A FINITE ELEMENT BASED APPROACH TO CHARACTERISING FLEXIBLE RING TIRE (FTIRE) MODEL FOR EXTENDED RANGE OF OPERATING CONDITIONS

BY

CHONGFENG WEI

A thesis submitted to the College of Engineering and Physical Sciences

of the University of Birmingham for the degree of

DOCTOR OF PHILOSOPHY

School of Mechanical Engineering

College of Engineering and Physical Sciences

The University of Birmingham

November 2014

ABSTRACT

In order to accurately predict vehicle dynamic properties when tires impact high obstacles or large bumps, appropriate tire models need to be developed and characterised. The Flexible Ring Tire (FTire) model is one of the models for predicting the transient dynamic responses when traversing obstacles. In this thesis, a combination of experimental tests and Finite Element (FE) modelling is used in deriving FTire models for different levels of tire/road interaction severity. A FE tire model is built to characterize tire properties including static properties, steady-state rolling properties and transient dynamic rolling properties.

A 235/60 R18 tire is cut in order that the tire cross-section can be captured and the tire rubber and reinforcement components can be extracted. A detailed method for the determination of geometrical and material properties of tires has been developed for tire modelling. The 2D and 3D models for static and dynamic analysis are both developed using a commercial FE code ABAQUS.

The parameters of FTire model are derived based on the experimental data and FE simulation data, and different FTire models are derived under different operation conditions. Multi-body dynamic analysis is carried out using these FTire models, and the transient dynamic responses using different FTire models are compared with each other.

It is shown that FE modelling can be used to accurately characterise the behaviour of a tire where limitations in experimental facilities prevent tire characterisation using the required level of input severity in physical tests.

The novelties of this study are: A new image processing method is applied to define the geometry of the tire model; Numerical simulations using FE method for tire rolling over large obstacles with different heights are carried out.

ACKNOWLEDGEMENTS

Firstly, I would like to express my greatest appreciation to Dr Oluremi Olatunbosun for taking over the supervision and guidance of my PhD work. I would like to thank him very much for his advice, support, and patience during my research. He is not only the supervisor of my PhD study, but also a father and a friend. I also learnt a lot from his attitude on academic research and social communication. It is difficult to express my gratitude to him using such few words.

Furthermore, I would like to thank Jaguar Land Rover for their support and the many favourable discussions on this research project.

I also would like to thank my colleagues Xiaoguang Yang, Mohammad Behroozi, Samaneh Arabi, Adebola Oluwaseyi Ogunoiki for their kind help and scientific discussions on my PhD work.

I would extend my thanks to my best friends Baosheng Shi and Guanxiong Wang for their supports and help when I came across some problems. Thanks are also delivered to my housemates, Qi Chen, Bing Liu and Shiling Zhang. I feel that I was joining a family when I was living with them.

My parents spent a lot on my studies from the time when I was a child. I have appreciated their patience and encouragement very much. I am really touched by their love.

Finally, I would like to thank my wife Beibei Chen for her non-technical support during my research work. Her encouragement gave me a lot of confidence for my study abroad.

List of publications

- **Chongfeng Wei**, Oluremi Olatunbosun. Transient Dynamic Behavior of FE Tyre Traversing Obstacles with Different Heights. Journal of Terramechanics. 56, 2014, Pages 1-16.
- **Chongfeng Wei**, Oluremi Olatunbosun, Mohammad Behroozi. Simulation of Tyre Rolling Resistance Generated On Uneven Road. International Journal of Vehicle Design. Accepted for publication.
- **Chongfeng Wei**, O. A. Olatunbosun. Detailed Finite Element Modelling Technology for Tire Parameters Derivation. Tire Technology International. 2013. 78-82.
- **Chongfeng Wei**, Olaremi Olatunbosun. Explicit Dynamic simulation for tire rolling over obstacles. Tire Technology International. 2014. 42-46.

Table of Contents

List of Figures

List of Tables

List of abbreviations

FE	Finite Element	FEA	Finite Element Analysis
FFT	Fast Fourier Transform	FTire	Flexible Ring Tire Model
NVH	Noise, vibration, and harshness	MBS	Multi-body System
CMM	Coordinate Measurement Machine	CAE	Computer aided engineering

Chapter 1 GENERAL INTRODUCTION

This chapter gives a general introduction on the research work described in the thesis. The motivation and background as well as objective and scope of this study are presented. This chapter also presents an outline of the thesis content.

1.1. Motivation and background

As a unique component of the vehicle contacts with the road, the tire plays an important role in the performance of vehicle/road interaction. Tire mechanical characteristics significantly influence the dynamic behaviour of the vehicle. With the development of new vehicle concepts and the improvements of dynamic behaviour of vehicle components, vehicle simulation with appropriate tire models is becoming more and more important. Engineers need to accurately predict the moments and forces transmitted from the tire to the wheel and the suspension. Prediction of the effect of tire characteristics on vehicle dynamic behaviour requires an accurate tire model.

Tire models used in vehicle dynamics simulation for handling, durability and ride comfort assessment need to be capable of predicting the non-linear deformation and enveloping characteristics which occur when traversing large road obstacles. The gradient of the cornering force vs slip angle (cornering stiffness) is the determining parameter for the handling properties of vehicles [122]. Vehicle durability can also be analyzing for tire rolling over different road unevenness, in which process accurate tire models are needed. Vehicle ride comfort performance is an important issue and tire models used for predict vertical and longitudinal responses are important for the ride comfort assessment. Tire model development for analysis of tire envelopment properties when the tire impacting road obstacles.

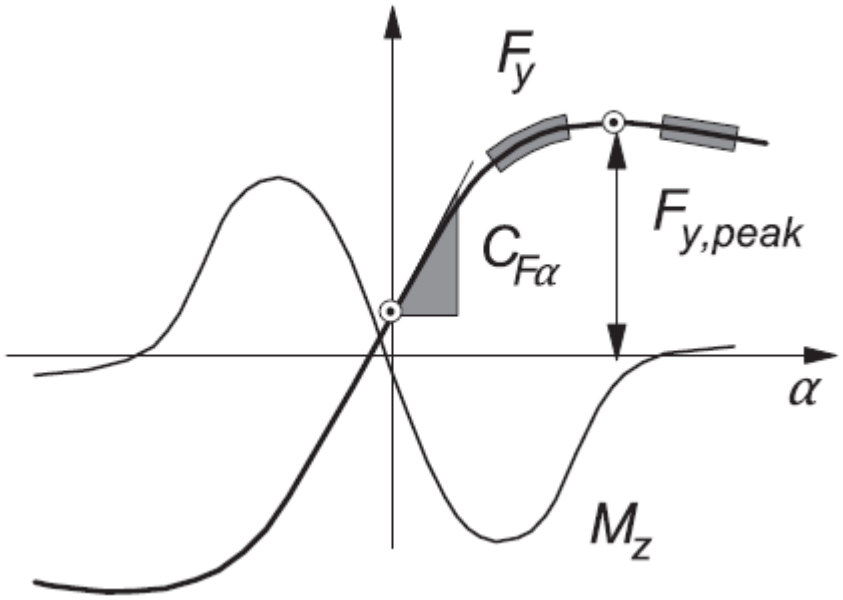

Figure 1.1 Characteristic shape factors of tire may influence vehicle handling properties (tire cornering force and aligning moment vs slip angle) [122].

The model FTire (Flexible Ring Tire Model), developed by Michael Gipser in 1998, serves as a sophisticated in-plane and out-of-plane dynamic and non-linear virtual tire model. FTire model has developed a reputation as the leading higher-frequency and short-wavelength tire model over the last few years. Today, FTire has become the major tire model used in the automotive industry for vehicle durability, road load, and ride comfort predictions [1].

For the tire/road contact, reaction forces generated from the interaction can be derived using FTire model and also, the responses can be taken as input for quarter-car vehicle or whole vehicle dynamic analysis. The main benefits of FTire consist of the following [1]:

i. simple and flexible interfacing to Multi-body System vehicle models
ii. fully nonlinear three-dimensional model
iii. good accuracy when passing single obstacles like cleats, pot-holes, and curb-stones
iv. validity for predicting steady-state rolling properties

In addition, FTire model can be applied for analysing all tire or vehicle vibrations in the frequency domain up to approximately 150 Hz, including tire-road contact [1]. The model is also valid for obstacle wavelengths in the longitudinal direction (rolling direction) up to half the length of the footprint, including sharp-edged obstacles.

Even though FTire has some advantages when being applied for CAE durability and ride comfort analysis today, further development of the model seems quite necessary because of the increasing requirements for model accuracy at high tire load conditions as well as at high frequency conditions. Basically, FTire model is determined from tire rig tests. Parameters such as static stiffness and cornering stiffness of FTire model can be easily obtained from the tests. However limitations in rig design and operating conditions mean that tests cannot cover all the different loading, inflation and road conditions which the tire will encounter in the most severe conditions, particularly for traversing high ramp or large obstacles, so that tire non-linear deformation and transient dynamic properties which occur when traversing large road obstacles cannot be accurately predicted. Some of the important issues that the current FTire models have not addressed properly can be categorised as:

i. The effect of high ramp or big obstacle on high speed rolling tire and the forces transmitted to the suspension and vehicle structure;
ii. Fatigue analysis of suspension structure and bushes under NVH loads provided by the FTire interface;
iii. The analysis of vehicle NVH under high-frequency road excitations – Frequencies which are higher than 200 Hz are outside the standard FTire range;
iv. The influence of material properties and layup structures of the tire on its steady-state and enveloping properties.

The above issues for tire and vehicle dynamic analysis including parametric studies

contributes to the limitation of FTire application for dynamic simulations. It has been shown that FTire model could not describe high-frequency deformations accurately, and thus is limited to excitations where the influence of these phenomena is not very serious. Also, a more accurately derived FTire model to deal with large road obstacles or high ramps for ride comfort, handling and durability analysis is needed. It is necessary to derive an extended FTire model to cover these conditions which the current FTire model cannot cope with, especially for the severe conditions.

Finite Element Analysis (FEA) for tire dynamic properties has been widely used by researchers and engineers in recent time. This is largely due to high performance property of computers and development of numerical simulation methods, therefore enabling the application of Finite Element tire models in analysing tire dynamic behaviour for extended range of operating conditions as an alternative to tire experimental measurements.

1.2. Objective and scope

As mentioned above, limitations in rig design and operating conditions restrict the range of test conditions under which the tire can be tested such that derivation of FTire parameters during extreme manoeuvres may not be possible using physical tests. However, Finite element methods can enable this to be realized as the advances in finite element modelling of tires have produced tire models capable of predicting tire dynamic properties when traversing large obstacles, from which the difficult physical tests can be carried out virtually. Therefore, a validated finite element (FE) tire model can be applied to predict tire dynamic responses in order to derive FTire models under operating conditions outside the capability of laboratory tire test rigs.

The research presented in this thesis is carried out at the Vehicle Dynamics Laboratory of University of Birmingham, and partly supported by Jaguar-Land-Rover. The objective of this

research is to develop an improved FTire model capable of overcoming the limitations of the current FTire model, particularly in accurate prediction of transient dynamic responses and enveloping properties produced in traversing high obstacles (higher than 25mm). In executing this project the experience in both physical testing and FE modelling of tires accumulated by the Vehicle Dynamics Group at University of Birmingham over many years is deployed.

Determination of FTire's data consists of geometry data, footprint shapes, static and steady-state properties validation as well as identification of transient dynamic properties when rolling over obstacles. In order to accurately predict transient dynamic properties, validation of the FE tire model needs to be carried out in static as well as steady-state and transient conditions.

Some other important objectives of this research are as follows:

- Understanding tire static, cornering and transient dynamic properties during FE tire model development.
- Parametric studies for the effect of material properties and operating conditions on tire performance
- Multi-body system (MBS) simulation using derived FTire model at normal conditions and extended operating conditions to find out the different dynamic responses

1.3. Outline of the thesis

In this chapter, the motivation and background of the current research was discussed. The necessity of developing an extended FTire model was analysed. Furthermore, the objective and scope of the research was also presented in this chapter.

In chapter 2, a review of literature on tire models and experimental methods for tire dynamics analysis is presented. Analytical tire models, empirical and semi-empirical tire models, together with numerical models and their behaviour at different operating conditions are described. By the comparison of different tire models, the reasons for choosing FE methods for tire modelling are addressed.

In chapter 3, the methods for determination of tire geometrical and material properties in the tire model are developed. Measurement methods of the material properties of rubber components are described and the processes of derivation of rubber material properties are presented. Based on definition of the geometrical and material properties of the tire, the 2D tire model is developed in chapter 3.

In chapter 4, the static properties analyses including inflation pressure analysis, static stiffness derivation, and tire/road contact footprint analysis are presented. Experimental validations for the tire static properties are also described.

In Chapter 5, the steady-state tire model was developed based on the static 3D model, cornering stiffness and aligning moment for different vertical loads and inflation pressures are predicted and validated. Parametric studies in terms of tire geometrical, material properties and different operating conditions are carried out in this chapter.

In Chapter 6, transient dynamic analysis for tire rolling over road obstacles with different heights is carried out. Validations of the transient dynamic responses in terms of longitudinal

spindle forces and radial spindle forces are presented. Furthermore, tire rolling resistance resulting from longitudinal forces generated on the uneven road is predicted. The rolling resistance for the tire rolling on different road surfaces is studied in this chapter.

In Chapter 7, the procedure of derivation of FTire model is presented. Different FTire models are developed based on different input data, and multi-body dynamic analysis for the rolling tire using three different FTire models is presented. Comparison of the transient dynamic responses with different FTire models is also described in this chapter.

The main works and important findings arising from the current research are presented in chapter 8. In addition, the possible works for improving the FTire model derivation in future studies are provided.

Chapter 2 LITERATURE REVIEW OF TIRE MODELS AND EXPERIMENTAL METHODS

2.1 Introduction

Due to the increasing requirements of predicting dynamic behaviour of tires and vehicles as well as the improvements of simulation techniques for vehicle design and development, reliable and effective tire models used to predict tire deformation, stiffness properties and rolling performance need to be developed. The tire model and vehicle model need to be able to reflect realistic behaviour of vehicle components. This chapter gives a development progress of tire modelling approaches and tire model application. Descriptions of analytical, empirical and semi-empirical, and numerical tire models developed over the years are given. Also, the development and application of FTire (Flexible Ring Tire Model) are presented in this chapter.

A literature review of the characterisation of tire behaviour under the following conditions is presented in this chapter:

- Normal condition: static behaviour, steady-state rolling conditions
- Severe conditions: tire traversing obstacles, bumps.

2.2 Analytical tire models

2.2.1 Tire models for tire behaviour at normal conditions

Analytical tire models have been developed to characterise the complex behaviour of the pneumatic tire and its interaction with the road surface. These models are developed based on the physical characteristics and behaviour of tires. Because of the low cost of such models on tire dynamic simulation, research on analytical tire models continues today.

Analytical tire model development has been carried out for more than 40 years. In order to calculate the areas of dynamic contact footprint, Clark [2], in 1965, modelled the dynamic rolling property of a pneumatic tire under load, and in the model the tire was treated as an elastically supported cylindrical shell. With the development of analytical techniques of tire/road contact, the contact areas and dynamic pressure distributions can be predicted. In the model, the parameters that affect contact area and pressure distribution are tire structure and traveling velocity. Tielking [3] also used an elastic shell to represent a pneumatic tire, and the equations of tire motions were established using energy methods. The effect of elastic property and inflation pressure of the cylindrical shell were considered for establishment of the equations of motion. The circular cylindrical shell was also used by Keltie [4] to represent a truck tire model. The objective of theoretically modelling truck tires, in this case, was to describe the sound radiation due to the vibration of in-service truck tire surfaces. The sound power radiation was calculated based on the influence of inflation pressure, structural damping and tire bending stiffness.

In the model developed by Soedel [5] in 1975, the tire was assumed as an equivalent thin shell, which can be used to define displacements of every particle in three directions. A dynamic Green's function was developed with regard to natural frequencies and modes of the tire, and dynamic responses of the rolling tire were predicted based on the dynamic Green's function.

In 1987, Huang and Soedel [6] developed a rotating ring on elastic foundations model, in which Hamilton's principle was used to derive the equations of motion that cover both lateral and longitudinal motion. Due to the completeness and simplicity of the ring on elastic foundations (REF) theory, it has been the most frequently used for tire rolling analysis. Similar foundations for ring models have been developed by Gong [7], Dohrmann [8], Kim and Savkoor [9] , and Wei et al. [10].

In 1988, Springer et al. [11] developed a general mechanical rolling tire model for prediction of tread deformations under transient conditions. The equation of motion for steel belts and the tread were applied to predict the deformation of the tire circumference. Newmark's integration method and Finite Differences were applied to solve the equations of motion, and the transient tire model is suitable for both even and uneven road surfaces. Sjahdanulirwan developed an analytical tire model for the prediction of friction on the tire/road contact surface in 1993. Some parameters in the model such as braking coefficient, static stiffness of the tire, and the longitudinal and lateral forces generated on the contact patch were predicted for a specific tire. In addition, the slip ratio and orientation relative to the road were given. In the same year, Qiu et al. [12]investigated three kinds of analytical tire models: point contact tire model, fixed footprint tire model and adaptive footprint tire model, from which they found the point contact tire model was only suitable for calculation of vertical response for the tire of low natural frequency, while the footprint tire model was difficult to be adopted in a terrain-vehicle system for dynamic simulation because of its nonlinear and complex properties although they had satisfactory validations of the vertical responses. A modified tire model was developed based on the point contact tire model with a satisfactory modified function of the vertical response function and gave better accuracy of the vertical response properties.

In the mechanical tire model developed by Mastinu et al. [13], the carcass of the tire is constructed using the sidewalls and the belt. A circular Euler beam which is flexible in radial and lateral direction and fixed in longitudinal direction was used to define the belt, and a distributed stiffness was applied between the beam and the rim centre to represent the tread elasticity. The area of the contact patch, pressure distribution, tread deformation, sliding forces and moments, adhesion forces and moments can be predicted using the computer system based on the tire model.

Ramji and Goel [14] used part of circles at the ends with rectangle at the middle to represent the tire model (Figure 2.1), in which the normal pressure distribution at the contact patch is symmetric and trapezoidal. The rectangular and circular parts were defined to represent the contact patch and the deformed tire separately. Based on this tire model, Rao et al. [15] developed a new one with different normal pressure distributions. Different shapes of vertical pressure distributions within the contact patch in circumferential direction were studied to describe different manoeuvres. And they found tire models with trapezoidal pressure distributions (high range of slip characteristics) show smaller lateral force and longitudinal force.

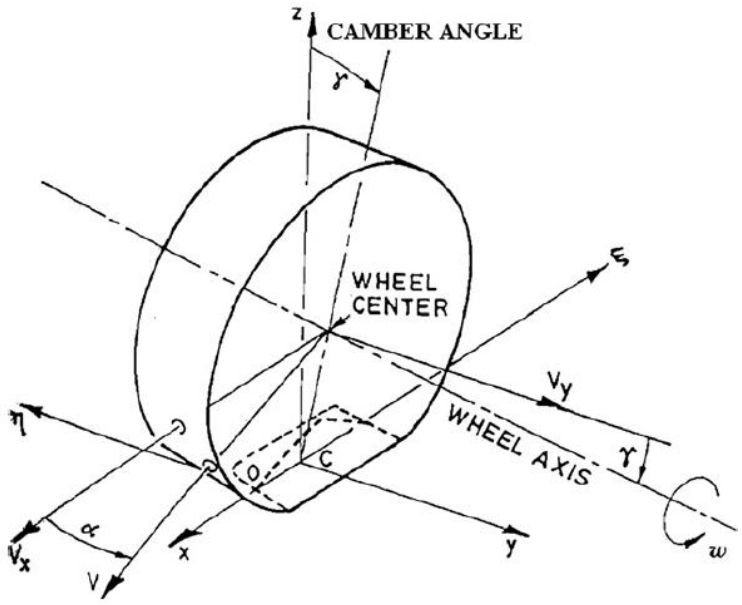

Figure 2.1 Tire axis system and kinematic variables [14]

As one of the basic properties, tire static stiffness has been investigated by many researchers. In the research of Kao about tire radial stiffness, the tire model was defined by a two-spring-and-two mass system, and the tire stiffness was independent of the acceleration of the tire. In their model, the radial stiffness is determined by the tire patch enveloping stiffness and the sidewall stiffness, which was determined by the measurement of the length of the contact patch [16, 17].

Shim and Margolis [18] presented a new analytical tire model for simulation of tire braking and cornering at normal driving conditions. As there is a linear region for the low slip angle of the tire, the analytical model was developed for prediction of pure braking, pure cornering and combined braking and cornering properties in this region. The longitudinal forces and cornering forces of the tire were derived as a function of tire/road friction coefficient, slip angles, and normal load.

In order to efficiently carry out steady state simulation, some researchers used analytical approach for prediction of steady state tire forces and moments. With description and comparison of the string model, beam model and spring-damper models, Peng et al. [19] developed a new analytical tire model for the lateral dynamic behaviour of a rolling tire. The tire carcass of the model is represented by a parallel spring and hysteretic damper, while the interaction between the tire and road is represented by a viscous damper. The results showed that the new model provided more satisfactory lateral forces prediction than other normal spring-damper models. Similarly, Wang et al. [20] proposed a mathematical method for estimation of cornering stiffness coefficient and tire/road friction coefficient.

2.2.2 Tire models for prediction of tire behaviour at special conditions

With the objective of characterizing the enveloping properties of a rolling tire, Kilner [21] developed a tire model using a toroidal membrane. Road surface was modelled with large discrete surface obstacles shorter than the length of tire contact patch. Tire/road contact patch, tire column, and the normal and drag loads were calculated using an explicit set of equations.

Guo [22] developed a rigid roller contact tire model for investigation of vehicle vibration properties. The geometric filtering concept and the method to transfer road unevenness into effective input were proposed. In the rigid roller contact model, there is at least one point contact with the road and the radius of the rolling tire is kept constant. Based on the rigid

roller contact model, Guo and Liu [23] developed a flexible roller contact model, in which the single point contact was replaced by a tire/road contact surface, and the contact length can be variable in rolling. Although the geometric filtering work has been improved in flexible roller contact model, it could not accurately predict the enveloping properties of rolling tires, especially tire deformations.

Based on the REF model and its analytical formulations developed in [10], Wei et al. conducted a study on the dynamic contact responses between tire and road/cleat [24]. A dynamic explicit program was developed to obtain time domain solutions of tire rolling over an obstacle. In addition, in order to investigate the effect of damping on dynamic responses, the tire was modelled as a ring on viscoelastic foundation, and they found the damping has a significant influence on tire dynamic responses when rolling over a cleat.

Analytical tire models can be easily applied because of their high computing efficiency and simplified tire structures on which they are based. However, analytical models based on physical properties have some limitations because of their simplified structures and application restrictions such as in-plane deformation or static property investigations.

In addition, tire models used in vehicle dynamics simulation for CAE durability and ride comfort assessment need to be capable of predicting the non-linear deformation and enveloping characteristics which occur when traversing large road obstacles. However, the pure analytical tire models could not represent accurate enveloping behaviour of rolling tires, and some important parameters such as tire material properties and tread deformation were not considered.

2.3 Empirical and semi-empirical tire model

2.3.1 Tire models for tire properties at normal conditions

Empirical models were often derived based on the experimental data. Some purely empirical tire models have been developed to get over the inaccuracy of simple analytical tire model. The Magic Formula Tire model developed by Pacejka is a widely used empirical model for tire dynamic analysis [25, 26]. The general form of Magic Formula can be written as

$$y = D\sin[C\arctan\{Bx - E(Bx - \arctan Bx)\}] \qquad (2\text{-}1)$$

In which D is the peak value, C the shape factor, and B and E represent the stiffness factor and curvature factor respectively. The formula is capable of producing the curves for side force F_y, longitudinal force F_x, and aligning moment M_z with regards to the slip angle α and the longitudinal slip κ, and the input x is described by α and κ.

Guan et al. [27, 28] established a tire model for cornering properties by extracting experimental modal parameters under different inflation pressures, vertical loads and friction coefficients. Experimental modal parameters were extracted from longitudinal and vertical responses under excitations. The lateral force distribution in the contact patch and the deformation of carcass and tread were predicted based on the empirical tire model. Results obtained from simulation of the tire model fitted well with the Magic Formula model.

However, it needs many input variables to derive the lateral force and aligning moment, which means lots of test data are needed to obtain the outputs. Also, empirical models are often described in terms of typical curves which describe the relationship between inputs and outputs, and the curves are then adjusted using test data without giving physical property explanations of the forces or moment generation.

Some tire models were derived by the combination of mathematical approximation of measured tire performances and physical characteristics of tires, this kind of tire model can be referred to as semi-empirical models. The development methods of semi-empirical models were used by some tire researchers for improving the accuracy of tire behaviour predictions, including braking, cornering and transient dynamic conditions. Also, sometimes tire measurements were conducted for acquiring important parameters which should be used in the physical tire models for further development.

Guo and Ren [29] developed a unified semi-empirical tire model, the input parameters of which can be identified by pure longitudinal slip and side slip tests of the rolling tire, from which the lateral force, longitudinal force as well as self-aligning moment can be predicted. Basically, the improved tire model was developed based on their previous tire model, Uni-Tire model [30, 31], and it can produce better accuracy and requires fewer input parameters from measurements.

In order to efficiently carry out steady state simulation, some researchers used an analytical approach for prediction of steady state tire forces and moments. Rao et al. [32] developed an analytical tire model based on different normal pressure distributions. The rectangular contact patch is positioned at the middle and parts of two circles are positioned at the ends. Different shapes of normal pressure distribution on the contact patch have been considered for the tire models, and they found that the trapezoidal normal pressure distribution tire model predicts low magnitudes of lateral forces, longitudinal forces and aligning moment. By considering the description and comparison of the string model, beam model and spring-damper model, Peng et al. [19] developed a new analytical tire model for the lateral dynamic behaviour of a rolling tire. The tire carcass of the model is represented by a parallel spring and hysteretic damper, while the interaction between the tire and road is represented by a viscous damper. The results showed that the new model provided more satisfactory prediction of lateral forces

than other normal spring-damper models. Similarly, Wang et al. [20] proposed a mathematical method for estimation of cornering stiffness coefficient and tire/road friction coefficient based on the longitudinal tire force difference between the two sides of a rolling vehicle.

2.3.2 Tire models for special road conditions

In 1988, Transient rolling simulation was conducted by Bandel and Monguzzi [33]. They developed a "black box" mathematical tire model on the basis of experimental test results for studying a tire running over an obstacle at low speed and high speed respectively. In the "black box", the parameters and input data were acquired from experimental tests on the tire, which derived an empirical relationship between the obstacle dimensions and the displacement of the damped oscillating system. Low-speed forces can be obtained by using the empirical relationships, while the high-speed forces were derived by using the low-speed forces at the hub as the input to an oscillating system with one degree of freedom. The shape of the basic curve obtained from a limited number of tests is interpreted as the shape of the obstacle "filtered" by the tire, while it is independent of tire deflection and inflation pressure.

Guan and Fan [27, 34] established a semi-analytical tire model derived from experimental modal parameters below 350Hz, which were extracted from the radial and tangential responses under radial and tangential excitation. The tire model could not only calculate the static vertical stiffness of a non-rotating tire on a flat surface and distributions of contact and shear forces, but tire static enveloping properties with different operating conditions could also be investigated. Based on the work of investigation of static enveloping properties, further study of Guan and her colleagues [35] was concentrated on the enveloping properties of the dynamic tire model. With consideration of the nonlinear stiffness of the tire sidewall, a quantitative in-plane rolling tire model was developed to investigate tire dynamic responses and enveloping properties when the tire rolls over different cleats with different values of

inflation pressure and wheel load in both time domain and frequency domain. Validation results showed the tire model had a disadvantage that the contact time of the tire model was shorter than that in the experiments with higher radial load condition.

Because of the limitations and inaccuracy in the characteristics of analytical tire models, the development of empirical and semi-empirical models can improve the accuracy of physically based analytical models. However, most of this kind of models can only be used in the low frequency range. In addition, because of their simplified structures, tire designers and researchers cannot investigate the effect of material properties and reinforcement layup on static or dynamic performance of tires.

Most of the Empirical models and semi-empirical models are derived from experimental data, which are used as input of the tire model. In order to build a tire model suitable for different operating conditions, many parameters need to be derived from tests, which will significantly increase the experimental cost.

As one of the most important enveloping properties, tire deformations when impacting road obstacles have been ignored in most of the empirical models and semi-empirical models. In addition, tire viscoelastic property plays an important role in tire transient dynamic behaviour when the tire traverses an obstacle, but this property is often replaced by simple tire damping model, which is unable to represent the real behaviour of the rolling tire.

2.4 Numerical tire models

2.4.1 Tire models for normal conditions

Numerical simulation for tire static and dynamic properties has been applied for more than thirty years, and has been increasingly used by tire designers and researchers for tire design and analysis. Finite Element Analysis (FEA), as a widely used approach for tire performance investigation, is a powerful technique with high accuracy. The principle of the finite element

method is to obtain approximate solutions by integrating the mechanical properties of finite elements over the whole structure [36]. At present, many tire tests can be carried out virtually using FE tire models.

2.4.1.1 Static properties

Tire basic static properties (behaviour under inflation pressure, static stiffness, and footprint) are very important tire characteristics. The natural frequencies of the vertical vibration of tires are related to the tires' vertical stiffness. Likewise tire excitation resulting from road unevenness is generated through static tire stiffness. The footprint property of a tire (size and shape) is important for the shear force generation in the contact area. As one of the important parameters, the inflation pressure significantly affects steady-state rolling behaviour and transient rolling behaviour of tires.

Finite element modelling for tire static properties has been conducted for different operating conditions. Burke and Olatunbosun [37] developed a tire model based on derivation of material properties from a real tire. Different samples of the tire were extracted for tensile testing and material property definition. The load/extension data obtained from tensile testing were imported into MSC/NASTRAN to develop the FE tire model. Based on the tire model, modal analysis of the tire model was carried out at various inflated and deflected conditions, and they found that the inflation pressure has a great influence on the tire stiffness and hence tire dynamic behaviour. In addition, a new procedure to define tire/road contact was developed by Burke and Olatunbosun [38, 39]. In their study, the tire/road contact was modelled by a gap element formulation, with which the footprint shape, contact area as well as the tire deformation can be obtained automatically. And also, the approach provided flexibility in setting operating conditions such as inflation pressures and radial loads.

Bolarinwa and Olatunbosun [40] developed a two-dimensional axisymmetric FE tire model for tire burst analysis based on a P195/65R15 passenger car tire cross section using ABAQUS (Figure 2.2). In order to model the tire burst phenomenon, the inflation pressure was increased until the ultimate strength of the tire reinforcements, which were modelled with rebar elements, was reached. They found that the burst pressure is dependent on the cross-section area, yield strength, and spacing of carcass reinforcements. Further study [41] concentrated on the cornering properties analysis with regard to cornering forces and aligning moment. The 3D FE tire model was developed based on the definition of rubber material and reinforcements. Solid elements were used to define hyperelastic rubber material and rebar elements were used to define carcass and steel belts embedded in the rubber. However, viscoelastic property was not included in the tire dynamic analysis.

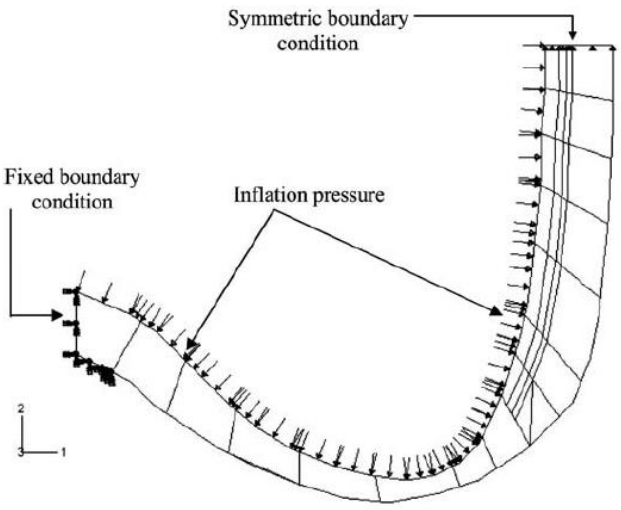

Figure 2.2 Two-dimensional axisymmetric tyre model with reinforcement materials [40]

Recently, Yang et al. [42] developed a procedure to determine material property by using the rubber and reinforcement components extracted from a tire. Combination of experimental testing and FE modelling were applied to derive the hyperelastic parameters and viscoelastic properties of the rubber as well as the elastic property of the reinforcements. Static validation was carried out based on tire radial deformation and footprint comparison between

measurements and tests, and the finite element tire model showed satisfactory correlation with test results. Furthermore, Yang and Olatunbosun [43] investigated the influence of reinforcement turn-up on tire durability and operating properties using finite element analysis (Figure 2.3). They found that the strain energy density of elements in the critical region of the tire is greatly affected by the height of reinforcement turn-up. Also, the turn up height of bead reinforcement has a significant effect on tire operating properties, including static stiffness and cornering stiffness.

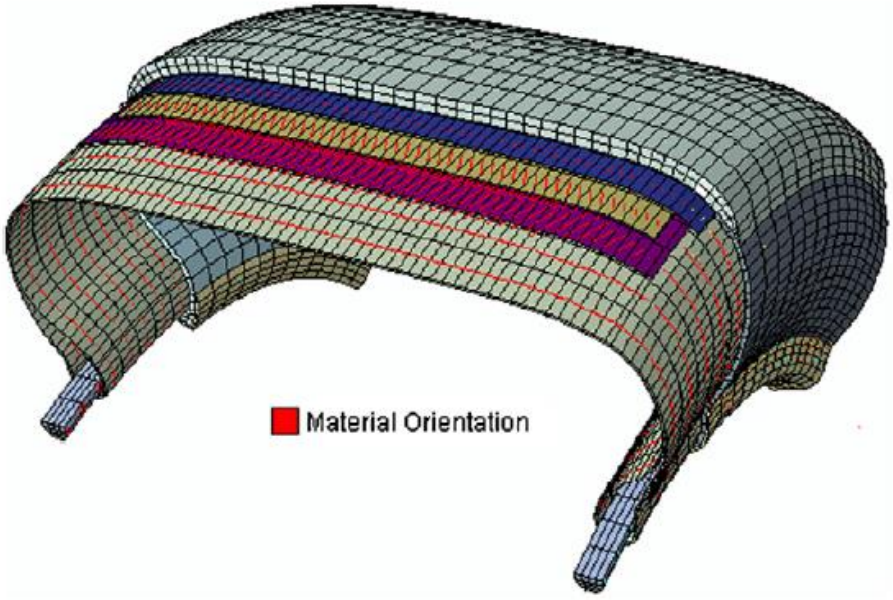

Figure 2.3 Detailed view of 3D finite element tyre model [43]

Apart from vehicle tire modelling, a comprehensive work was also conducted on the aircraft tire modelling at University of Birmingham. Behroozi et al. [44] demonstrated the capability of FE analysis to model the very complex structure of an aircraft tire with many layers of reinforcement both in the carcass and the belt of the tire. They analysed the influence of model complexity on aircraft tire performance properties using finite element analysis. Composite layup and rebar elements were applied on the FE modelling of aircraft tire performance. Particularly, cords spacing, cords orientation as well and the material property have been defined using rebar elements. Different mesh sizes for rubber and reinforcement

components were employed to generate different FE tire models, from which the effect of mesh size on stresses and deflections of the tire were studied.

As an initial simulation step of tire static properties analysis, inflation behaviour of the tire has been applied for basic research. Allen and his colleagues [45] developed a numerical approach to calculate the inflated shape and stress distribution of a pneumatic aircraft tire using axisymmetric model, the deformation characteristics of the tire were studied to determine the heat generation based on the rubber material properties.

Some researchers have carried out static simulations using different tire models. Pelc [46] developed a static three dimensional tire model using finite element program MARC, in which the radial stiffness and the shape of the tire footprint as well as the pressure distribution were predicted using the tire model. Hamid [47] developed a steel-belted radial model using another FE program Abaqus, in which different belt angles were applied on the tire model to investigate the effect of belt angles on radial stiffness, also distribution of the contact pressure were analysed with simple tread pattern and complex model with detailed tread blocks. He found that the belt angle has a significant influence on the maximum pressure because of the variation of lateral stiffness when different belt angles applied on the model.

With regard to footprint investigation, Hu and Abeels [48] developed a 2D agricultural tire model for prediction of the deformation of the tire profile as a function of inflation pressure and vertical load. The normal and tangential contact forces, vertical and lateral displacement of the tire, and stress distributions were analysed using the 2D finite element model. However, material properties of reinforcements were not considered in their investigation. Different from Hu and Abeels's model, Xu et al. [49] proposed a piece-wise Ritz procedure for investigation of interaction between tire and rigid road surface. The footprint contour as well

as stress distribution of radial tires were predicted using the piece-wise Ritz procedure and FEM code separately. Their results showed that the tire radial stiffness was approximately linear, and the tire pattern has little influence on it.

With regard to tire/soft-road static interaction, Nakashima and Yong [50] pointed out that analysis of tire/terrain interaction was very important for prediction of contact geometry. And attempts have been made to build efficient tire/terrain interaction models by applying finite element methods [51, 52]. The tire was assumed as an elastic system and the soil was considered as a piece-wise elastic material, and Hertz theory of contact between two elastic bodies was used to predict the length of tire/terrain contact patch. Based on the mechanics of Pneumatic tires investigated by Clark et al. [53], the contact area can be considered as an ellipse at small deflection and can be approximated as rectangular at large deflection. In the study of Nakashima and Yong [50], the contact patch was assumed to be rectangular and the influence of inflation pressure on tire dimension was ignored. Mohsenimanesh and Ward [54] developed a detailed and efficient methodology for estimating the three dimensional contact footprints of a truck tire. Based on the measured tire/soil contact length, the width and depth of the ruts formed in the soil as well as the tire/soil interface pressure were used in the method to estimate the footprint under different inflation pressures and vertical loads.

2.4.1.2 Steady state rolling properties of tires

As an important property for tire rolling analysis, cornering property of a tire has a significant effect on the directional control and handling stability of the vehicle, and cornering stiffness is one of important parameters in full vehicle dynamics simulation. Normally, cornering analysis is conducted at free rolling conditions. Therefore, it is necessary to derive the free rolling condition through braking and traction analysis. Korunovic et al. [55] developed a FE tire model for straight line steady state rolling analysis, in which the travelling velocity was

constant and the angular velocity of the tire varied in given increments. Later on, they carried out an analysis for tire rolling on the drum using finite element methods and experimental tests, and the rolling surface was changed to cylindrical road from flat road [56]. In order to find the accurate value of friction coefficient, they used tread blocks extracted from another tire for friction rolling tests on a Mini-μ-road.

Different from the analytical methods [19, 20] for cornering property prediction, Olatunbosun and Bolarinwa, using a 3D FE tire model, investigated the effects of material and geometric properties variation on dynamic responses of the tire, especially on tire cornering behaviour, including lateral forces and moment [41]. Xu and his colleagues [57] demonstrated that the inflation pressure is of scarcely any effect on cornering stiffness of the tire when the slip angle is less than 6 degrees, while the inflation pressure has a positive influence on the cornering stiffness when the slip angle is above 6 degrees. Zhao et al. [58] took the detailed tread blocks into account in modelling Force & Moment properties of a treaded tire in cornering using implicit to explicit FEA solving strategy.

In order to demonstrate the feasibility of explicit finite element code PAM-SHOCK™ for prediction of cornering property, Koishi et al. [59] developed a 3D FE tire model. The reinforcements components were modelled with shell elements and the rubber components were modelled with solid element. The hourglass control was applied in the reduced integration elements to eliminate numerical instability. Explicit program was also used by Rao et al. [60] in ABAQUS™. Cornering behaviour, braking behaviour, and the effect of camber angle on cornering behaviour were investigated by them. However, there was a need to filter the simulation results as numerical noise was generated in explicit dynamic simulations.

Because of the complexity of the tire structure and time consuming characteristic of finite element analysis, some researchers try to build reduced finite element tire model by simplifying the sidewall and tread of the tire. In order to simplify the finite element tire model, Faria et al. [61]used a combination of layered anisotropic thick shell elements in the carcass and blocks representing tread section to describe the cross section of the tire. The interaction between tire and road has been obtained as extensions of the Hertz theory of elastic contact.

With the advent of computer system and development of FE software, some researchers prefer to use detailed FE tire model to conduct tire static and rolling analysis. Zhang et al. [62] used a detailed finite element model to analyse tire vibration problems in time domain by means of application of explicit nonlinear finite element code LS/DYNA3D. The new three-dimensional finite element approach for vibration analysis they used had the advantages that it can consider both material and geometrical nonlinearity, can employ different kinds of contact algorithm, and also it could incorporate different damping effects. What is more, NVH post-analysis was conducted in frequency domain by transforming the resultant time domain data into frequency domain using FFT. However, compared to the traditional implicit formulation, this approach requires more CPU time, and it can also lead to unsatisfactory accuracy of the FFT results at a low frequency range.

2.4.2 Rolling Tire models for special road conditions

2.4.2.1 Tire rolling on soil or snow covered road

Most of the rolling studies were focused on the interactions between tires and rigid road surfaces. However, some researchers attempted to investigate tire behaviours for tire rolling on snow and soil recently. Choi et al. [63] employed the 3D patterned tire model to investigate tire traction characteristics on snow covered road. Euler-Lagrange coupling method was implemented on the tire tread blocks and snow deformation, which was defined

using the Mohr-Coulomb yield. Lee [64]conducted simulations for tire rolling on low-strength snow at longitudinal-slip-only condition and combined-slip condition. A 3D FE tire model was constructed with reduced integration and hourglass control. The low-density fresh snow was modelled using the modified Druchker-Prager Cap model, which is assumed to be isotropic and its yield surface is composed of two main segments: a shear failure surface, providing dominantly shearing flow, and a "cap," representing plastic compaction. 168000 3D eight-node elements were used in the FE snow model. The motion resistance, tire deformation and distribution of normal pressure and shear stress on tire/snow contact patch were predicted, and he found that the longitudinal slip and normal load have significant influence on the interfacial forces.

Drucker-Prager/Cap model implemented in ABAQUS has also been used by Xia [65] to model soil compaction. Only tread, sidewall and rim of the tire model in his study were considered, and sidewall and tread were constructed from fiber-reinforced rubber composites, the rim was modelled as a rigid body using kinematic coupling. The terrain section was modelled as a system with two layers, in which the top soil layer was modelled using Drucker-Prager/Cap model, and the bottom soil layer was assumed to deform elastically because of its stiffer characteristic. The effects of operating conditions including inflation pressures and rolling velocity on traction and acceleration of the tire have been predicted. However, the simulation was focused on the straight line rolling analysis, and cornering behaviour has not been addressed in the research. Different from Xia's research [65], tire/soil interaction simulation was conducted by Fervers [66] in two-dimensional space. Tire components like tread, steel belts, and rim of 3D FE tire model can be easily transferred into the 2D space. The carcass in a 2D tire model was replaced by the relation between contact force and tire deflection. A wet loose loam soil with high cohesion and low compaction resistance and a dry sand soil with low cohesion and high compaction resistance were used in

the model. As the simulation was conducted in 2D space, lateral slip was ignored in Fervers's model.

2.4.2.2 Tire rolling over obstacles or steps

In 1994, Mousseau and Clark [67] used the ring on elastic foundation model consisting of beam finite elements as a pneumatic tire to simulate a tire rolling over large obstacles. In their tire model, the tread is represented by a ring of two-noded beam elements, and ABAQUS nonlinear finite element program was used in the simulation. Interaction between the ring beam elements and the road surface was modelled using Lagrange multipliers, and tangential friction was determined by friction coefficient and shear stiffness of elements. A tire rolling over a large step was simulated using the ring on elastic foundations model (REF model) including beam finite elements. The reduced FE tire model only takes about 30 minutes to simulate the rolling process with a 2-MFLOP computer, which means the tire model may have the capability for use in vehicle dynamic analysis. By examining the influence of Model DOF and sensitivity of model parameters, they found the response of the tire rolling over a step is influenced primarily by the radial deformation of the foundation and inflation pressure. However, the beam element in the ring on elastic foundation model is unable to support large deformations.

To overcome the inaccuracy and simplicity of simplified models such as the ring on elastic foundation model [67] and radial spring model, Mousseau and Hulbert [68] developed the tire model by using an inextensible, circular membrane in combination with an elastic arch to approximate the sidewall behaviour, while the tread was modelled by using a geometrically nonlinear beam element (Figure 2.4). In order to investigate the enveloping properties of the tire rolling over a step at low speed, a rolling tire model was constructed by implementing the finite element model in the ABAQUS code. Dynamic responses for an inflated tire rolling over a step were simulated and measured in their study at low speed. From the good

agreement between the simulation and measured results and the simplified construction of the structure of the tire, the new model was shown to be more accurate than simple tire models and more efficient than detailed finite element models. It was also shown that the tire model is more accurate in predicting longitudinal forces and vertical forces than the ring on elastic foundations when a tire impacts large obstacles.

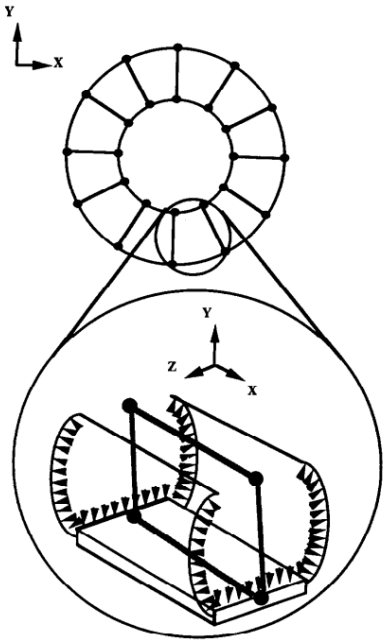

Figure 2.4 Finite element tire model developed by Mousseau and Hulbert [68]

Further studies of the transient dynamic response of a rolling tire impacting an obstacle at high speed (i.e., more than 30 km/h) was carried out in 1996 [69]. From the characteristics of the tire model it was found that it was capable of predicting tire transient dynamic performance at different rolling speeds, and more accurate than conventional simple tire models and more efficient than detailed FE tire models. However, while the tire model is suitable for vehicle dynamics simulation with the capability of analysing durability events, it could not provide sufficient parameters information for the tire designer due to the simple construction of the tire model. In addition, it is difficult for the user to determine the sidewall length and tread width for the tire model definition accurately.

As the reduced FE model has the potential for full vehicle dynamic analysis, Mousseau et al. [70] applied a coupled multibody and finite element model to simulate the dynamic response of ground vehicles on uneven road. In their model, a nonlinear FE tire model was developed and a multibody system simulation vehicle model was simulated by using an interface which transfers data between these two models. In the tire contact model, the Finite Element method was used in modelling the deformation of the tire structure and the contact between tire and the ground. In comparison to the detailed FE tire model which uses the special nonlinear FE to model the tire structure, the efficiency of the overall simulation was greatly improved. In order to improve the efficiency of the combined tire and vehicle simulations, the force Jacobian calculation was used. This comprehensive model also had a good accuracy in predicting the vertical spindle forces in the case of a vehicle driving over an obstacle. However, it did not perform very well in predicting the longitudinal forces.

Cho et al. [71] developed a 3-D patterned tire model with detailed tread pattern definition for transient dynamic response analysis of a rolling tire impacting with a small obstacle with a width of 50.8mm and a height of 12.7mm (Figure 2.5). ABAQUS^{TM}/Explicit was applied for the tire rolling simulation. Rubber components were modelled using the Mooney-Rivlin material model with a strain-energy density law. For the transient dynamic contact between the tire and road, they adopted the Lagrange multiplier approach and penalty method to formulate the contact problem. From the tire transient dynamic responses in the time domain and frequency domain, they found that the rolling velocity had a significant effect on both horizontal and vertical responses. In addition, the tire inflation pressure produced slight variation on the horizontal dynamic forces while it had significant effect on the transient dynamic response of the vertical forces.

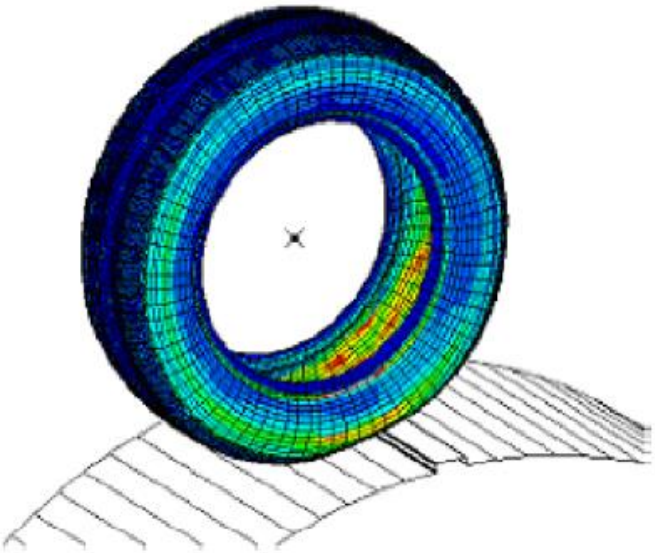

Figure 2.5 A FE tire model impacting with a rigid cleat of the rotating circular drum [69]

Kamoulakos and Kao [72] developed the Finite Element approach using PAM-SHOCK™ for studying the transient dynamic properties of a rolling tire impacting a road imperfection. In their study, the influence of impact between a rolling tire and a spinning drum with road imperfection was examined numerically using explicit time integration scheme. Up to 21 tire revolutions were simulated to demonstrate the reliability and stability of the program in resolving tire impacting problems. Olatunbosun and Burke [73] used MSC/NASTRAN™ to develop a time domain rotational FE tire model for the study of the dynamic performance of a 195/65 R15 radial tire traversing a small cleat (Figure 2.6), in which the tire carcass was represented by laminated anisotropic shell elements as it was capable of defining the non-linear material properties and had satisfactory computational efficiency, while the rigid wheel was represented by beam elements.

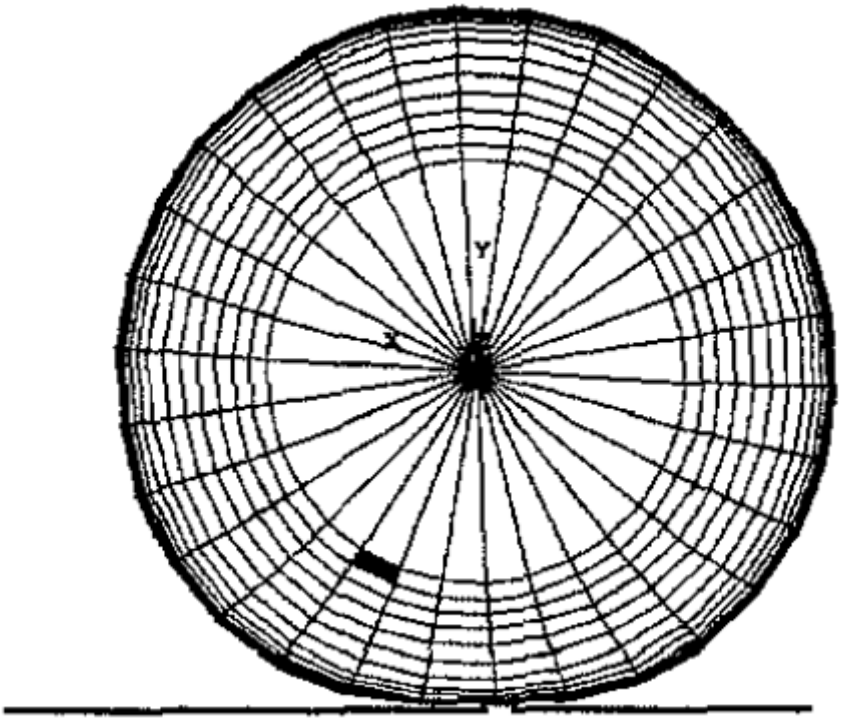

Figure 2.6 Tire rolling over a small road obstacle [71]

Besides pure tire modelling and tire dynamic analysis, some researchers have attempted to assemble the tire model into a quarter-car model to investigate vehicle dynamic performance. Yu and Aboutorabi [74] used ABAQUS to assemble the tire model, suspension model and wheel model together. Road roughness, potholes and bumps were taken as input excitation of the simple quarter-car model to predict the vibration of the tire spindle. They discovered the first radial mode has a significant effect on the spindle vibration amplitude, and only at certain frequencies can the spindle forces transmit to the vehicle. Similarly, Kerchman [75] developed a tire-suspension-chassis system to investigate ride comfort and impact harshness property of vehicles. A detailed FE tire-wheel model was modelled to connect the wheel hub and the suspension system. Simulations of the quarter-car rolling over different cleats with different velocities were conducted. He found that the rolling contact force variation and tire vibration modes are very important factors affecting the responses of the hub. Also it was verified that stresses and deformations of the impacted tire may affect tire endurance

seriously. However, as the whole tire-suspension-chassis system simulation was carried out using explicit program, much calculation time is needed to find out the performance of the system on an uneven road, which could be very expensive.

Mousseau et al. successfully applied the FE tire model in full vehicle analysis. However, most of their work was concentrated on the tire enveloping properties, and the out-of-plane properties of the tire have been ignored. As the tread was defined by simple beam elements, the tire model may not be able to accurately predict cornering properties. For some of the other detailed finite element tire models, the researchers did not provide appropriate methods for applying these models into quarter vehicle or full vehicle analysis. Besides, there is a lack of a complete tire enveloping properties study as only a single cleat was adopted in the investigations, which means the effect of the size of the obstacle has been ignored. Reference [74] and [75] give the quarter vehicle model in ABAQUS, but the suspension has been greatly simplified and much more computation time needs to be taken compared to the tire model itself.

2.5 Experimental test methods

As an alternative to tire static property investigations using simulations, Taylor et al. [76] introduced different measuring methods to derive tire vertical stiffness under different conditions. Based on the measurement results for static load-deflection and non-rolling vertical free vibration as well as rolling vertical free vibration, they found that the stiffness at the condition of non-rolling vertical free vibration showed the greatest value. Also, from their results, a conclusion was obtained that using pure combination of a spring and viscous damper to determine vertical tire stiffness in the analytical tire model was not adequate at low inflation pressures.

Due to the complexity of the tire/obstacle impacting problem and limitations in numerical techniques for predicting transient dynamic behaviour of rolling tires, experimental approaches were developed by some researchers for estimating the tire enveloping characteristics at low speed and transient dynamic properties of tire rolling over obstacles for different types of tires.

In the study of Alkan and his colleagues [77], different tire inflation pressures, vertical loads and types of obstacles were considered to investigate tire enveloping properties by experimental tests. In addition, different tires were tested in the experiment, and data was collected in terms of in-plane and out-of-plane forces and moments. By comparison of the tire dynamic behaviour at different vertical loads and different inflation pressures, they drew the conclusion that vertical load has a considerable effect on vertical and lateral forces of the tire, while the inflation pressure does not have significant influences on tire force and moment responses.

Upadhyaya et al. [78] tested three different tires at different soil conditions to obtain the traction prediction equations for radial tires. They found the soil-tire contact area and inflation pressure were very important parameters which affect the traction properties of radial tires. Lyasko [79] derived mathematical equations to obtain tire/road contact area, contact length and contact width for tires with different inflation pressures, sizes and deformations.

Although most of the simple tests can be carried out for investigating the tire transient dynamic property, some severe conditions could not be conducted because of the limitations of laboratory facilities, particularly for large obstacles and road unevenness. In addition, tire transient dynamic analysis using experimental methods is an expensive work for engineers, as different types of tires and different kinds of road obstacles need to be adopted in the tests.

2.6 Development and application of FTire model

2.6.1 FTire model development

FTire is a mechanically based tire model, suitable for application in general vehicle dynamic analysis. The development of FTire began in 1998 [80], and the first version of it was released by Michael Gipser in December 1998. It has become the major tire model being used in the automotive industry for CAE durability and ride comfort investigations, and prediction of road load [1] .

There were two other tire models influencing the development of FTire, one is DNS-Tire (Dynamical Non-Linear Tire Model), the other is BRIT (Brush and Ring Tire Model). DNS-Tire is a coarse non-linear time-domain FE model, which has been under development since 1986, and is still being used today for certain tire development studies. Despite all this, DNS-Tire required too much computing time to be used as standard tire model in full vehicle simulations. In order to resolve the limitation of DNS-Tire in terms of computation time requirement, BRIT was developed using a simple rigid-body approach since 1990. In the BRIT model, the belt structure was given six degrees of freedom of motion relative to the rim. The distribution of normal load on the contact patch of the BRIT model is derived from experimental test data and finite element tire models. However, the initial version of BRIT was not valid for road unevenness with short wavelength such that the validity range was restricted for tire transient dynamic investigation. With the improvement of BRIT in 1997, the model is now valid for road unevenness with wavelength up to the length of the contact patch[81]. After the modification of BRIT, the main drawback of this model is concentrated on the limited capability to predict contact forces and deformation for all kinds of rough road unevenness [82]. A new tire model named CTire (Comfort Tire Model) was developed for accurately predicting in-plane dynamic forces and moments of tires when traversing extremely rough road surfaces [1]. The CTire, however, cannot be used for vehicle handling

and ride comfort analysis without empirical models like Magic Formula tire model. Due to the insufficient versatility of CTire model for prediction of lateral force and aligning moment, new degrees of freedom of belt elements were applied to CTire, and in the new tire model with new degrees of freedom, torsional displacement of the belts about the circumferential axis can be described. This important improvement resulted in the generation of FTire.

Generally, FTire features a flexible belt provided with friction elements. The tire belt is represented by a slim ring, which could be displaced and bent in arbitrary direction relative to the rim (Figure 2.7).

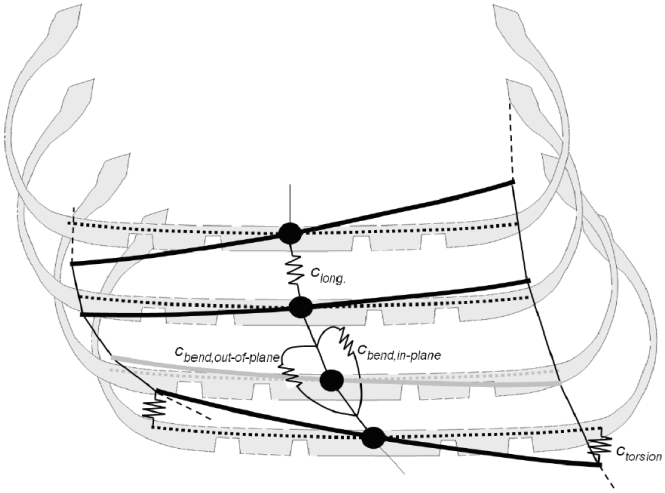

Figure 2.7 Some force elements between adjacent belt elements and the rim

Most of the Mechanical tire models are composed of two separate parts, the structural model and the tread/road contact model. In terms of FTire, the structural model is used to describe the structural damping, stiffness and inertia characteristics of the tire, while the tire/road contact model is used to determine the normal contact pressure and friction distribution on the contact patch. The structural model of FTire is composed of 80-200 lumped-mass nodes, which are connected to each other and also connected to the rim by some damping, stiffness and friction elements. These nodes are subject to the forces of the tread model and inflation pressures. The belt segment is such a tire structure which is associated with one belt node, and has five degrees of freedom (Figure 2.8). The nonlinear force elements in the radial,

transverse and circumferential directions are applied to describe the connection between the rim and the belt nodes, and the force element in the radial direction of one single belt node is illustrated in Figure 2.9, where the force element is composed of dampers, springs and spring-friction series connections. In order to establish tread/road contact, a certain number of contact and friction elements without mass are placed between two adjacent belt segments. The number of contact and friction elements can be specified by the user according to the construction of road unevenness. Figure 2.10 describes the contact forces distribution during a parking manoeuvre of the tread/road contact model. References [83] and [84] give the detailed description of the structure model and tread/road contact model.

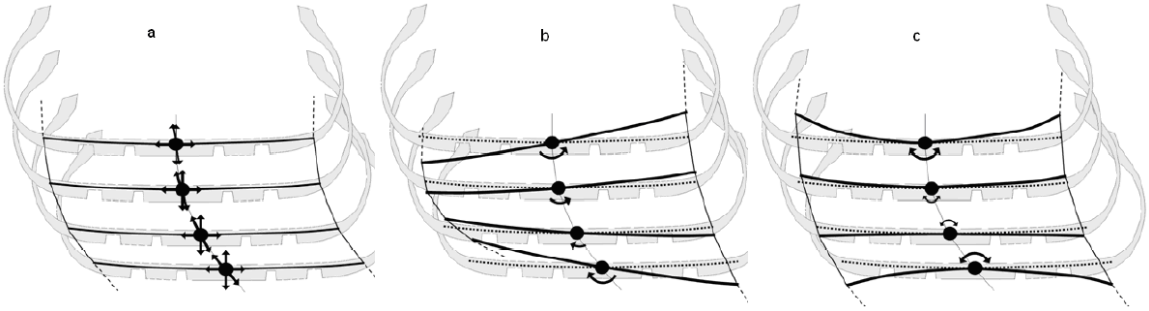

Figure 2.8 DOF of the belt segment: (a) translation; (b) torsion; (c) lateral bending [83]

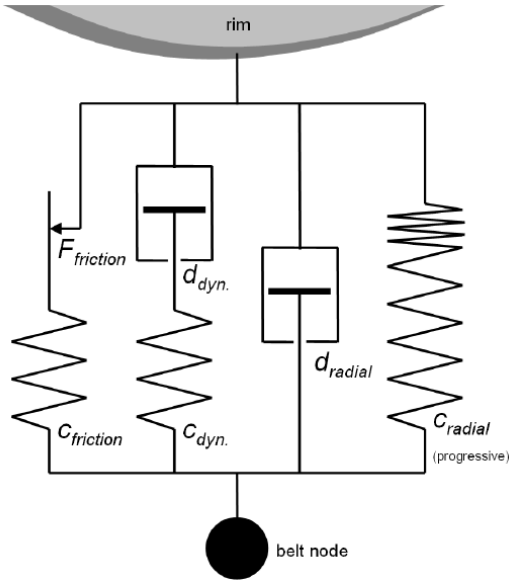

Figure 2.9 Force elements between single belt node and the rim in radial direction [84]

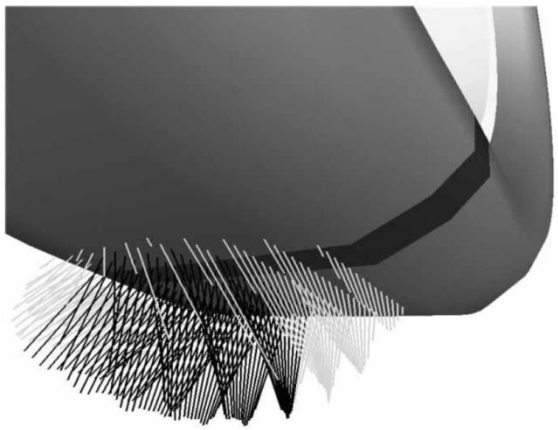

Figure 2.10 Contact force distributions at a parking condition [83]

FTire has many benefits such as: ease of implementation with multiple instances, fully nonlinear, valid for obstacle wavelengths in rolling direction up to half the length of the foot print, and good accuracy when passing single obstacles like cleats and potholes. Compared with simple empirical handling models which describe steady-state measurements using mathematical formulas, FTire could calculate the forces even on shortwave road unevenness or in highly unstable situation.

2.6.2 Application of FTire

Nowadays, FTire is widely used by engineers in the vehicle and tire industries worldwide, and the application of FTire includes the following studies: generation of load histories for durability simulations, handling and traction on extremely uneven roads, rolling resistance calculation for different road surfaces, and ride comfort analysis. Riepl et al.[85] applied FTire model for the automotive development at MAGNA STEYR Fahrzeugtechnik in the multi-body application tasks such as suspension analysis, vehicle handling, and ride comfort simulation. The inner-drum test rig was used to record test data, which was applied on FTire/tool to generate the FTire model. With the tire model FTire, full-vehicle simulations and equivalent measurements on the rough road and Belgian block were carried out. The objective of these tests was to determine the accuracy of using FTire under different road excitation conditions. The calculation of vehicle dynamic manoeuvres with FTire gave good

quality results for both the rough road section and Belgian block section. Also, Riepl and his colleague [86] carried out a virtual rough road ride simulation with tire model FTire and RMOD-K, in which the tire models are compared for six measurement rides performed with one and the same vehicle on the MAGNA STEYR Fahrzeugtechnic test track [85]. In terms of calculation time efficiency, FTire performance was considerably better than RMOD-K.

Haga [87] made an evaluation of tire models for durability loads prediction using a suspension on a drum environment. In the evaluation, FTire was one of the two tire models used for vehicle dynamics simulation. The spring rate, damping factor, inertia moment together with the mass of components in the "suspension on a drum" system were specified in the simulations. The vertical and longitudinal responses in the time domain were obtained using multibody simulations (MBSs) with FTire and LMS CDtire. With the application of tire models, Haga concluded that MBSs using the tire model FTire is suitable for real world applications for durability performance. However, the input parameters of FTire model are not shown in Haga's study. Dorfi [88, 89] attempted to analyse cleat impact and force transmission properties using FTire, the input parameters of which were obtained with simple vibration testing of a P235/75R17 tire on a fixed hub, unloaded and inflated. Three different belt angles and two different bead filler heights of tire were used in their study to build different constructions. From the results of parametric studies, Dorfi found that the inflation pressure affects both force magnitude and resonant frequencies of spindle responses, and the FTire is capable of accurately predicting in-plane spindle forces in the case of the resonant frequencies up to 100Hz.

2.6.3 Characterisation of FTire model

FTire model development is based on the input parameters (such as inflation pressure properties, static stiffness, footprints, cornering stiffness, transient dynamic properties etc.). Normally, the input parameters were determined by measurements. According to FTire,

parameters such as tire geometry properties, tire static stiffness, contact footprints, tire rolling steady-state properties, and tire transient responses for tire rolling over cleats are used to characterize the tire properties. Some simple stiffness and tire steady-state properties are relatively easily measured in the laboratory. However, some tire properties cannot be carried out because of the laboratory limitations, particularly for tire traversing large obstacles, high bumps or uneven road. Without the input data under severe conditions for characterising tire properties, the derived FTire model may not be suitable to be used in quarter-vehicle or full-vehicle models. Thus, the transient dynamic properties may not be accurately predicted. However, some input parameters like camber stiffness and transient dynamic responses under severe conditions can be obtained by numerical simulations.

The following input data need to be prepared for FTire model characterisation:

- Tire static properties (tire cross-section, tire size, tire static stiffness, tire footprints)
- Tire steady-state properties (tire cornering properties)
- Tire in-plane responses for tire impacting cleats
- Tire out-of-plane responses for tire impacting cleats

2.7 Tire geometrical and material properties modelling

As pneumatic tires have composite structure with complex reinforcement layups and hyperelastic rubber material, tire researchers have attempted to develop efficient methods to define the geometry and material properties. Kenny et al. [90] used a powerful tool named Cured Tire Layout (CTL) to provide the geometry input of the tire for the pre-processing phase of finite element analysis. The overall diameter, tread width, inflated crown radius, and section width were defined using CTL. Boundary conditions were defined by controlling the nodes of the tire model. Inflated and deflected tire shapes were then predicted by finite element simulation. Similarly, Konde et al. [91] used finite element approach to model the

interaction between aircraft tire and the rigid ground surface. Tire structure was obtained by cutting the tire cross-section using a water-jet, in which method the geometry of the tire can be obtained more accurately. In order to define the hyperelastic properties of rubber components, uniaxial tension tests were carried out to acquire the stress-strain curves. With static analysis of the tire model, the effects of carcass orientation, material property, belt orientation and rebar spacing on tire stiffness were studied.

With the increasing requirements for great accuracy and improvements of modelling capabilities, material properties have become more important in tire modelling, such as rolling losses analysis in tire, tire vibration analysis, and tire enveloping analysis. However, it is still a challenge to characterize the material properties in FE modelling of tires.

Many researchers have attempted to develop accurate models to define the hyperelastic property of rubber material. Also, different experimental methods have been designed for hyperelastic characterization. Mooney [92] made the first important attempt at the mathematical theory of large elastic deformations of rubber materials. The strain energy function was derived by Mooney, and it is given by

$$U = C_1(\lambda_1^2 + \lambda_2^2 + \lambda_3^2 - 3) + C_2(\lambda_1^{-2} + \lambda_2^{-2} + \lambda_3^{-2} - 3) \tag{3.1}$$

Where C_1 and C_2 are temperature-dependent material paremeters, and λ_1, λ_2 and λ_3 are the principal stretch ratios. Rivlin [93] assumed the rubber material is homogeneous, isotropic and incompressible, and the strain energy function was derived and expressed as

$$U = \sum_{i+j=1}^{\infty} C_{ij}(I_1 - 3)^i (I_2 - 3)^j \tag{3.2}$$

in which C_{ij} are material parameters, I_1 and I_2 represent the first and second strain invariants of the Green's deformation tensor. If only two terms of the power series are taken, the strain energy function is reduced to

$$U = C_{10}(I_1 - 3) + C_{01}(I_2 - 3) \tag{3.3}$$

which is known as the Mooney-Rivlin equation. Following this, Yeoh et al. [94, 95] derived the Rivlin's strain energy function by omitting the dependence on the second invariant as I_2 has much less influence on the changes of strain energy function than the first invariant I_1. The reduced function is given by

$$U = \sum_{i=1}^{3} C_{ij}(I_1 - 3)^i \tag{3.4}$$

In 1997, the Ogden strain energy form was developed by Ogden [96], and the strain energy function can be expressed by

$$U \overset{def}{=} \sum_{i=1}^{N} \frac{2\mu_i}{\alpha_i^2}(\lambda_1^{-\alpha_i} + \lambda_2^{-\alpha_i} + \lambda_3^{-\alpha_i} - 3) \tag{3.5}$$

However, the nonlinear regression method for derivation of the Ogden strain-energy function, which is based on stress-strain data from one mode of deformation tests, is not able to predict behaviour in other deformation modes, and the reason has been explained by Yeoh [97]. Also, some other constitutive material models (such as Neo Hookean, Arruda-Boyce, Van der Waals models) can also be used to fit the test data and define the hyperelastic property of rubber or rubberlike materials.

Different experimental and data-fitting methods have been designed for fitting these constitutive hyperelastic models. Ogden et al. [98] used simple tension, equibiaxial tension

and general biaxial tension tests to obtain experimental data, which was used for determining material parameters in incompressible isotropic hyperelastic models. The non-linear least squares optimization method was also applied to fit experimental data. However, based on the investigation of modelling hyperelastic property of rubber by Beda [99], it is shown that the identification methods like the usual least squares may not be suitable for the hyperelastic modelling in some cases.

In the experimental test methods presented by Kim and his colleagues [100], they found it is more appropriate to carry out the simple tension test using a narrow strip specimen (the length is 10 times longer than the width) rather than using a dumbbell type specimen. In order to eliminate the influence of friction, they used a tapered platen to carry out the compression test. Also, they found that the mechanical preconditioning has great influence on the prediction of material behaviour. Castellucci et al. [101] attempted to use different test specimens for characterization of dynamic properties of rubber material, and they concluded that the simple rectangular shear specimen can be considered as the most appropriate geometry to characterize the dynamic properties of rubber. Kupchella et al. [102] tried different test methods (biaxial, planar, uniaxial stress test) to identify accurate methods to define hyperelastic property of tire rubber. Two and three dimension digital image correlation systems were utilized to measure strains of rubber samples. They found that hyperelastic characterization can be improved by combination of uniaxial, biaxial and planar test data, rather than uniaxial test mode itself, although the uniaxial test is considered as the simplest test mode for material testing. In practice, however, based on the biaxial stress testing approaches reported in the literature [103-105], the biaxial tensile test mode has challenges to be implemented or to determine the biaxial stress magnitudes accurately.

Recently, Yang et al. [42] used simple uniaxial tension test to obtain minimum data to determine the parameters of hyperelastic models. The Yeoh strain energy function was

chosen to model the hyperelastic material property with combination of uniaxial tension test data. Because of the limitation of laboratory conditions and lack of material samples from tire manufacturers, a strip specimen extracted from tire product was used to replace the dumbbell sample for tensile tests. Martins et al. [106] used a computational/experimental scheme for the investigation of nonlinear mechanical behaviour of rubber-like materials. Inverse methods were applied to determine the material constants for seven different hyperelastic constitutive models. The silicone-rubber and soft tissues were taken for verifying the correlation between test data and theoretical data. Guo et al. [107] developed a detailed aircraft FE tire model to investigate safety criteria of the tire. Rubber components in the tire were considered as hyperelastic material in FE analysis, and the energy function of Yeoh model was chosen to represent the mechanical properties. Tire safety assessment was carried out by analysing the relationship between tire loads and landing speeds of the airplane. The most satisfactory results were obtained from Yeoh, Ogden and Martins [108] models, and Neo-Hookean model could not capture the nonlinearity of mechanical properties of the two types of samples.

In terms of viscoelastic property of rubber material, Gracia et al. [109] applied the overlay model [110] for prediction of hysteretic property of industrial rubber components. Two different industrial filled rubber components (cube and disc) were used for shear test and uniaxial test to obtain the hysteretic responses. They found that a greater amount of energy was dissipated from the overlay model fitted from uniaxial test data than the model fitted from shear data. In order to eliminate the frictional contribution on the hysteresis behaviour, calibration of material parameters of overlay model was based on the quasi-static stress-strain data. Ghoreishy et al. [111] employed the Marlow and Yeoh hyperelastic models into Prony series model to develop the linear hyperviscoelastic model. Because of the nonlinearity in rubber material behaviour at higher deformation, they developed a nonlinear

hyperviscoelastic model by taking the nonlinear viscoelastic model proposed by nonlinear Bergstrom-Boyce model [112-115] into account.

2.8 Summary and Conclusions

In the present chapter, the literature review regarding the tire models and experimental test methods has been presented. In addition, the development history and characteristics of FTire as well as the application of FTire has been given.

Analytical tire models, empirical and semi-empirical tire models can be easily applied because of their high computing efficiency and simplified tire structures on which they are based. However, they are not able to accurately predict enveloping properties and transient dynamic properties of tires. Besides, as one of the important parameters, tire deformation is often ignored because of the simple structures of this kind of models. As empirical and semi-empirical models are dependent on the experimental data, and the laboratory limitations reduce the application scope of the models significantly, it is very difficult to accurately predict the enveloping and transient dynamic properties for tire impacting large or high obstacles. However, due to the advance of numerical simulation, tire behaviour simulation by applying FEA method can cover all the scenarios, which experimental tests or empirical models cannot carry out.

As a reduced finite element tire model, FTire is capable of predicting tire in-plane and out-of-plane properties. Based on the literature surveys of the application of FTire, it has been shown that this model can predict accurate in-plane spindle forces in the case of the resonant frequencies up to 100Hz. However, because most of the parameters of FTire are derived from

experimental tests, the tire model is not able to accurately predict some transient dynamic properties under severe conditions, particularly for tire rolling over large obstacles. This may make FTire users lose confidence in quarter vehicle and full vehicle dynamic analyses under severe conditions, such as traversing large obstacles and high bumps.

Because of the high accuracy capability for predicting tire static and dynamic properties, the finite element method has been widely used and from the literature surveys of finite element tire models for tire dynamic properties when impacting obstacles, it has been shown that satisfactory validation was obtained between predictions of tire responses and measurements. Therefore, transient dynamic properties for tire impacting larger obstacles can be predicted using the validated FE tire model. In addition, the increasing growth of computer performance and the advances in tire modelling techniques considerably reduce the computational cost of transient dynamic analysis. This opens up the possibility that FTire parameters in severe conditions can be derived using FE simulation. As Abaqus/Standard employs solution technology ideal for static and low-speed dynamic events, tire static properties and steady state simulations were conducted using Abaqus/standard. In terms of the transient dynamic analysis for the tire impacting large road obstacles, Abaqus/explicit was applied as it has a robust contact functionality that readily solves complex contact simulations. In addition, the implicit finite element method may encounter numerical difficulties when solve complex nonlinear problems as the interative approach applied in implicit program may be troublesome to achieve convergence for solving tire/obstacle impacting behaviour. What's more, for the same simulation, Abaqus/Explicit can save much less disk space and memory comparing with Abaqus/standard. Therefore, the transient dynamic analysis for tire rolling over obstacles was carried out using Abaqus/Explicit.

Chapter 3 DEFINITION OF MATERIAL AND GEOMETRY PROPERTIES

3.1 Introduction

This chapter presents a detailed definition method of geometry and material properties which are important for the development of 2D tire model in the subsequent chapter. Section 3.2 gives a literature survey of material and geometry properties modelling methods. Section 3.3 gives a detailed review of image processing method of tire cross-section and layup structures including cords spacing, cords positional orientation and cords cross-section area. This tire cross-section geometry and cords distributions are needed for describing the physical lay-up of tires and also, parametric studies for tire dynamic responses can be carried out by modification of the structures.

Section 3.4 reviews methods to define hyperelastic property and viscoelatic property of rubber components. Different hyperelastic material models are used to fit the experimental stress-strain data.

3.2 Determination of geometrical properties of the tire

3.2.1 Image processing of tire cross-section

Before image processing is carried out, one of the important and imperative processes for 2D tire modelling is image acquisition, in which a technical camera was applied in order to capture the image of the cross section. The cords in the tire photograph need to be as clearly defined as possible, in order that they could be properly recognised by digitizer software. Before taking a photograph of the tire cross section, some parts of the boundary were

constrained to meet the requirements of the dimensions of a rimmed tire in the 0 kPa pressure condition. In addition, some important distances were measured along with the image capture (Figure 3.1).

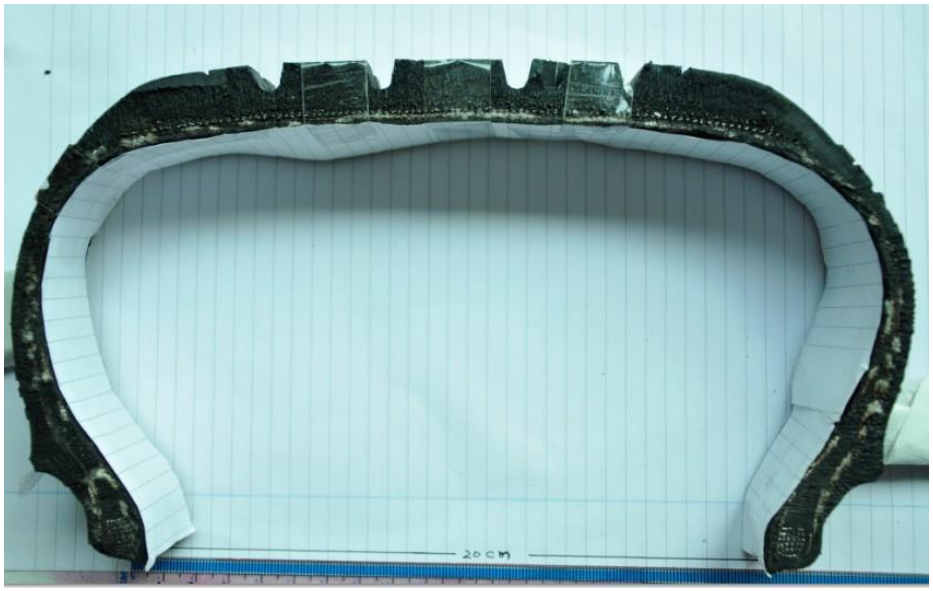

Figure 3.1 Photograph of the Tire Cross-section

In order to obtain a reasonable and effective image of tire cross-section for tire modelling in Finite Element software, it is necessary to carry out the image processing. It is pertinent to mention that the tire cross-section specimen was obtained from cutting of a whole 235/65 R18 tire. The whole procedure of image processing from boundary processing to modification of the image in ABAQUS™ is illustrated in Figure 3.2. Generally, the process could be divided into two parts, one is digitization of the image, which is presented in the second row, and the other part is graphic design from the digitized image, which could be seen in the third row. Although the diagram could reflect some information of image processing of the tire cross-section, comprehensive description of the process is also illustrated in the following introduction.

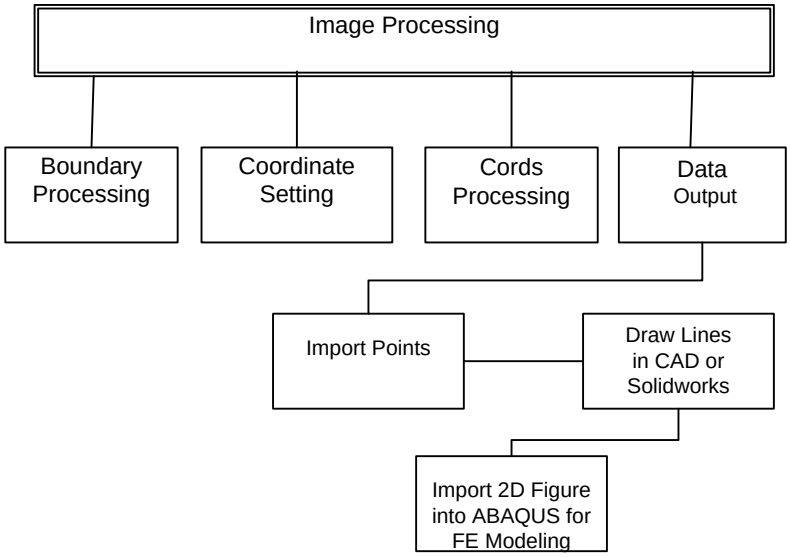

Figure 3.2 Whole Procedure of Image Processing

A further procedure after image capture is boundary processing, in which the photograph was imported into the Photoshop software to delete the image excluding the tire cross-section (Figure 3.3). After removing the unnecessary parts of the photograph, it is necessary to mark the important points and distances described in the process of image capture, which would be useful in determining the coordinates and the veritable dimension of the cross-section.

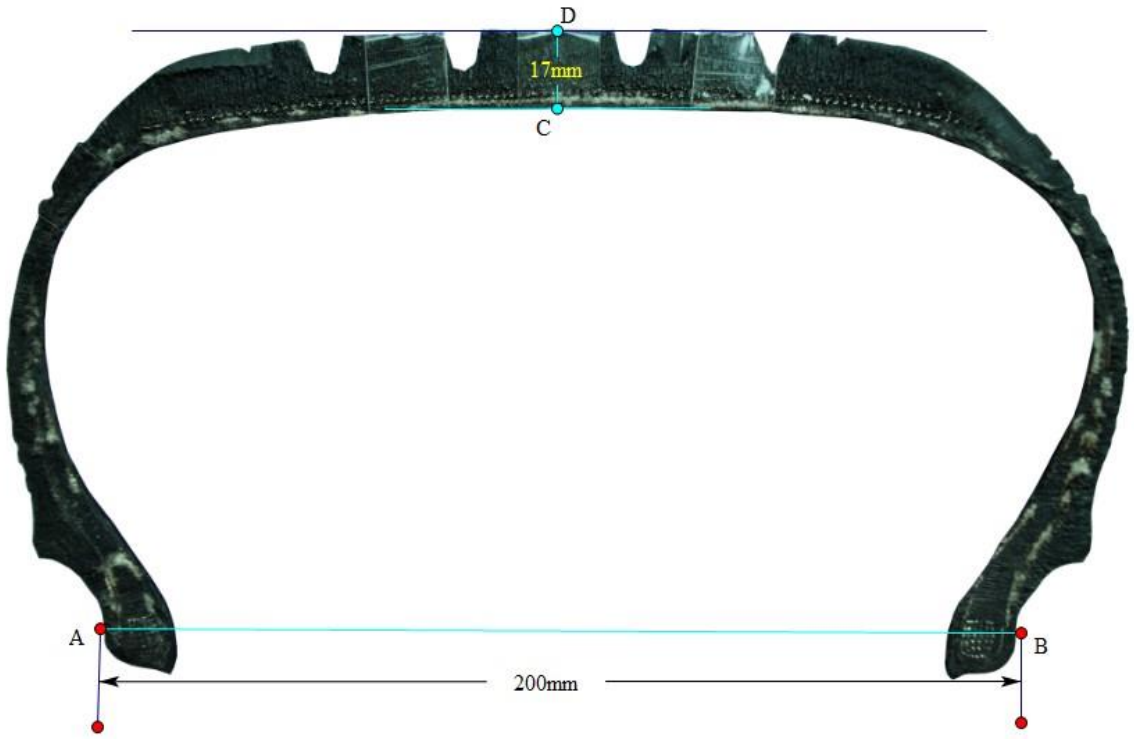

Figure 3.3 Cross-section after Photoshop processing

The image was clearly defined to facilitate digitization when the boundary processing is completed. By using the GetData Graph Digitizer (a software can transfer the image to data), it is possible to get the data of the tire cross-section, including the boundary, the cap ply, the steel belt, the carcass, the bead and the bead reinforcement (Figure 3.4). Subsequently, the whole structure of the cross-section could be described. In the process of cross-section digitization, the principal procedure is coordinates setting, in which the marked points and distances are used. By using the length of line AB and points A and B, the X axis the location of A and B in X axis, associated with the distance of A and B in the digitizer could be defined, while Y axis and the location of C and D could be determined using the same method, and then the scale of the tire cross-section is established by the method of comparing the dimensions with the real tire cross-section at their width and height.

Furthermore, cords processing is needed to be carried out to acquire their coordinates data, from tire boundary to the inner cords, from cap ply to carcass. From the Figure 3.4, it could be seen that all the cords, boundary and bead included, are described by lines and several arrays of colorized points, which are applied to define their real locations. However, as these points are manipulated manually, it is necessary to quite carefully depict the points in accordance with the real tire cross-section that was acquired by tire cutting. From this method of points' acquisition, their coordinates are recorded simultaneously, which can be seen in Figure 3.4. The coordinates' data of these points are then exported from the digitizer for further processing. It is noted that the points seem to be not very accurate compared with the actual cross-section. However, it can be corrected when imported to ABAQUS™ for Finite Element modelling in further steps.

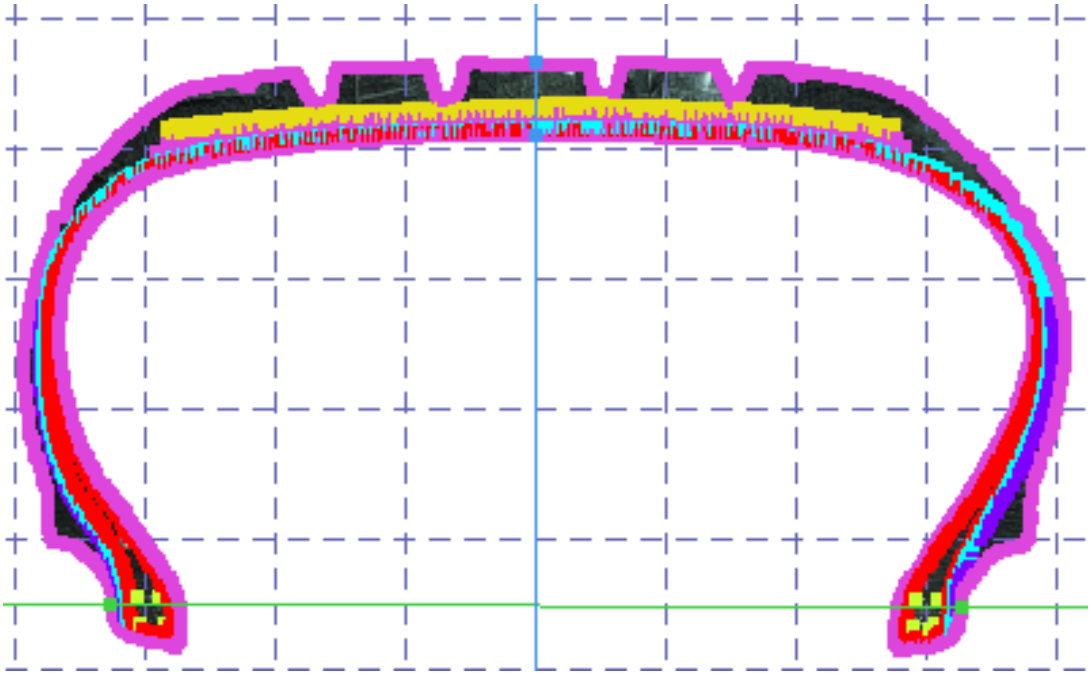

Figure 3.4 Tire Cross-section from digitization

When the geometry coordinates of the tire cross-section has been obtained, it is appropriate to import them into CAD software, such as Solidworks or AutoCAD, for further processing. In this study, these points were imported into Solidworks via a notepad file, in which they would be drawn by a method of spline interpolation, as this could be more accurate to satisfy the FE modelling requirements and also could modify some unreasonable points to some degree.

Figure 3.5shows the tire cross-section generated by these points in Solidworks. With the application of spline interpolation, the cords and the boundary curve seem to be smooth, which could reflect the accurate property of the real tire cross-section. However, as some irregular curved sections exist in the graph, the new cross section was imported into ABAQUS™ for further processing, including deleteting some small grooves, and smoothing some rough reinforcements (Figure 3.6). Geometrical optimization in FE software is not only capable of improving the cross-section image, but also favourable for meshing of tire components. It is worth noting that the rubber components and reinforcement components are coupled by the interaction constraint supported by ABAQUS™.

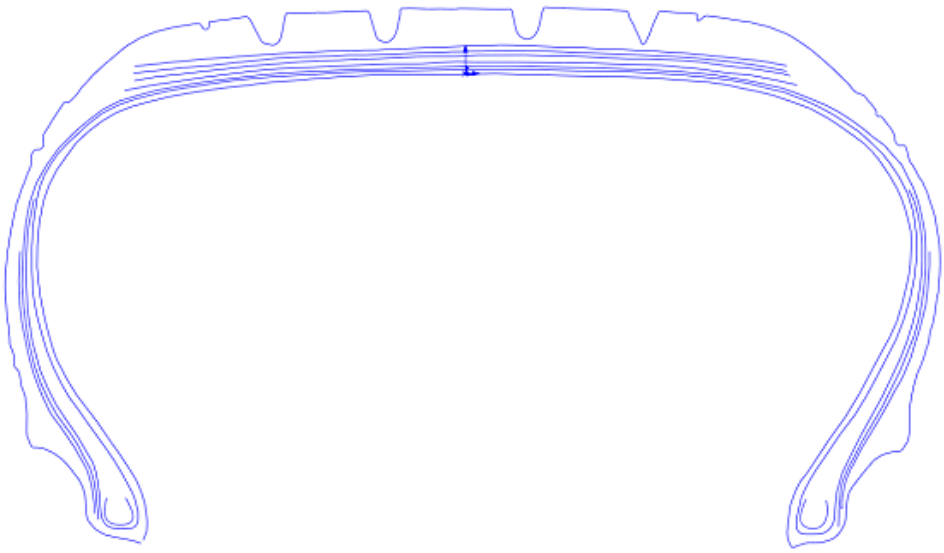

Figure 3.5 Solidworks geometry cross-section generated by the points

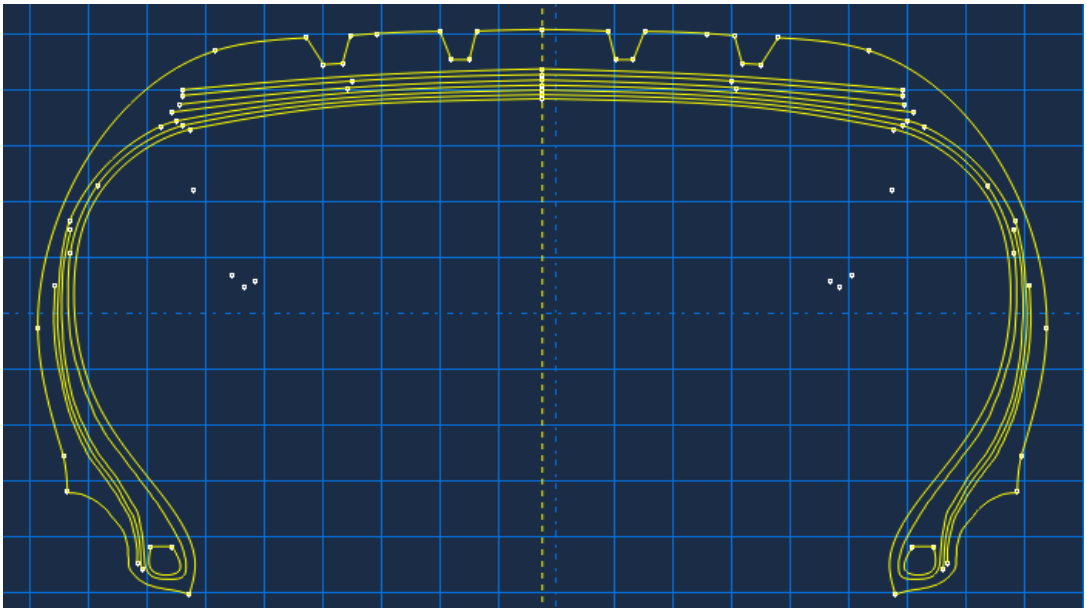

Figure 3.6 modified geometry of tire cross-section

3.2.2 Layup Structures of Reinforcements

As is well known, the tire contains different reinforcements, and the reinforcements are embedded in rubber component in terms of layers. Different reinforcement components are positioned in rubber material with different characteristics. Rebar elements in ABAQUS are able to define the structures for different layers in membrane and surface elements. Rebar

spacing, rebar cross-section area, rebar orientation angle are all necessary parameters for definition of the structure of reinforcements. A representation of distribution of reinforcement components is shown in Figure 3.7, in which the orientation angles are given.

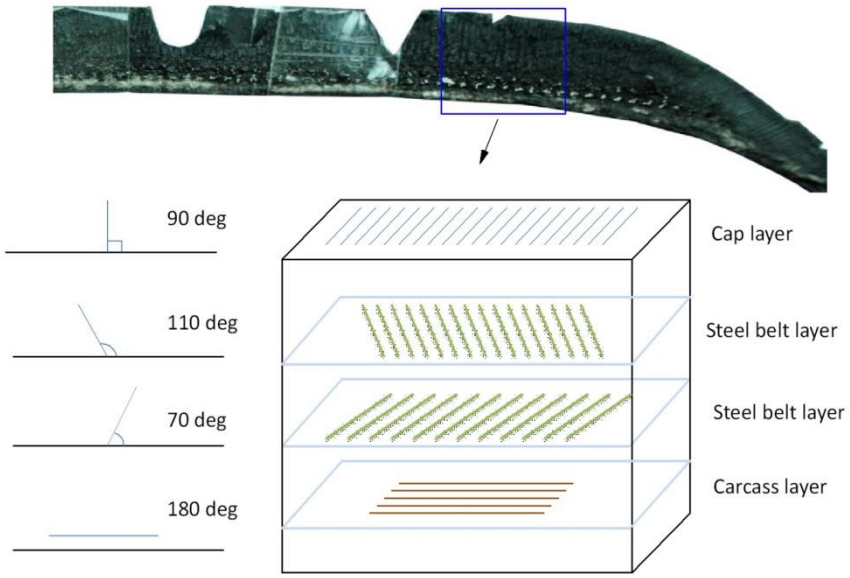

Figure 3.7 Layup structures and reinforcements distribution

The area of rebar cross-section can be obtained by measurement of the diameter of the reinforcement using micrometer Figure 3.8. The space between the centre of two neigboughing cords and orientation angles can be easily obtained using image processing techniques.

Figure 3.8 Area measurement for cross section of steel belt

Measurements for the structure characteristics for different reinforcements were carried out and the test data are shown in Table 3.1.

Table 3.1 Reinforcement structure detail

Component	Area per Bar (mm^2)	Spacing(mm)	Orientation Angle (^{o})
Cap ply	0.1521	0.5128	90.0
Steel belt 1	0.3424	1.2983	110.0
Steel belt 2	0.3424	1.2983	70.0
Carcass	0.2917	0.5928	0.0
Reinforced strip	0.1898	0.8055	80

3.3 Material Properties of Rubber and Reinforcement Components

3.3.1 Hyperelastic Property Test of Rubber

In this study, material properties of rubber components and reinforcements of the tire are defined by experimental tests and computational processing. Therefore, the specimens of rubber components and reinforcements of the tire need to be extracted from the tire product. Rubber components of a tire in finite element analysis are represented using the hyperelastic

model and viscoelastic model to describe the properties of rubber material, and the properties of reinforcements are represented by parallel layers of unidirectional rebar with isotropic material properties. The hyperelastic property provides the nonlinear and incompressible property of rubber material. In this study, the Yeoh model [97] is applied to define the hyperelastic property of rubber components. The reason for using Yeoh model in the tire rubber material model is described in detail in the following paragraph.

With review of a number of elasticity models of rubber material, which are used to describe the hyperelastic property, it is found that most of these models are determined based on the polynomial expression of strain energy function. Among these material hyperelastic property models, Mooney-Rivlin energy density function has been widely applied for tire dynamic properties analysis in the finite element simulation [59, 72]. However, the Mooney-Rivlin function has a limitation that it could not be accurately applied to large deformation problems of the rubber material [116]. In order to determine the parameters of rubber hyperelastic property, most of the material models need to combine three deformation tests (uniaxial, biaxial tension and pure shear), which is recognized as a complex and time consuming procedure. Although Neo Hookean material model is supported in ABAQUS, it also has a limitation that the coefficients derived from uniaxial deformation tests are not suitable to describe other deformation modes. Ogden strain energy function derived from stress-strain data obtained from one deformation mode is also unsatisfactory for predicting rubber behaviour in other modes [97]. The Yeoh hyperelastic material model is not only suggested and supported in ABAQUS, but also capable of predicting different deformation modes using data from a simple deformation mode like uniaxial tension test.

Rubber material of the tire is composed of different components, which have different material properties. Figure 3.9 **(a) rubber components of the 2D tire model (b) reinforcement**

components of the 2D tire model shows rubber materials and reinforcement materials of half cross section of the tire. By cutting a tire product, rubber samples were extracted from the tread, the sidewall, and the apex sections separately. Normally, the tensile testing sample should be better extracted as a dumbbell or ring shaped specimen. However, because of the requirement of narrow strip and the limitations of support from tire manufacturers, it is not realistic to acquire either a dumbbell or a ring specimen. In this study, however, some straight specimens for rubber testing were prepared, and those specimens can satisfy the requirements in ASTM-D412 [117]. In this case, the length of the sample needs to be more than 10 times longer than its width and thickness, and it can produce the same reliable testing data as the other two shaped samples in hyperelastic property test of rubber.

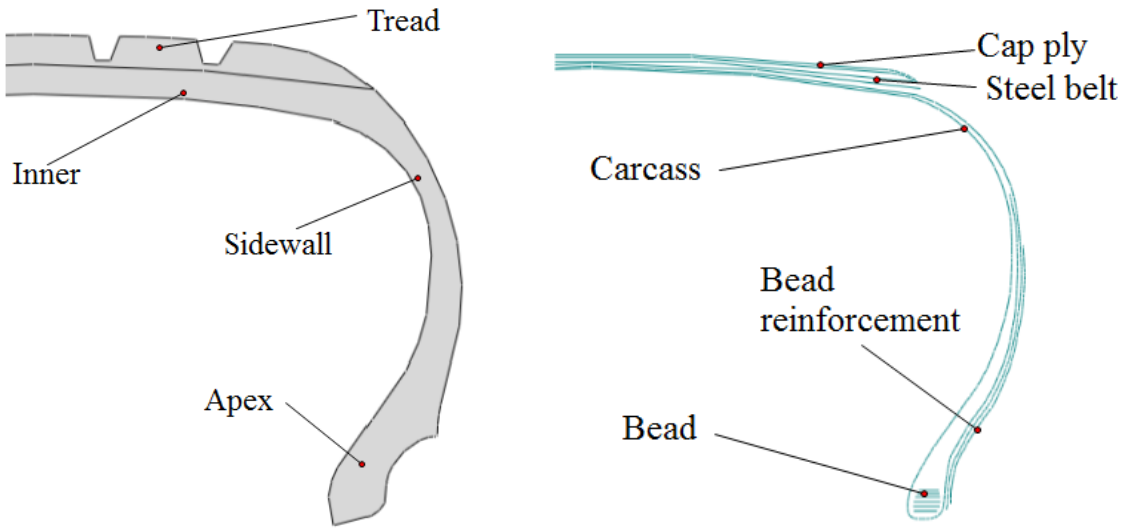

(a) (b)

Figure 3.9 (a) rubber components of the 2D tire model (b) reinforcement components of the 2D tire model

The testing method applied in the rubber test was uniaxial extension method. In addition, the tension test rig used for rubber testing is a power driven machine illustrated in Figure 3.10, and the temperature for the test was set about 23 ℃ according to the standard in ASTM-D412 [117].

Figure 3.10 power driven test machine-INSTRON

In the uniaxial test, the specimens from different components of the radial tire were pre-stretched separately at the velocity of 50mm/ min up to 100% strain for about 10 cycles before the nominal test was carried out. As different components have different property and strength, some special samples like apex rubber could be allowed to be stretched up to 50%-60% strain. In the procedure of pre-conditioning, five minutes relaxation time in the interval between two cycles is needed to eliminate the influence of stress softening [116]. After the completion of the pre-conditioning of rubber test, the specimens were removed from grips of the machine and allowed to have half an hour relaxation time.

Following test was the standard test after relaxation of the samples. During the standard testing, all the samples were stretched at least three times to get an effective test data. Similarly, five minutes relaxation time was given between each loading and unloading of the specimen as well.

After completion of the tension test, the data acquired in the test was normalized by converting the extension force F_h to stress σ_h and converting the elongation ΔL_h to strain ε_h. The transforming formula is illustrated in Eq.3.6 and Eq.3.7.

$$\sigma_h = \frac{F_h}{A_h} \tag{3.6}$$

$$\varepsilon_h = \frac{\Delta L_h}{L_h} \tag{3.7}$$

Where A_h is area of the specimen, L_h is the original length of the specimen.

By using hyperelastic property models in ABAQUS to fit the test data of different rubber components, the fitting functions were acquired and shown in Figure 3.11. In order to examine the fitting properties of different hyperelastic material models, Mooney-Rivlin model, Neo Hookean model and Yeoh model were used in the process of function evolution. It is not difficult to recognize that Yeoh hyperelastic property model provided the most effective fitting in all the three components. By the consideration of the material model accuracy and test rig simplicity and time, the Yeoh model has been chosen to define the hyperelastic property of the rubber in tire models. The strain energy function is presented in terms of Eq. 3.8.

$$\begin{aligned} U = {} & C_{10}(I_1 - 3) + C_{20}(I_1 - 3)^2 + C_{30}(I_1 - 3)^3 + \\ & \frac{1}{D_1}(J^{el} - 3)^2 + \frac{1}{D_2}(J^{el} - 3)^4 + \frac{1}{D_3}(J^{el} - 3)^6 \end{aligned} \tag{3.8}$$

where U represents the strain energy density; C_{i0} (i=1, 2, 3) and D_i (i=1, 2, 3) are material constants to be determined by testing and test data fitting in ABAQUS, which describe the shear behaviour and material compressibility separately; J^{el} is the elastic volume ratio, while I_1 is the first deviatoric strain invariant.

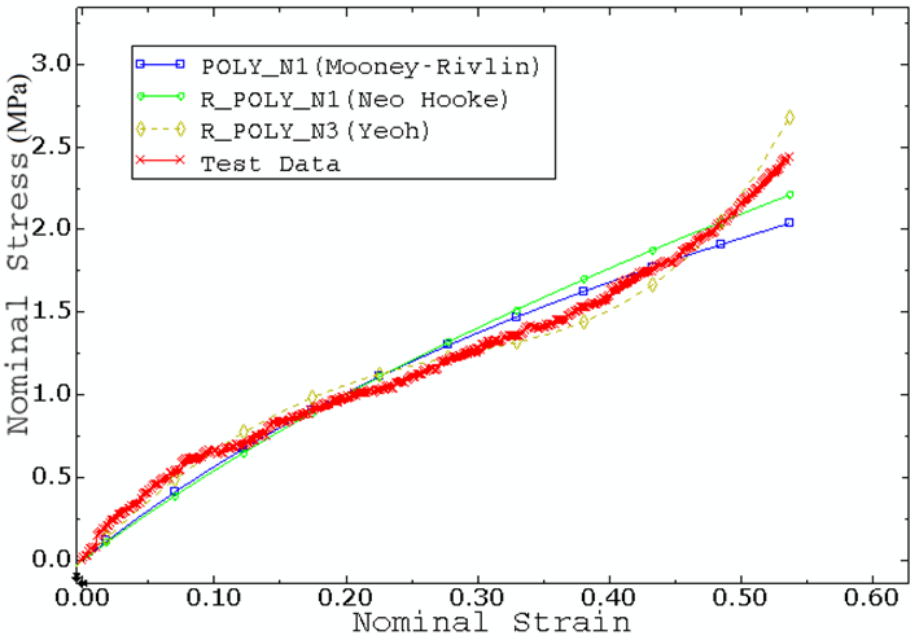
POLY_N1(Mooney-Rivlin)
R_POLY_N1(Neo Hooke)
R_POLY_N3(Yeoh)
Test Data
Nominal Stress (MPa)
Nominal Strain
0.0
0.5
1.0
1.5
2.0
2.5
3.0
0.00
0.10
0.20
0.30
0.40
0.50
0.60

(a)

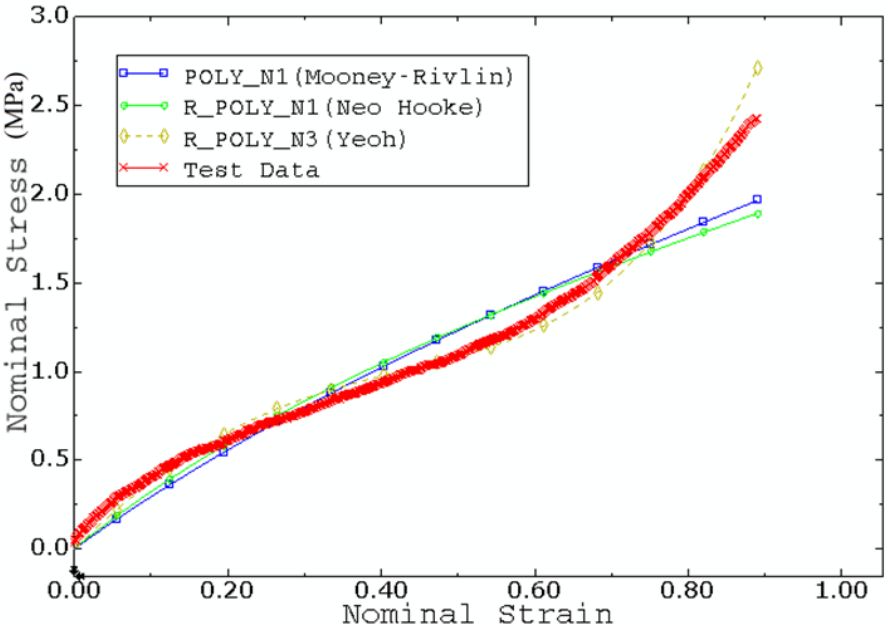
POLY_N1(Mooney-Rivlin)
R_POLY_N1(Neo Hooke)
R_POLY_N3(Yeoh)
Test Data
Nominal Stress (MPa)
Nominal Strain
0.0
0.5
1.0
1.5
2.0
2.5
3.0
0.00
0.20
0.40
0.60
0.80
1.00

(b)

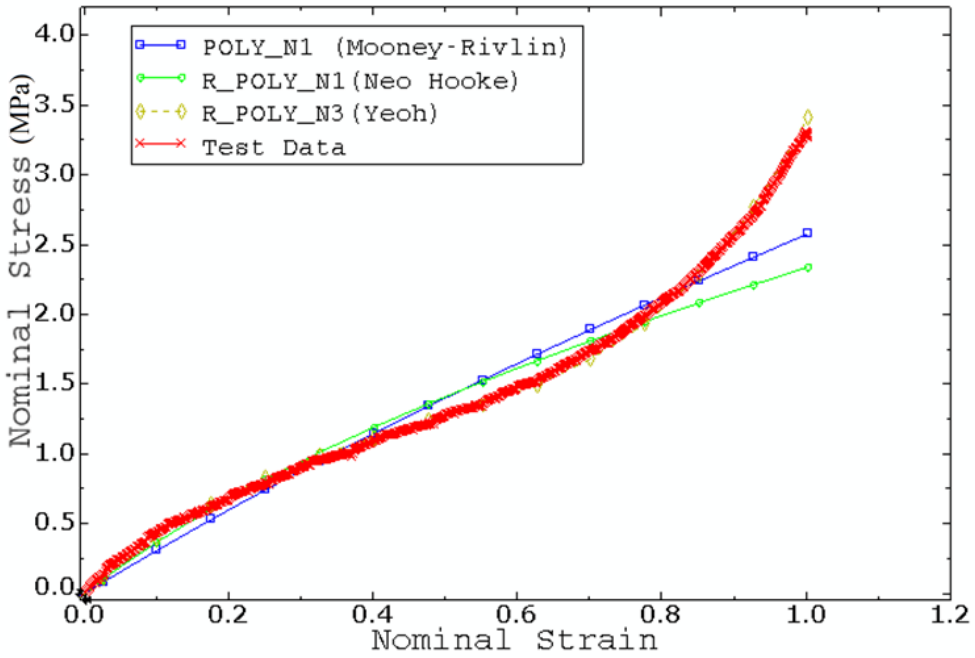

(c)

Figure 3.11 (a) Hyperelastic Property Fitting for Apex (b) Hyperelastic Property Fitting for Sidewall (c) Hyperelastic Property Fitting for Tread

Based on the hyperelastic property fitting between test data and Yeoh model, the constants of Yeoh model for the three components of tire product were obtained, which could be seen in Table 3.2.

Table 3.2 Hyperelastic property constants for rubber materials

Rubber Material	Yeoh strain energy potentials constants					
Component	C_{10}	C_{20}	C_{30}	D_1	D_2	D_3
Tread	0.73	-0.18	7.96E-02	2.76E-02	0	0
Sidewall	0.71	-0.28	0.13	2.85E-02	0	0
Apex	1.28	-1.25	1.20	1.58E-02	0	0

3.3.2 Viscoelastic Material property Test

Viscoelastic property, in conjunction with hyperelastic property of the rubber material, is also considered in this study. The viscoelastic property of the material provides a more accurate representation of the real world rubber behaviour, and the finite element model should include consideration of this characteristic, especially for transient dynamic analysis. Also,

the rolling resistance, tire thermal properties and internal damping are highly dependent on viscoelastic properties of tires.

The viscoelastic property test of rubber material was carried out based on the method of stress relaxation, and the test data was collected and analysed in the time domain. The MTS test machine for stress relaxation is illustrated in Figure 3.12.

Figure 3.12 MTS test system for stress relaxation test

The viscoelastic property is determined from the shear stress response time history when a constant strain is applied to the test specimen. In the process of viscoelastic property testing, the specimens used in the hyperelastic material property test were also subjected to the rubber relaxation test. Pre-conditioning of the samples from different components of tire product was conducted in the same manner as in the hyperelastic material property test. Likewise, these samples were allowed to be given half an hour for relaxation.

During the standard viscoelastic property test of rubber material, these samples were stretched up to 50% of their original length respectively, and then they were held for more than 900 seconds while recording stress levels from the beginning to the end of the test. In

order to get more accurate results, this test was repeated three times to determine the average stress relaxation curve.

After completion of the viscoelastic property test of different samples, the test data was obtained and converted to standard variable, which could be used for evaluation in ABAQUS. Time coordinate was kept the same as the test data, while the uniaxial stress relaxation modulus was converted to tensile stress. And the conversion formula is illustrated in Eq.3.9.

$$S_v = \frac{F_v}{A_v} \tag{3.9}$$

Where S_v is tensile stress, while F_v and A_v represent tensile force and area of rubber sample, respectively.

The normalized time domain viscoelastic property test data obtained from stress relaxation testing was implemented for evaluation in ABAQUS. The relaxation function $g_R(\mathrm{t})$ in terms of a series of exponentials known as Prony series is used to fit viscoelastic property data [118]

$$g_R(\mathrm{t}) = G_0\left(1-\sum_{i=1}^{N}\overline{g_i}^{p}(1-\mathrm{e}^{-\mathrm{t}/\tau_i^{\mathrm{G}}})\right) \tag{3.10}$$

where $\overline{g_i}^{p}$ represents the shear relaxation modulus ratio, τ_i^G represent relaxation time, these material constants are determined by modelling the physical test in ABAQUS. The evolution results of different material components are illustrated in Figure 3.13, and the Prony series parameters were calculated and listed in Table 3.3.

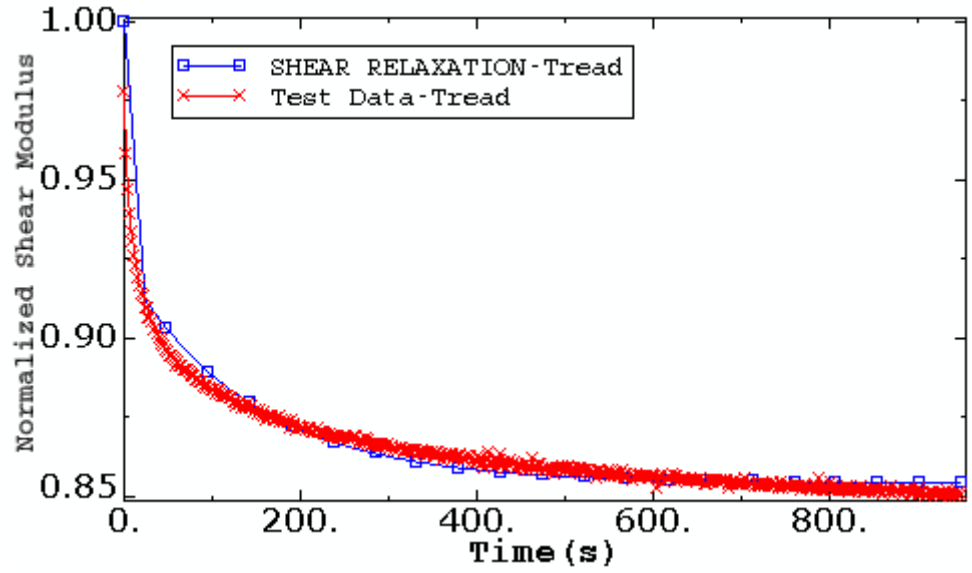
SHEAR RELAXATION-Tread
Test Data-Tread
Normalized Shear Modulus
1.00
0.95
0.90
0.85
0.
200.
400.
600.
800.
Time(s)

(a)

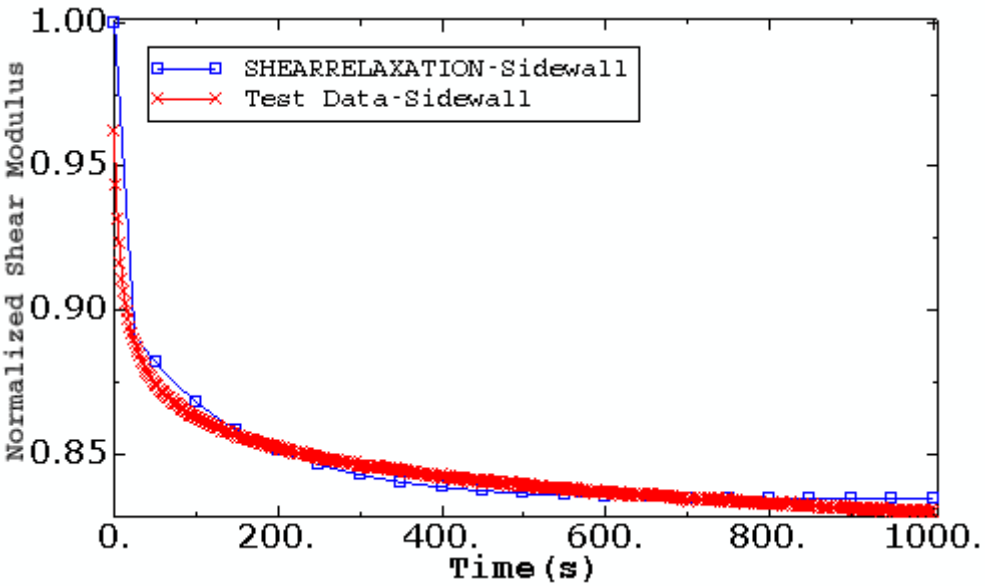
SHEARRELAXATION-Sidewall
Test Data-Sidewall
Normalized Shear Modulus
1.00
0.95
0.90
0.85
0.
200.
400.
600.
800.
1000.
Time(s)

(b)

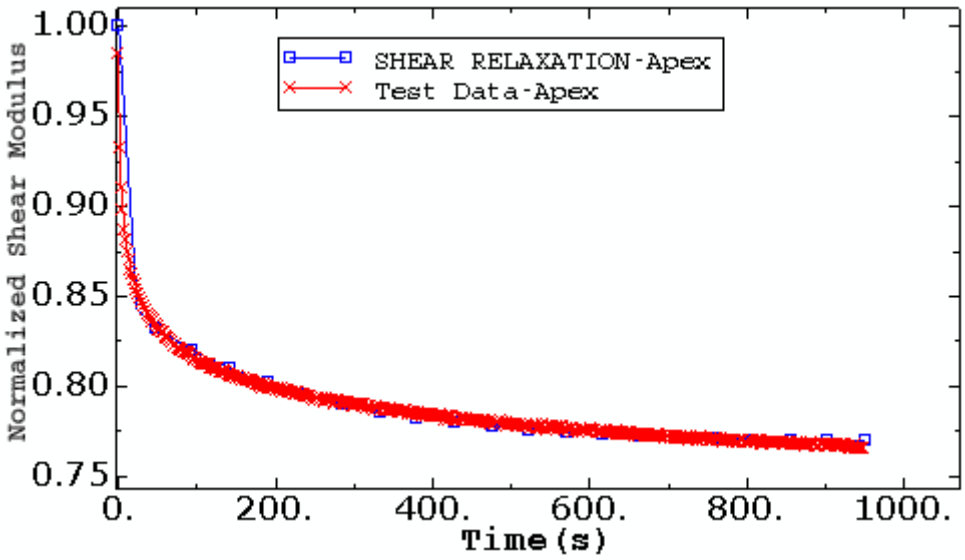

(c)

Figure 3.13 Viscoelastic property evolution: (a) Sidewall, (b) Tread, and (c) Apex

Table 3.3 Viscoelastic property constants for rubber materials

Rubber Material	Prony series parameters			
Component	g_1	τ_1	g_2	τ_2
Tread	0.08	2.39E-5	0.07	142.83
Sidewall	0.10	2.07E-6	0.07	146.11
Apex	0.15	5.76	0.08	220.41

3.3.3 Elastic Property Test of Reinforcement Materials

As important components embedded in rubber matrix, reinforcement material properties mainly control the overall performance of pneumatic tires. Tire performance such as burst, bruise, endurance and power loss depend in some way on the tire reinforcements.

In this study, the properties of cords are characterised as linear elastic. The specimens for the test of reinforcement material property were extracted from tire product. However, some cords in tire components such as cap ply reinforcements could not be extracted due to the limitation of laboratory facilities. In this study, steel belt specimen and carcass reinforcement specimen were acquired for testing and analysis.

The property of the cords could be characterized using Yong's Modulus E and Poisson's Ratio v, but the Poisson's Ratio could not be obtained due to the limitation of available test facilities in the laboratory. Based on the review [119], the Poisson's Ratio of the cords were set as 0.3 approximately.

The objective of the reinforcement property test is to acquire Young's Modulus of the cord. u-, and uniaxial tension test was carried out to meet the requirements . In the process of the tension test, the cords were stretched up to 4%-5% of their original length. The test rig is the same as the machine used in hyperelastic material property test. During the test, the stretching force F and the corresponding elongation ΔL were recorded, and they were going to be used for derivation of Yong's Modulus E , which is illustrated in Eq. 3.12,

$$E = \frac{\sigma}{\varepsilon}, \tag{3.12}$$

In the equation, $\sigma = \frac{F}{A}$ and $\varepsilon = \frac{\Delta L}{L}$, in which A is area of the cross-section of the specimen.

As the stress-strain curves of steel belt and carcass cord are linear within their elastic ranges, the tangent modulus of elasticity of the cords were selected to represent their Young's Modulus. The Stress-Strain curves of reinforcement test data of steel belt and carcass cord are illustrated in Figure 3.14 and Figure 3.15.

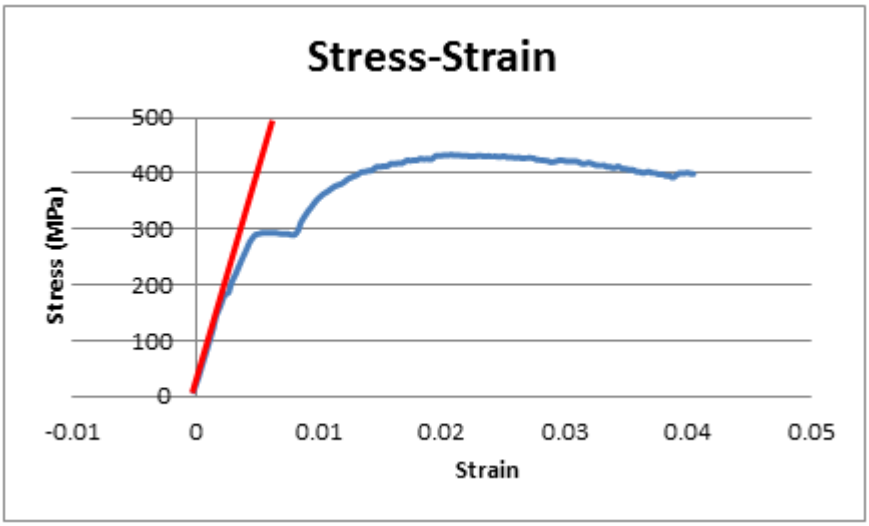

Figure 3.14 Normalized reinforcement test data of steel belt

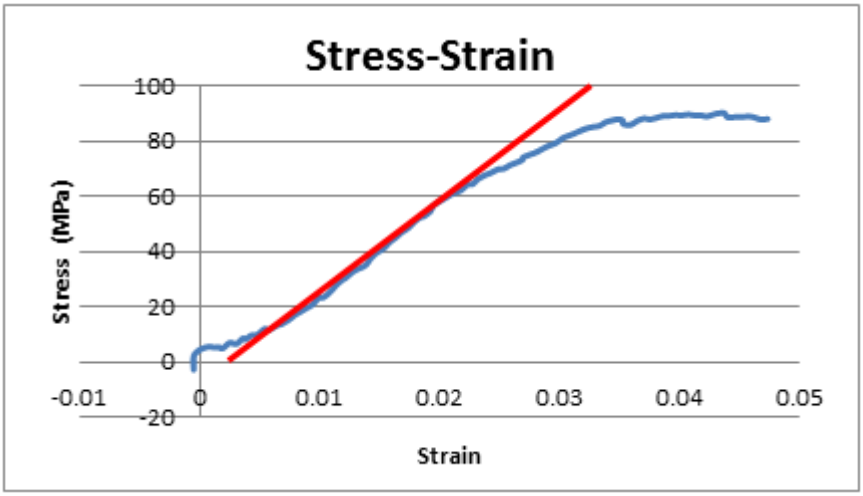

Figure 3.15 Normalized reinforcement test data of carcass cord

By calculation of the gradient of stress-strain, the Young's Modulus of the steel belt and carcass cord are 180GPa and 4.5Gpa, respectively. And then, the results were imported into Finite Element code ABAQUS for material property modelling.

In addition, the density of cords such as carcass and cap ply were assumed as 1300kg/m^3 according to the density database for different kinds of cords, and the density of steel belt and the steel bead were set as 7800kg/m^3 [120]. Based on the experiments from tire research group at University of Birmingham, the Density Measuring Device was applied to measure

the density of different rubber components, results show that all the values were very close to 1200kg/m^3. Therefore the density of all rubber components was set as 1200kg/m^3.

3.4 Summary and Conclusions

1. In this chapter, the geometry property of tire cross-section and layup structures has been determined by measurement. Image processing method has been developed to capture the tire cross-section geometry data. Rebar elements were used to define layers properties including cords spacing, cross-section area of cords and positional orientation of cords.
2. Material properties of the tire model have been developed. Rubber specimens were extracted from a real tire, and parameters of Hyperelastic and viscoelastic properties were obtained by fitting the tensile test data for rubber components. With the comparison of different hyperelastic material models, the Yeoh model was chosen as the best model for definition of rubber components. Also, Prony series in ABAQUS was used to define the viscoelastic property of rubber components.
3. Reinforcement material property was considered as linear elastic because of its small strain during tire deflection conditions. In the explicit dynamic analysis of rolling tire, the weight of the tire is a necessary parameter. Therefore, rubber and reinforcement density have been defined.
4. The approach developed to define material and geometry property is considered to be very important for parametric studies in future. It allows researchers to investigate the sensitivity of tire dynamic properties to rubber and reinforcement properties.

Chapter 4 STATIC TIRE PROPERTIES ANALYSIS AND STATIC PARAMETERS DERIVATION

4.1 Introduction

This chapter presents the static properties which are necessary for the development of steady-state and transient tire models in the further analysis.

Inflation pressure analysis can provide important information for the tire designers and researchers about the shape variation of the tire cross-section under different inflation pressures. For the tire traversing obstacles, the rolling tire is excited by road obstacles through vertical stiffness of the tire. Static vertical stiffness validation was carried out for different inflation pressures. Longitudinal stiffness is also an important parameter for the longitudinal characteristics of the tire, such as braking analysis and rolling resistance generated on the uneven road, which will be described in the further chapters. As the only connection between the road and the tire, the contact footprint is another important characteristic in the static property of the tire, in which the shape and size together with pressure distribution of the contact footprint are important in ride quality and handling properties of a vehicle.

In this chapter, measured tire cross section shape with different inflation pressures, vertical stiffness together with the footprint are compared with the simulation results in order that the accuracy of the FE tire model in static condition can be validated.

4.2 Inflation Property Analysis

The application of inflation pressure is perhaps the simplest and most fundamental method, and the inflation analysis can be conducted conveniently using Finite Element code. Tire

inflation modelling is the first step of tire static properties simulations, and the inflation pressure analysis can be carried out using two dimensional axi-symmetric tire models.

As one of the fundamental steps for tire properties investigation, inflation pressure analysis of the tire has been applied for basic research. Behroozi et al. [44] used the two dimensional model to investigate the effect of the complexity of the finite element models on the accuracy of predicting the tire properties by simulating the tire inflation behaviour with different mesh characteristics. Bolarinwa and Olatunbosun [40] presented a numerical method to simulate tire burst phenomenon under different values of inflation pressure using finite element code, from which the effect of tire design parameters on the tire burst pressure was investigated for identifying the critical inflation pressure. Allen and his colleagues [45] developed a numerical approach to calculate the inflated shape and stress distribution of a pneumatic aircraft tire using axisymmetric model, the deformation characteristics of the tire were studied to determine the heat generation because of the rubber material properties.

4.2.1 Inflation pressure simulation

As a commercial Finite Element code, ABAQUS^{TM} is capable of modelling deformation of rubber material under different values of inflation pressure. In order to carry out inflation analysis, boundary conditions were defined in the 2D axisymmetric model. In this study, the wheel centre was fixed by constraining four degrees of freedom of the tire cross-section (two translational degrees and two rotational degrees). In order to constrain the bead nodes of the tire model, a rigid body between rim node and the tire-rim assembly nodes was defined using the tie function in ABAQUS. From this way, it is more convenient to apply boundary conditions on the rim reference node to stabilize the tire-rim interface. The inflation of the tire is modelled by application of a uniform internal pressure, which is shown in Figure 4.1.

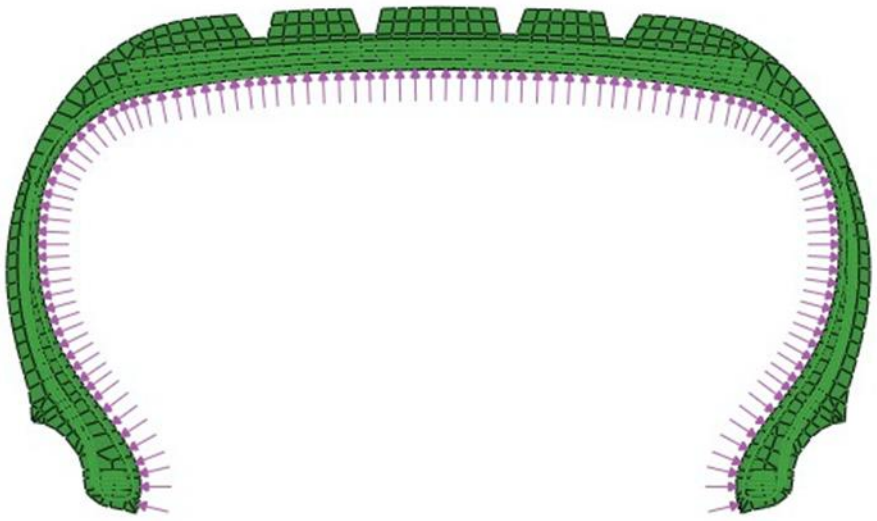

Figure 4.1 Inflation pressure on the 2D tire model

In order to investigate the effect of inflation pressure variation, five different inflation pressures were applied on the tire model for simulation, which were 40kPa, 80kPa, 120kPa, 160kPa and 200kPa. About 16 nodes at half of the cross-section were selected to describe the inflation behaviour at different operating conditions by calculating the displacement variation of these points. Because of the axisymmetric property of the tire, half of the cross-section displacement is sufficient to describe inflation behaviour of the whole tire model. The coordinate data of these nodes at different values of inflation pressure is shown in Figure 4.2.

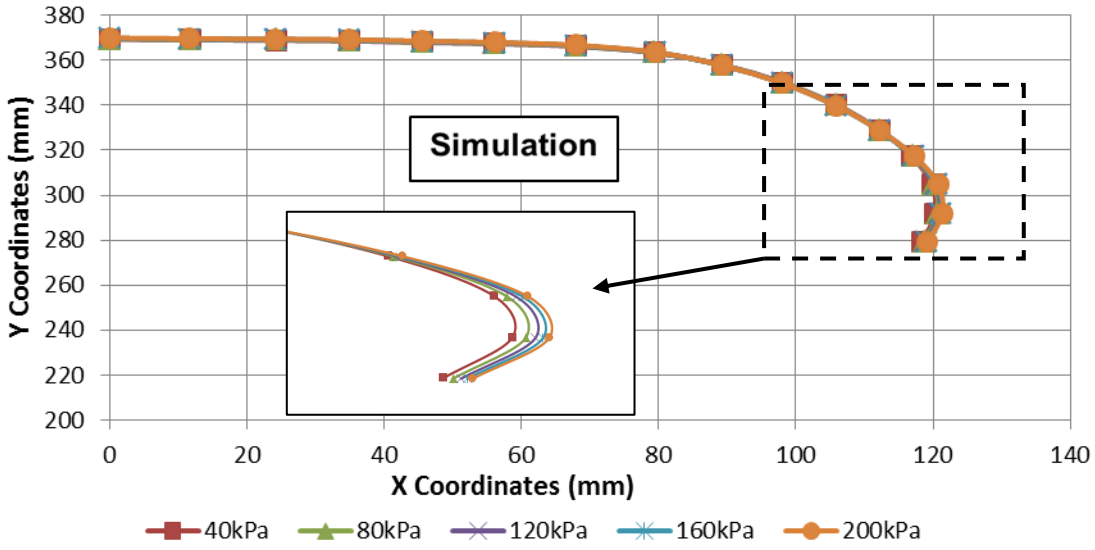

Figure 4.2 Pressure/Displacement profile at different inflation conditions in simulation

4.2.2 Experimental measurement of inflated tire

Properties of inflation pressure were investigated in terms of the relationship between inflation pressure and tire deformation, which could be measured at the nodes' positions of the tire cross-section. The displacement of any prescribed node can be determined by comparing the node positions at non-inflated status and inflated status. In order to validate the nodes position variation, some points need to be marked on the profile of the tire in advance. The coordinate's data of the marked points at tire profile were obtained by using the Coordinates Measurement Machine (CMM), which is shown in Figure 4.3. With a flexible touch trigger of CMM, the facility could be efficient in measurement of the tire profile geometry with different values of inflation pressure, so that the relationship between pressure and displacement can be determined.

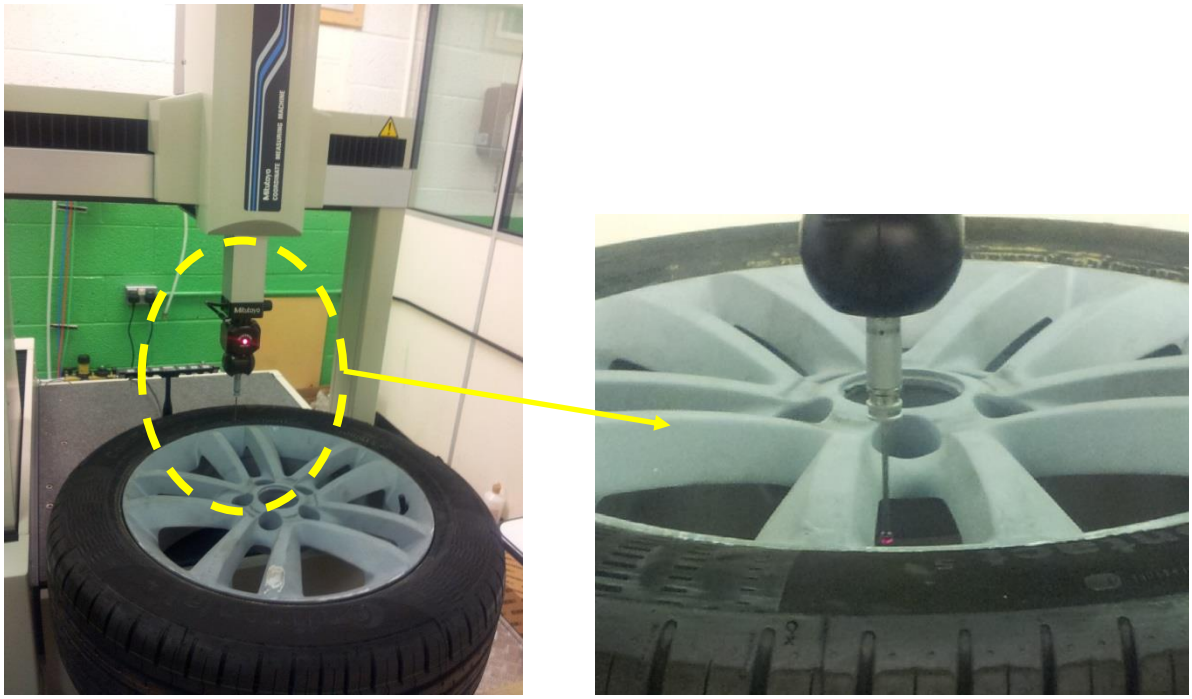

Figure 4.3 Coordinates Measurement Machine for tire inflation shape measurement

However, because the modelling file of tire cross-section data was extracted from tire cutting, and the tire file for measurement data was from an assembled balance tire with rim, not all the corresponding nodes of the FE tire cross-section model could be located on the real tire file, which is one of the difficulties in carrying out displacement testing of the tire profile. However, enough points were marked on the tire profile, which could reflect the pressure/displacement properties with coordinate measurements at different values of inflation pressure.

The CMM has the capability to measure the coordinates of the points in three dimensions. Because the measurement was carried out at the outside surface of the tire cross-section from the bead area to the centre of the tread area, only coordinates at X direction and Y direction were recorded, which is illustrated at Figure 4.4. Due to the axisymmetric characteristic of the tire, half of the cross-section measurement is used to represent the inflation behaviour of the whole tire profile.

Figure 4.4 Representation of the tire lying on the testing table

Eighteen different points were marked on the outside surface of the cross-section, which was convenient for the CMM to touch and acquire the coordinates of these points. Five different operating conditions were applied on the tire in terms of different values of inflation pressure. Corresponding to the condition of Finite Element model, the same range of inflation pressures were adopted in the measurement, which were 40kPa, 80kPa, 120kPa, 160kPa and 200kPa. The results at different inflation conditions are shown in Figure 4.5.

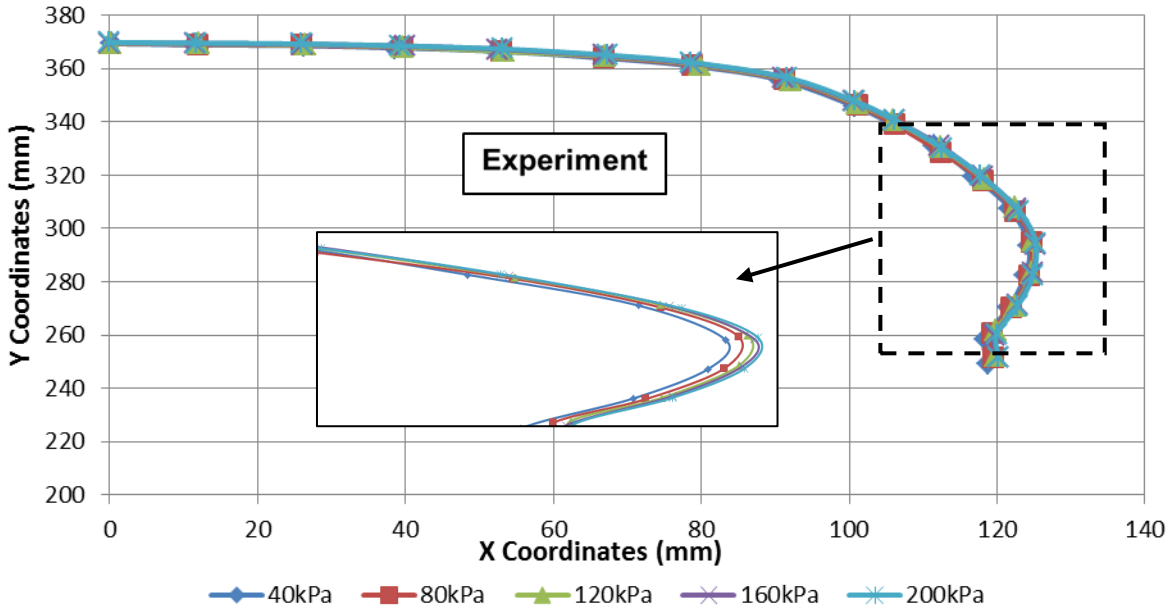

Figure 4.5 Pressure/Displacement profile at different inflation conditions in experiment

However, the above figure cannot clearly describe the difference between the original shape and inflated shape of the tire. In order to efficiently investigate the displacement variation of the tread and the sidewall when the tire was inflated, two representative nodes from the tread

and sidewall of the 2D tire model were chosen to validate their displacements. The displacement of the node A (in the centre of the tread area) of the tread section in Y direction and the displacement of the node B (at the outermost point in sidewall area) of the sidewall section in X direction were considered and calculated at different inflation pressure conditions (Figure 4.6). Note that node A's displacement represents the tread's displacement relative to the tire centre, while node B's displacement represents the width variation of the tire. The variation of the displacement of node A in Y direction under different inflation pressures is shown in Figure 4.7, while Figure 4.8 presents the variation of the displacement of node B in X direction with increase of inflation pressure.

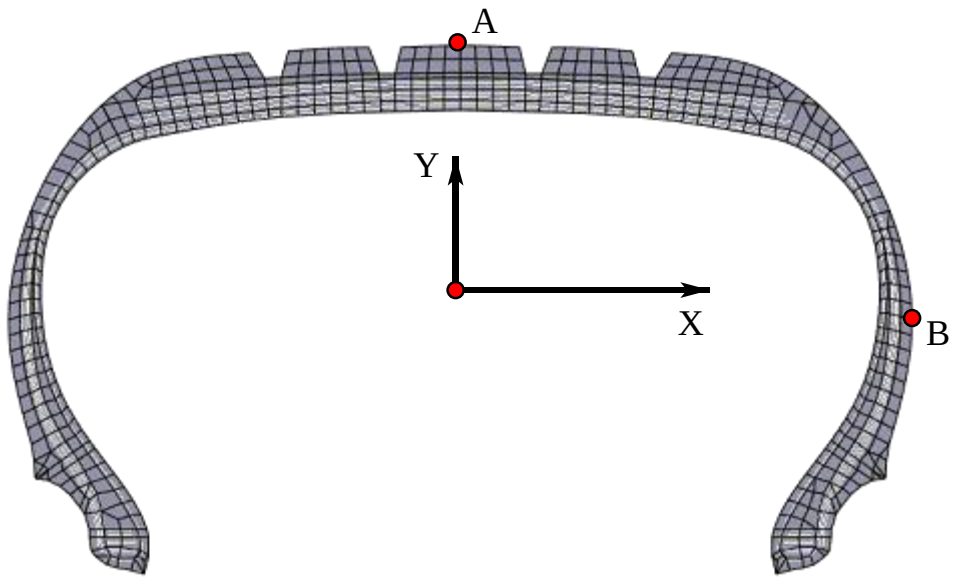

Figure 4.6 Tread and sidewall nodes

It can be seen in Figure 4.7 and Figure 4.8 that the simulation results agree well with the measurement results for both the sidewall node and the tread node. By analysing the variation of the displacement of the sidewall in different inflation pressure conditions, it was found that the displacement of the tread in Y direction has a nearly linear relationship with the inflation pressure. The displacement of the sidewall in X direction is increasing with the increment of the inflation pressure, but the increasing magnitude of the displacement is gradually reduced.

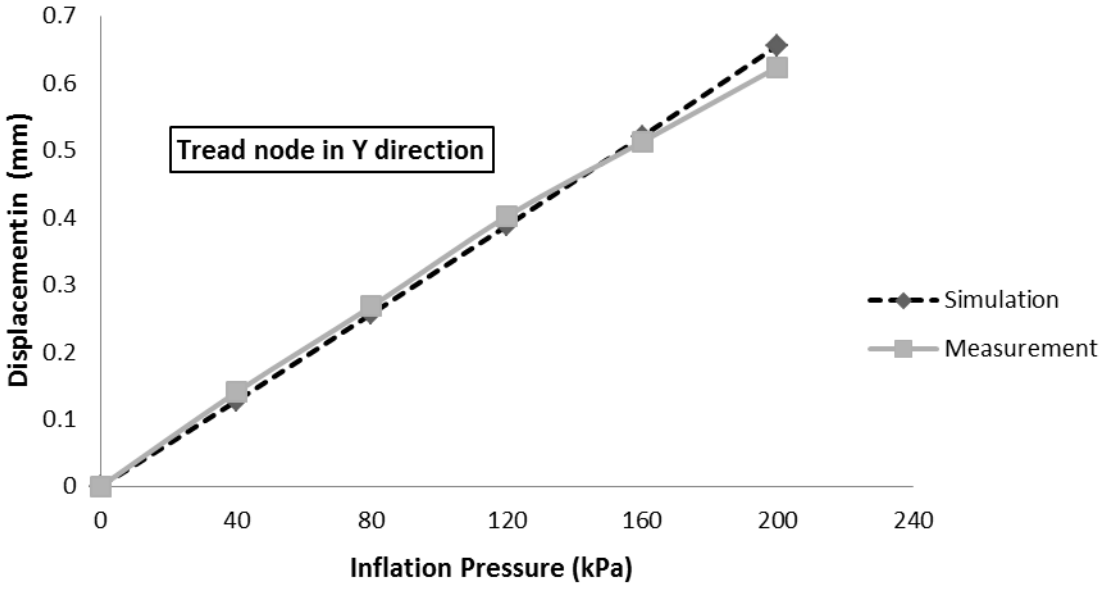

Figure 4.7 Displacement of tread node A in Y direction

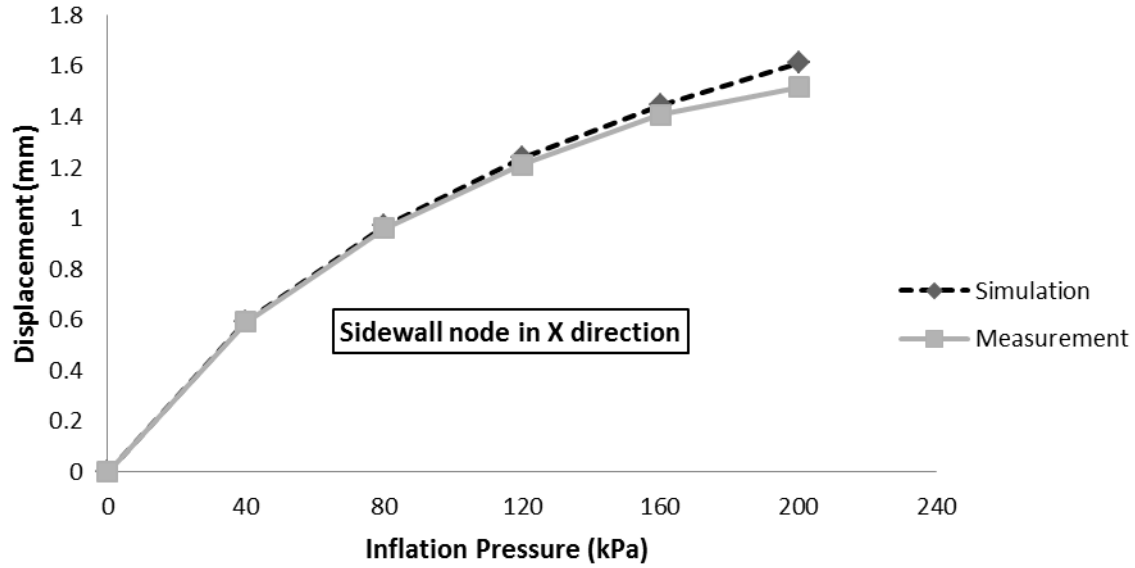

Figure 4.8 Displacement of the sidewall node B in X direction

4.3 Static Stiffness Analysis

4.3.1 Definition of tire/road contact

Normal contact qualification is used to restrict the movement of two contact bodies (Figure 4.9). Impenetrability is used to make the constraint that the configurations V^A of body A and V^B of body B cannot penetrate into each other in the process of movement [121]. In the tire/road contact model, V^A and V^B represent the tire and road respectively.

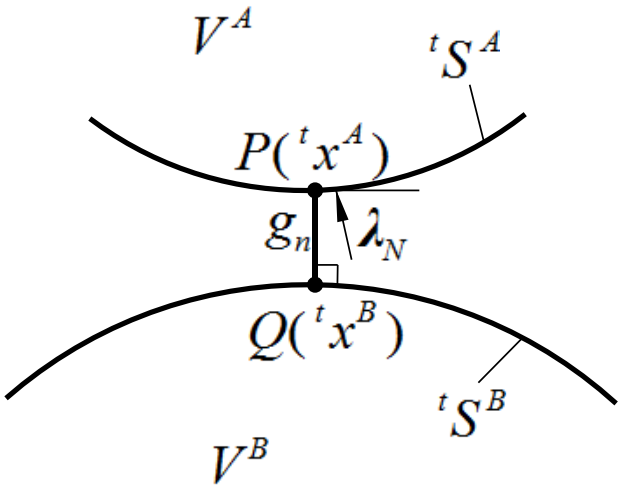

Figure 4.9 Schematic representation of two body's contact

We assume that ${}^tx_P^A$ represents the coordinate of the particle P on the surface ${}^tS^A$ of body A at time t, the distance g between the particle and the nearest particle $Q({}^tx^B)$ on the surface ${}^tS^B$ (Figure 4.9) can be expressed by

$$ {}^tg = g({}^tx_P^A, t) = \left| {}^tx_P^A - {}^tx_Q^B \right| = \min \left| {}^tx_P^A - {}^tx^B \right| \qquad (4\text{-}1) $$

in which ${}^tx^B$ represents the coordinate of any particle on surface ${}^tS^B$. In this study, the orientation of g should be the same with that of ${}^t\boldsymbol{n}^B$, which represents the unit vector normal to the contact plane. Therefore, the vector ${}^t\boldsymbol{g}$ can be obtained by

$$ {}^t\boldsymbol{g} = \boldsymbol{g}({}^tx_P^A, t) = ({}^tx_P^A - {}^tx_Q^B) \cdot {}^t\boldsymbol{n}_Q^B \qquad (4\text{-}2) $$

In order to meet the requirement of impenetrability for the two bodies (the tire and the road), we use the following constraint to define any particle P on the surface ${}^tS^B$

$$ {}^t\boldsymbol{g}_n = \boldsymbol{g}({}^tx_P^A, t) = ({}^tx_P^A - {}^tx_Q^B) \cdot {}^t\boldsymbol{n}_Q^B \geq 0 \qquad (4\text{-}3) $$

in which ${}^t\boldsymbol{g}_n > 0$ means a gap exists between the particle P and the surface ${}^tS^B$, while ${}^t\boldsymbol{g}_n = 0$ means the particle P has a contact with ${}^tS^B$. As the above function is effective for any particle on surface ${}^tS^A$ and ${}^tS^B$, the function can be described by

$$ {}^{t}\boldsymbol{g}_n = \boldsymbol{g}({}^{t}x^A, t) = ({}^{t}x^A - {}^{t}x^B) \cdot {}^{t}\boldsymbol{n}^B \geq 0 \qquad (4\text{-}4) $$

In addition, since the equivalent normal contact force is provided by the pressure, the condition of normal contact force λ_N （Figure 4.9）is given by

$$ \lambda_N \geq 0 \qquad (4\text{-}5) $$

In the tangential direction of rolling contact analysis, Coulomb model of friction is adopted to define the tangential contact conditions. In engineering analysis, coulomb model of friction is widely used because of its characteristics of simplicity and applicability [121]. The definition in the Coulomb friction model is that slip occurs when the tangential contact force (frictional resistance) $\tau_{eq} = \sqrt{\tau_1^{\,2} + \tau_2^{\,2}}$ equals to the critical stress $\tau_{crit} = \mu\lambda_N \geq 0$, which means that the friction force cannot be allowed to exceed the critical stress, which is

$$ \tau_{eq} = \sqrt{\tau_1^{\,2} + \tau_2^{\,2}} \leq \mu\lambda_N \qquad (4\text{-}6) $$

in which μ is the coefficient of friction, τ_1 and τ_2 are shear stresses in t_1 direction and t_2 direction respectively, and λ_N represents the normal contact force. On the other hand, no relative motion between the tire and the rigid road surface occurs when $\tau_{eq} < \tau_{crit}$. In ABAQUS, the stiff viscous behaviour is adopted to approximately simulate the non-relative-motion condition,

$$ \tau_\alpha = \kappa\dot{\gamma}_\alpha (\alpha = 1, 2) \qquad (4\text{-}7) $$

in which τ_α represents the shear stress in the tangential direction, $\dot{\gamma}_\alpha$ is the tangential slip rate in the tire/road contact plane, $\kappa = \mu\lambda_N / 2\Delta\omega R$ is the stick viscosity, ω is the rotation angular velocity and R is the rolling radius of the tire, and Δ is the slip tolerance defined by the users. In this study, Δ was set as 0.005.

4.3.2 Vertical (radial) stiffness

4.3.2.1 Experimental tests for vertical stiffness

As a prevalent parameter for tire static analysis and validation, static stiffness has an effect on vehicle ride performance and the properties of the static stiffness is very important for tire dynamic analysis. In the programme, the vertical stiffness experimental tests were carried out using the tri-axial electro-hydraulic tire dynamic rig with a 2.44 diameter drum, the configuration of which is shown in Figure 4.10. The procedure of the non-rolling tire vertical stiffness test includes three steps:

1. Apply an inflation pressure to the tire. As the tests need to consider vertical stiffness at different inflation pressures, an initial inflation pressure of 200kPa is applied on the tire, which is convenient to deflate it in order that the vertical stiffness at lower inflation pressure can be obtained.
2. Move the tire into contact with the drum. In order to acquire the position of the tire when it contacts the drum with a 0 vertical load, the tire needs to be pushed toward the drum gradually, and then the position of the tire is recorded. In this step, the centre of the drum, the centre of the tire, and the system fixed point need to be adjusted in the same line, which is illustrated in Figure 4.11.
3. Set a displacement of the tire. In this step, the position of the tire in vertical direction is determined in order to set the displacement of the tire. Different levels of displacement are applied to the tire, and the tire is pushed towards to the drum incrementally, the corresponding vertical loads are recorded by the calibrated load cell.

Figure 4.10 Tri-axial electro-hydraulic test rig

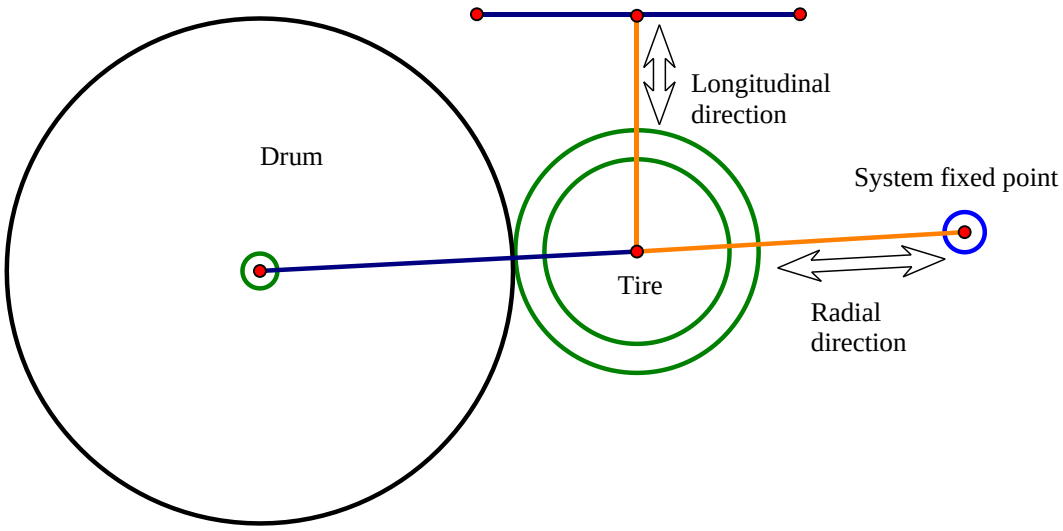

Figure 4.11 Schematic representation of the test rig

4.*3.2.2 Static vertical stiffness simulation*

The 3D tire model is obtained by revolving the 2D cross section of the tire about the rotational symmetric axis using *SYMMETRIC MODEL GENERATION, REVOLVE command. The 2D axisymmetric elements (CGAX4H and CGAX3H) were transformed into 3D solid elements (C3D8H and C3D6H). For the static contact analysis, only contact region of the tire need to be given fine meshes. The three-dimension model is composed of 50 sections, covering an angle of 320 degrees, while the rest of the model was separated into 60

sections in the tire-road contact patch region, covering an angle of 40 degrees. The objective of dividing such refined sections in contact patch region is to meet the requirements of steady state rolling analysis, and from which it should be convenient to acquire more accurate prediction of the forces and footprint (Figure 4.11).

In this three-dimension model, the tire was inflated to a pressure of 200kPa, the road was defined as an analytical rigid surface, the initial contact between the tire and the road was established with a small vertical displacement in order to avoid convergence difficulties which might be influenced by the unbalanced forces. Then a vertical load of 3000N was applied on the road towards the tire rim reference node. After completing the simulation of tire deformation, the reaction force to the displacement was recorded from the rim reference node. The deformed three-dimension tire model with road surface is shown in Figure 4.12.

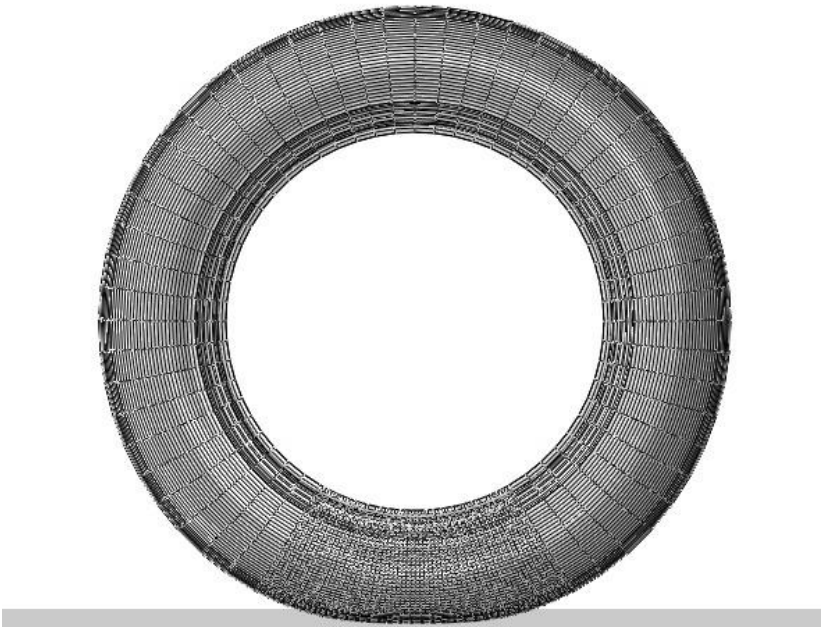

Figure 4.12 deformed 3D tire model

4.3.2.3 Comparison between the test results and simulation results

As the initial inflation pressure applied on the tire is 200kPa, it is convenient to carry out the static tests with lower levels of inflation pressure by deflating the tire. Different values of inflation pressure (200kPa, 160kPa, 120kPa, 80kPa, 40kPa) were applied on the tire for

simulations and tests. In the tests, the vertical loads were recorded at the tire displacements of 0mm, 3mm, 6mm, 12mm and 15mm. Figure 4.13 to Figure 4.17 describe the comparisons of vertical stiffness between corresponding simulation and experimental tests.

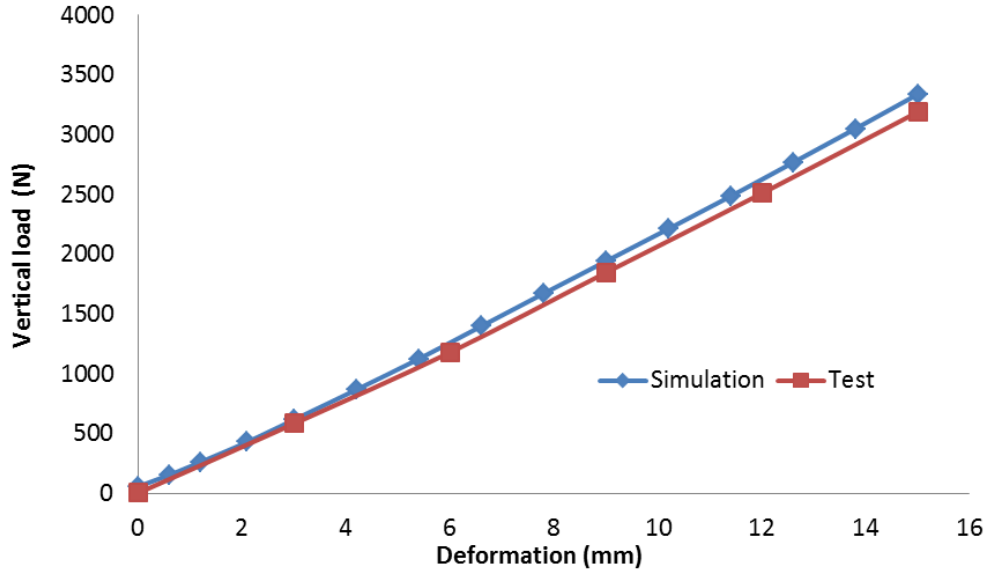

Figure 4.13 Force/Displacement relationships at 200kPa

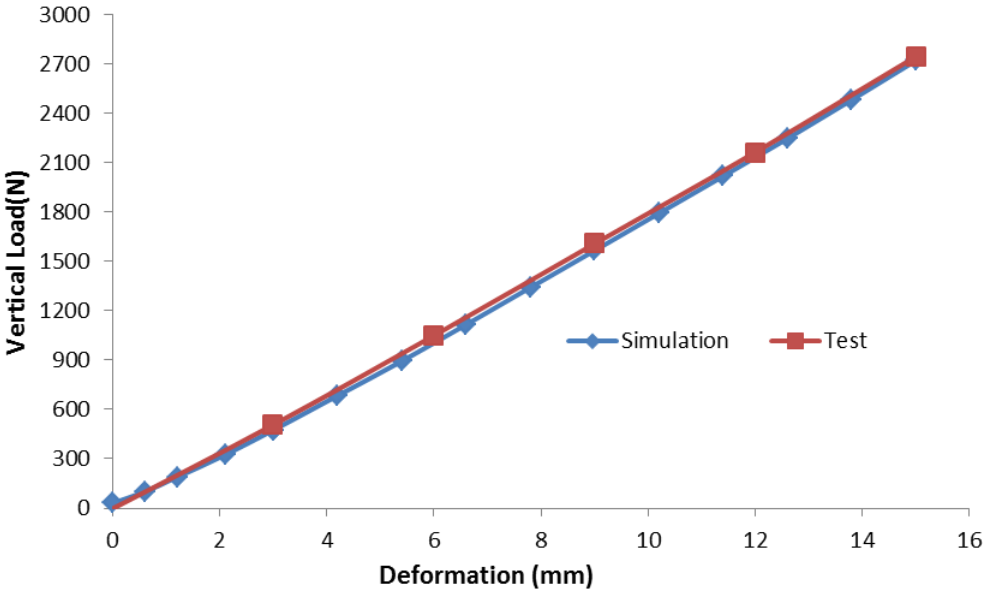

Figure 4.14 Force/Displacement relationships at 160kPa

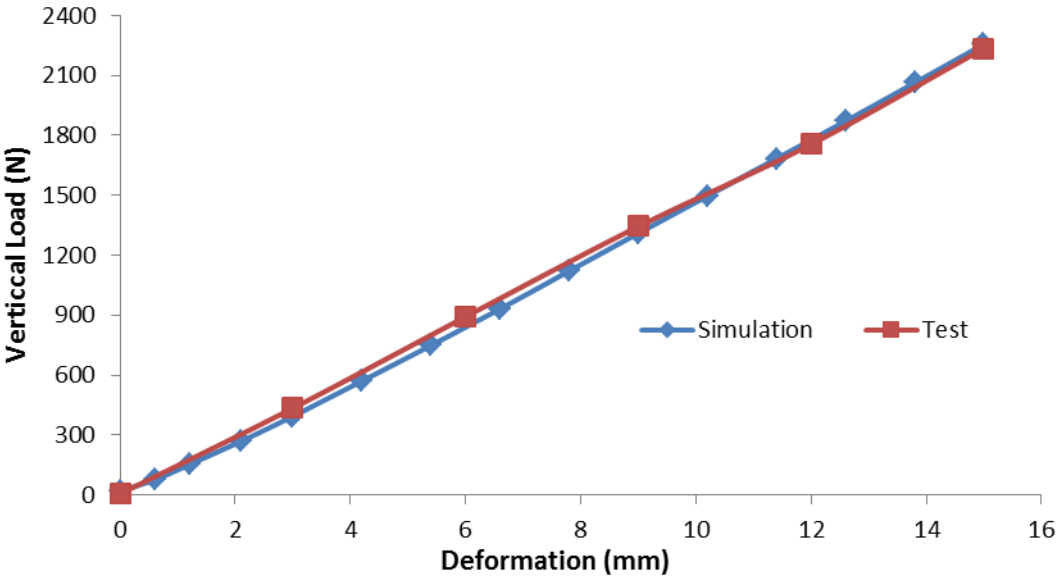

Figure 4.15 Force/Displacement relationships at 120kPa

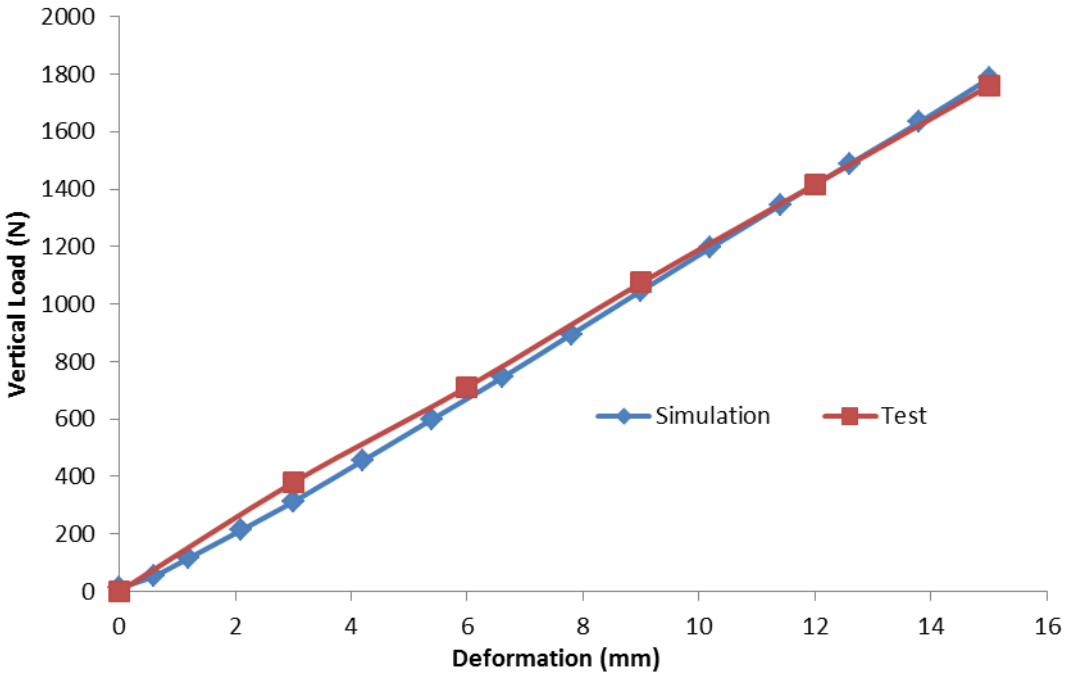

Figure 4.16 Force/Displacement relationships at 80kPa

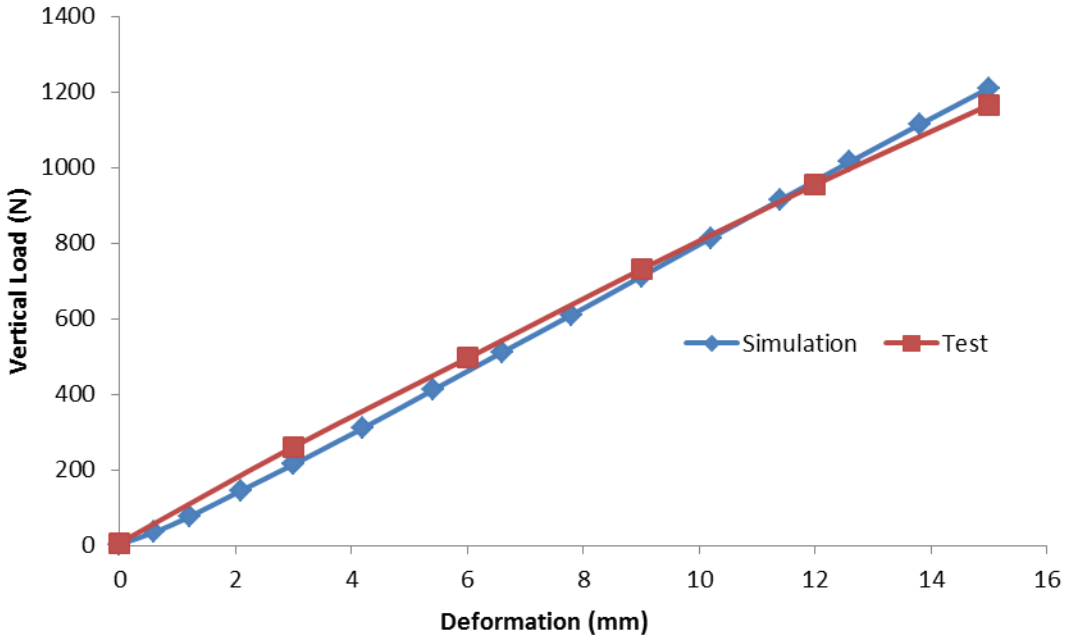

Figure 4.17 Force/Displacement relationships at 40kPa

From the force/displacement relationship figures shown above, it can be seen that there are approximately linear relationships between vertical loads and displacements at different inflation pressures. The vertical stiffness was obtained by fitting the relationship between vertical load and tire displacement in vertical direction using a linear curve. The comparison of vertical stiffness values between experimental tests and FE simulations is shown in Table 4.1. From Figure 4.13 to Figure 4.17 and Table 4.1, it can be seen that both of the force/displacement relationships and the vertical stiffness values at different inflation pressure conditions show satisfactory correlations between the experimental tests and FE simulations.

Table 4.1 Cmparison of vertical stiffness between test and simulation

Inflation pressures (kPa)	Vertical Stiffness Tests (kN/m)	Vertical Stiffness Simulation(kN/m)	Absolutely Difference (%)
200	222.53	212.83	4.36
160	180.21	178.19	1.13
120	146.31	146.8	0.33
80	118.05	119.39	1.12
40	79.55	82.23	3.26

4.3.3 Longitudinal stiffness and lateral stiffness

Unlike vertical stiffness, the longitudinal stiffness and lateral stiffness tests are difficult to carry out because of laboratory limitations. However, with the FE program, the simulations for derivation of longitudinal and lateral stiffness can be conducted sufficiently.

In the simulation of longitudinal movement, the tire was set to contact the road with a small deflection in the vertical direction in order that an initial vertical load is obtained. The friction of the road was set as 1.0 and no slip was allowed in the simulation, and then a small displacement in the longitudinal direction was applied on the tire spindle (Figure 4.18(a)). Longitudinal stiffness can be obtained from the gradient of the relationship between longitudinal forces and longitudinal displacement of the tire centre.

For the lateral stiffness simulation, a small deflection of the tire on the vertical direction towards the road was applied initially, and the same friction condition was defined in the simulation. The tire was then moved in the lateral direction up to a small displacement of 10mm, which is illustrated in Figure 4.18(b). Lateral stiffness can be obtained from the gradient of the relationship between lateral forces generated on the spindle and lateral displacement of the tire centre.

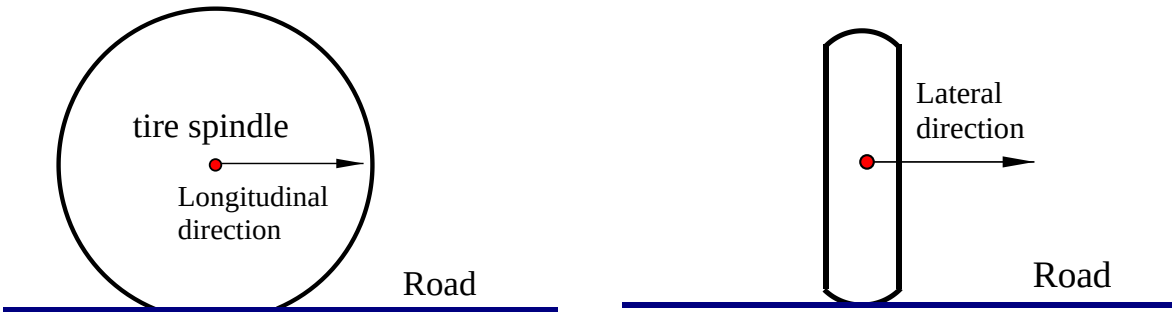

Figure 4.18 (a) Tire movement simulation for longitudinal stiffness derivation (b) Tire movement simulation for lateral stiffness derivation

In order to investigate the influence of operating conditions on longitudinal stiffness and lateral stiffness, different inflation pressures and different initial vertical deflection were applied on the tire/road contact model. Figure 4.19(a) describes the relationship between longitudinal forces and longitudinal displacement of the tire with different inflation pressures, a preload in vertical direction was applied in the simulation. On the other hand, the variations of longitudinal force with different initial vertical deflections are shown in Figure 4.19(b) when an inflation pressure of 200kPa was applied in the simulation. Figure 4.20(a) illustrates the relationship between lateral forces variation when the tire with different inflation pressures was stretched to a displacement of 10mm, and the initial vertical deflection of the tire was set as 9mm so that the preload was applied. For different initial deflections of the tire in the vertical direction, the relationships between lateral forces and lateral displacement of the tire were illustrated in Figure 4.20(b), and the inflation pressure of 200kPa was applied on the simulation.

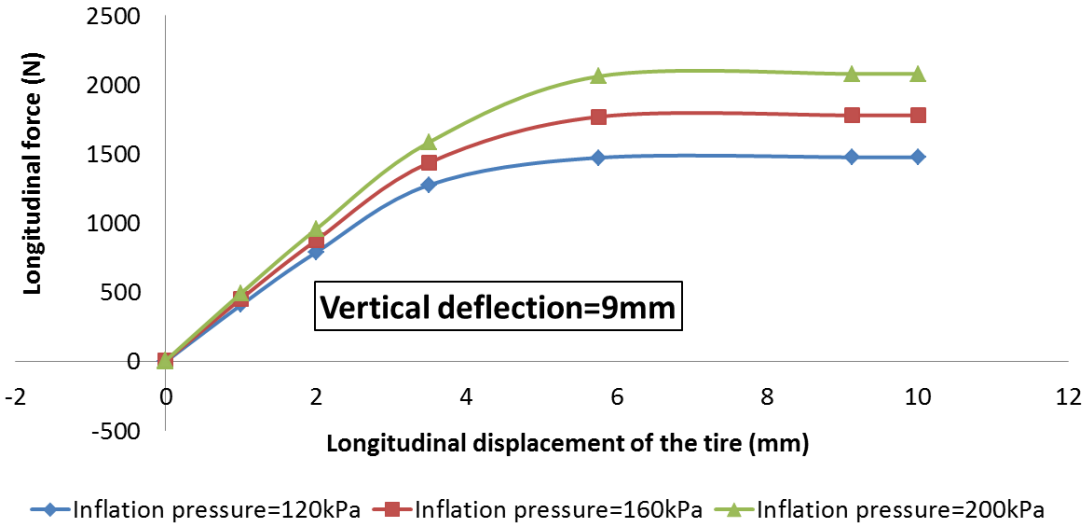

(a)

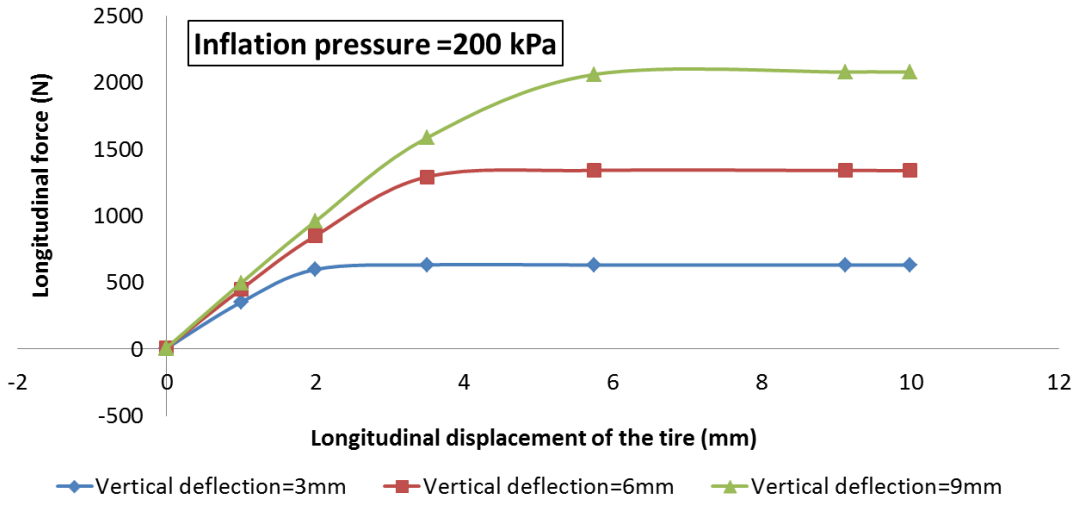

(b)

Figure 4.19 (a) Relationship between longitudinal forces and longitudinal displacement of the tire under different inflation pressures (b) Relationship between longitudinal forces and longitudinal displacement of the tire with different initial vertical deflection of the tire

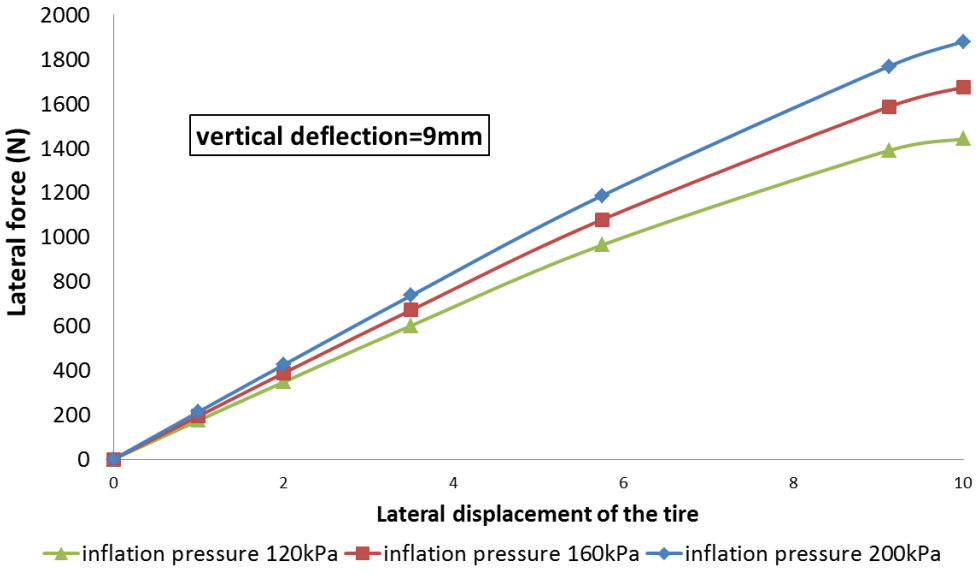

(a)

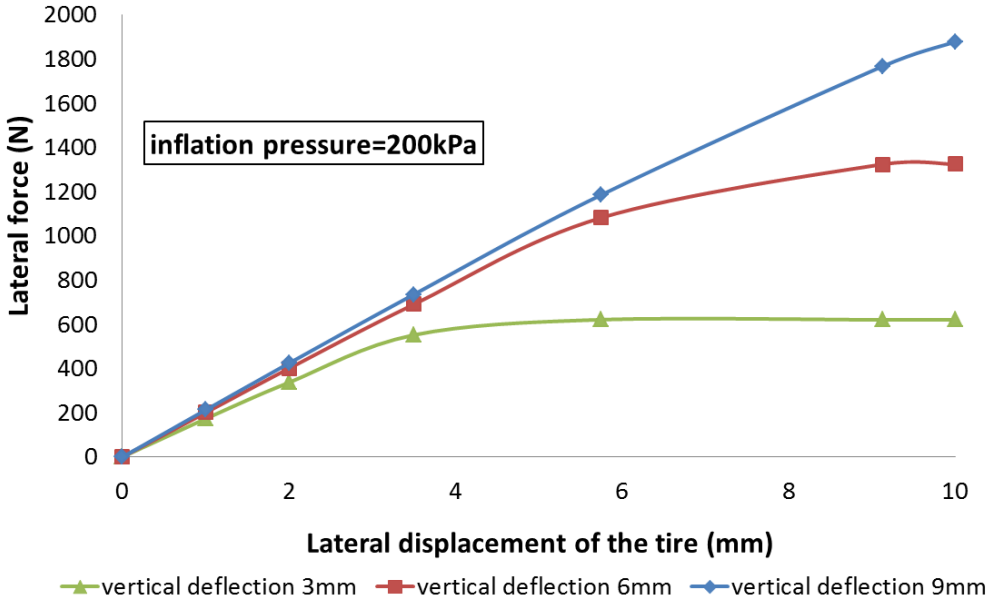

(b)

Figure 4.20 (a) Relationship between lateral forces and lateral displacement of the tire under different inflation pressures (b) Relationship between lateral forces and lateral displacement of the tire with different initial vertical deflection of the tire

The longitudinal stiffness can be derived by extracting the gradient of the relationship between longitudinal force and longitudinal displacement of the tire. Table 4.2 shows the longitudinal stiffness values at different operating conditions, from which it can be seen that higher inflation pressure leads to higher longitudinal stiffness and higher initial vertical deflection also leads to higher longitudinal stiffness. On the other hand, lateral stiffness was also derived using the same method as longitudinal stiffness. The values of lateral stiffness at different conditions are shown in Table 4.2. Likewise, the lateral stiffness increases with the inflation pressure and the lateral stiffness increases when higher vertical deflection is applied in the model.

Table 4.2 Static longitudinal and lateral stiffness at different conditions

Inflation pressure	Vertical deflection 9mm	Vertical deflection 6mm	Vertical deflection 3mm
	Longitudinal stiffness (N/mm)		
120kPa	790.30	686.40	434.96
160kPa	877.39	772.20	434.96
200kPa	957.58	848.98	597.13

	Lateral stiffness (N/mm)		
120kPa	346.84	326.99	272.21
160kPa	386.87	365.12	306.78
200kPa	423.99	400.66	337.14

4.4 Footprint analysis

The size and shape of the footprint of a tire as well as the pressure distribution within the footprint are significant factors for tire properties, especially ride performance and handling properties of a vehicle. The tri-axial electro-hydraulic tire dynamic rig was also applied for footprint tests. Black ink was smeared on the tire tread, and a sheet of white paper was attached on the drum in order that the contact patch was imprinted on it, described in Figure 4.21. The tire was pushed toward the drum slowly until the vertical load reached a pre-set value. In order to analyse the effect of inflation pressure and vertical load on the size and shape of the footprint, different levels of inflation pressure and vertical load were applied on the tire. The acquired footprint image was scanned into the computer and the contact area was calculated by extracting its outline and importing it to Solidworks, which are illustrated in Figure 4.22.

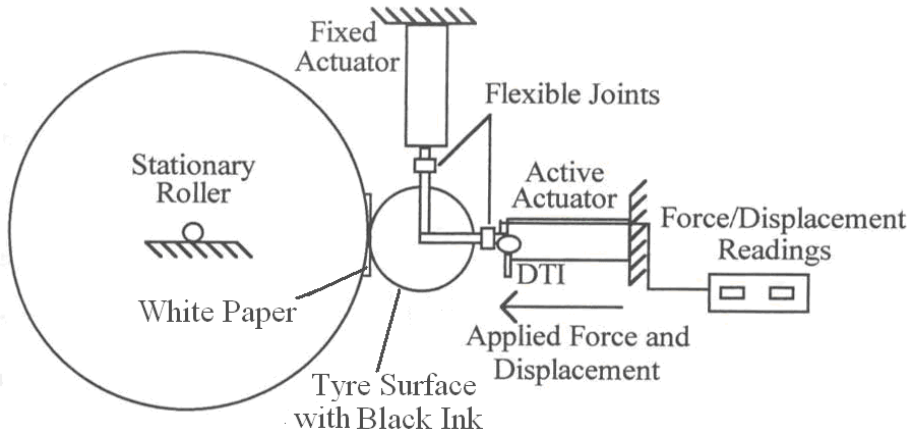

Figure 4.21 Configuration for footprint experiment

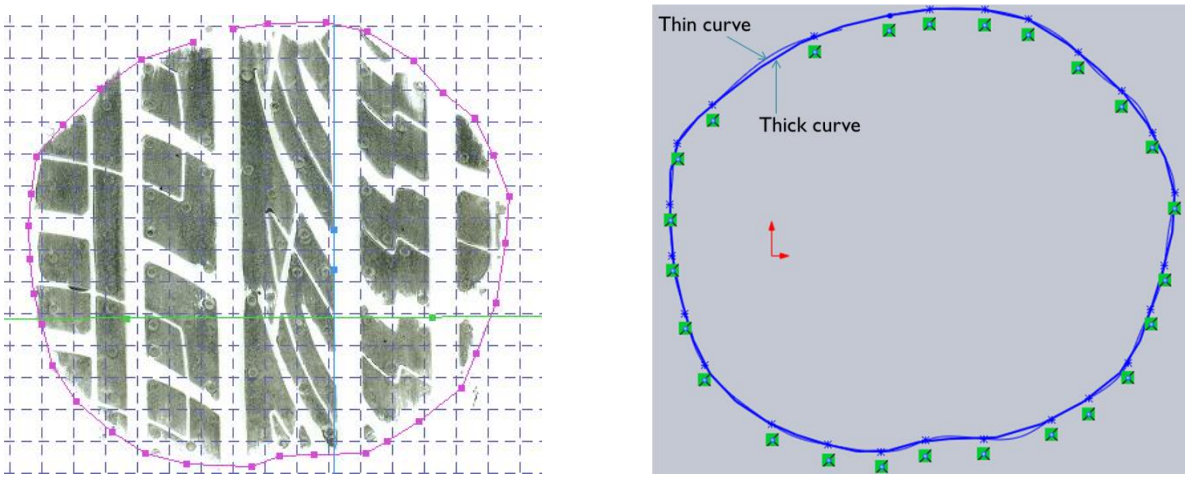

(a) (b)

Figure 4.22 (a) Extracting the outline of footprint, (b) Contact area calculating in Solidworks (the thick one is the curve from (a) and the thin one is the fitted curve in Solidworks)

In the FE simulation of footprint analysis, footprint shapes and pressure distributions at different operating conditions were easily acquired by using "CAREA" and "CPRESS" in ABAQUS, in which "CAREA" described the contact area between the tire and the road, while "CPRESS" illustrated the tire/road contact pressure distribution (Figure 4.23). As it is difficult to measure the pressure and force distribution in the contact region using experimental tests, it is necessary to use the tire model for the simulation. In addition, the corresponding area of footprint can also be calculated in the process of footprint analysis. In the first step of the procedure of footprint simulation, the inflation pressure was set as 200kPa, and different vertical loads of 1000N, 2000N, 3000N and 4000N were applied on the tire. In the second step, the vertical load was fixed as 3000N, and the inflation pressures of 80kPa, 120kPa, 160kPa and 200kPa were applied on the tire for footprint extraction.

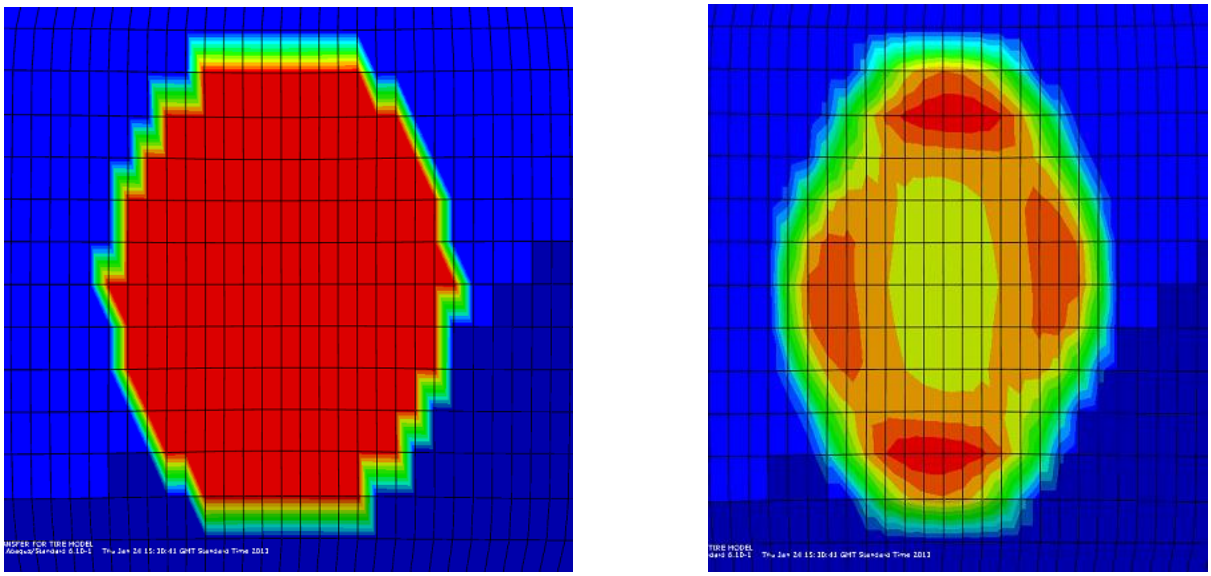

(a) (b)

Figure 4.23 (a) Footprint for "CAREA", (b) Footprint for "CPRESS"

As mentioned above, the area of footprint from experiment can be obtained using CAD software processing, and the FE analysis is also capable of predicting the area of tire/road contact patch. The validation of footprint areas at the operating conditions with different vertical loads is shown in Figure 4.24, while Figure 4.25 describes the validation of footprint areas at different inflation pressures. With the increase of vertical load, the tire has a higher deformation, which will lead to a greater contact area. On the other hand, the higher inflation pressure leads to a lower deformation, which makes the contact area smaller.

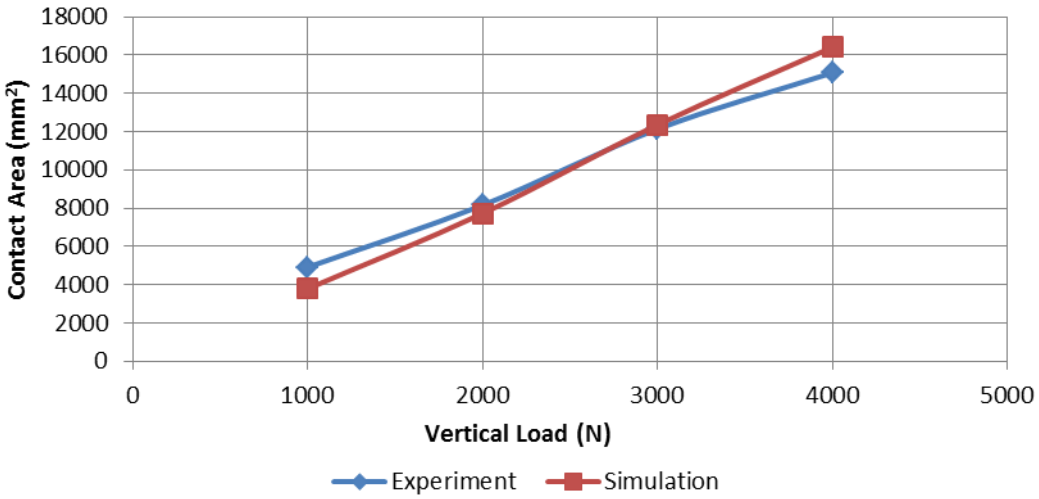

Figure 4.24 Footprint area at different vertical loads

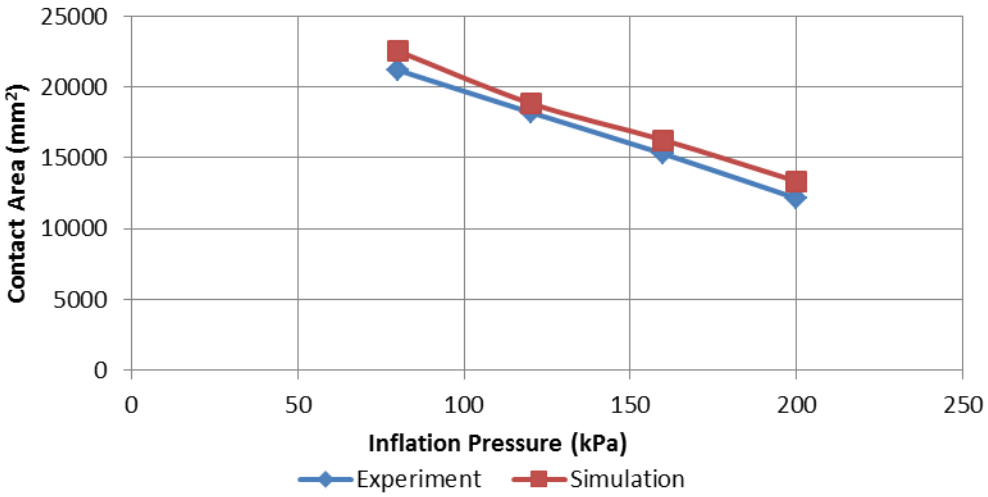

Figure 4.25 Footprint area at different inflation pressures

Figure 4.26 to Figure 4.28 show the footprint shapes at different vertical loads from simulations and experiments, while Figure 4.29 to Figure 4.32 describe the contact patch shapes at different operating conditions with different inflation pressures.

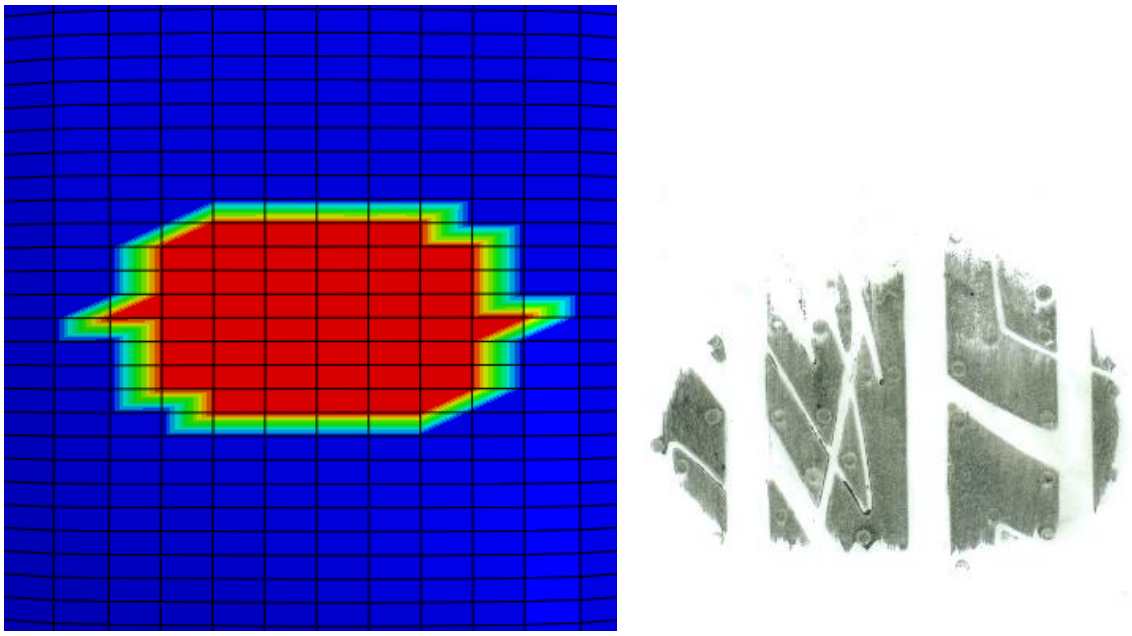

Figure 4.26 Footprint for 1000N vertical load, 200kPa inflation pressure

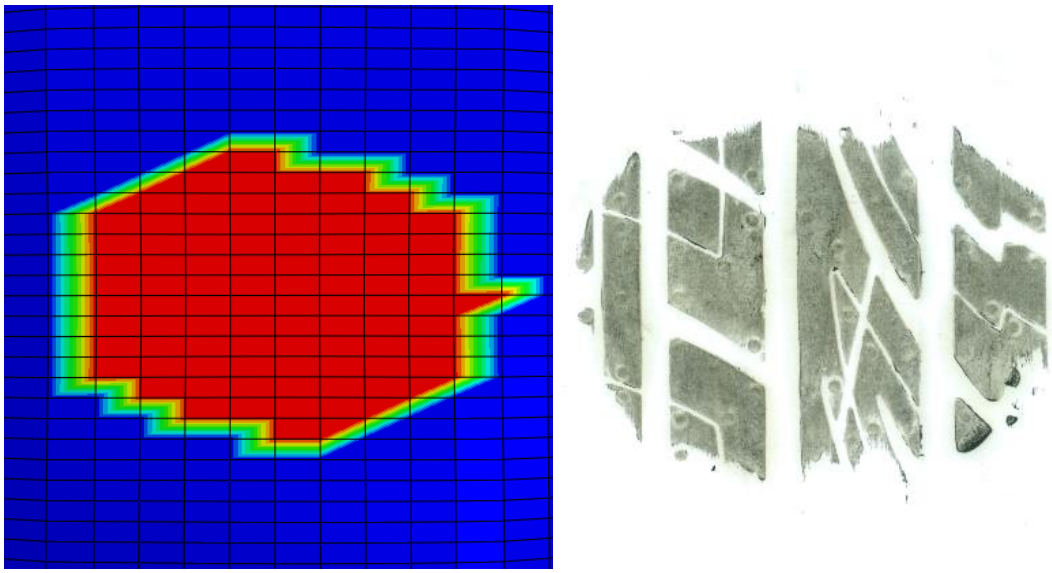

Figure 4.27 Footprint for 2000N vertical load, 200kPa inflation pressure

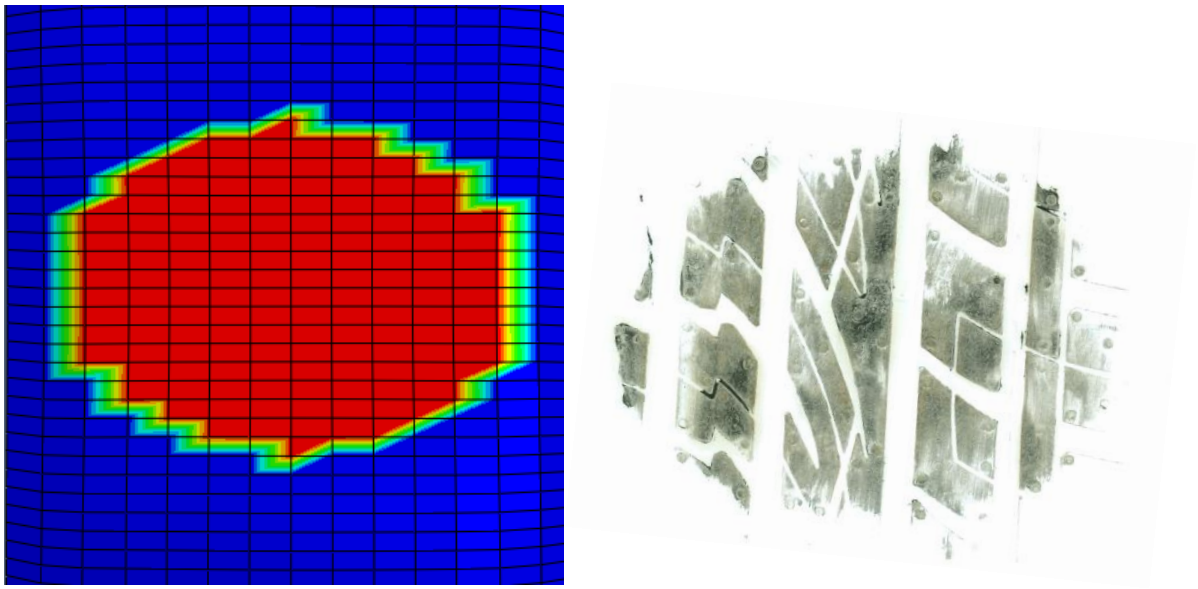

Figure 4.28 Footprint for 3000N vertical load, 200kPa inflation pressure

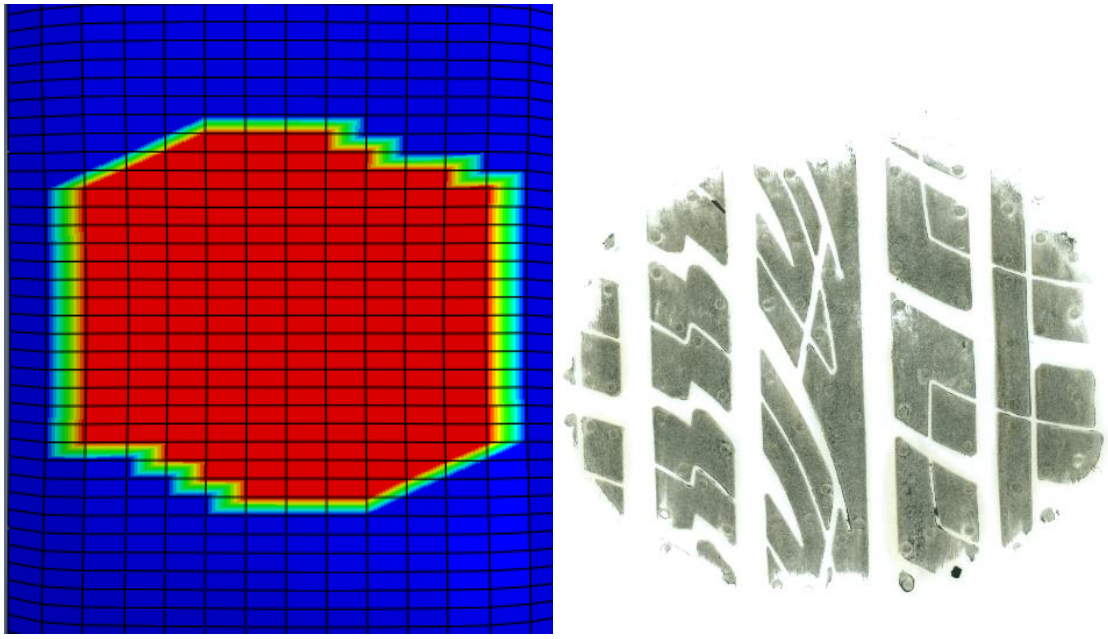

Figure 4.29 Footprint for 4000N vertical load, 200kPa inflation pressure

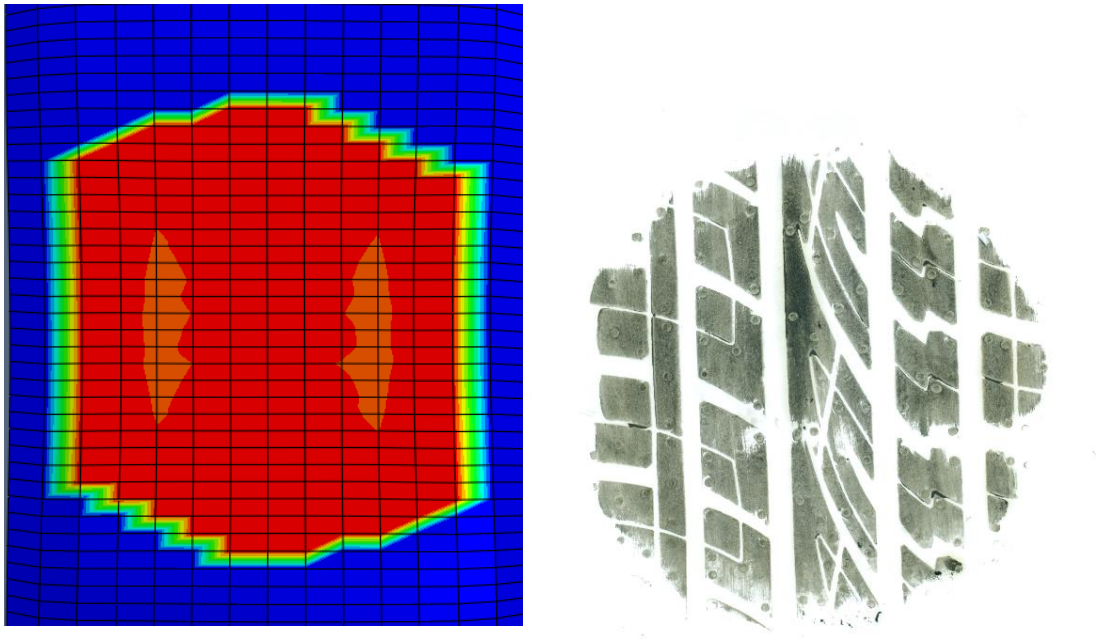

Figure 4.30 Footprint for 3000N vertical load, 80kPa inflation pressure

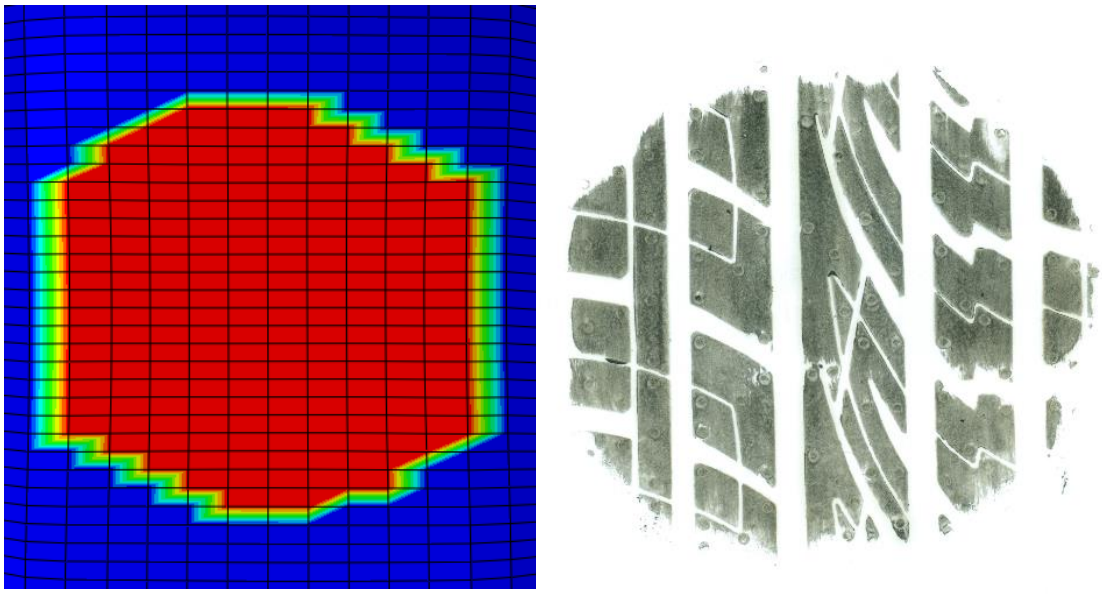

Figure 4.31 Footprint for 3000N vertical load, 120kPa inflation pressure

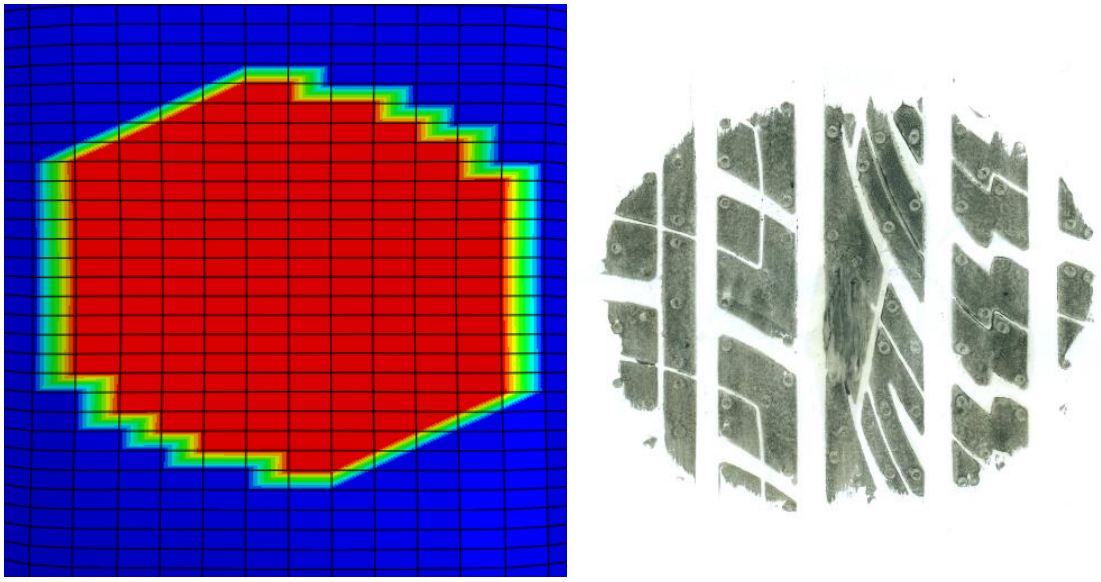

Figure 4.32 Footprint for 3000N vertical load, 160kPa inflation pressure

It can be seen that at the condition of 200kPa inflation pressure, the width of the contact patch is greater than the length of the contact patch for vertical loads of 1000N, 2000N, 3000N and 4000N. In addition, when the vertical load reaches 3000N, the contact width meets the shoulder of the tire, which is the reason that the footprint shape is not an elliptical form. For the condition with a vertical load of 3000N, when the inflation pressure is up to 80kPa, the contact length of the footprint is greater than the contact width, which is shown in Figure 4.32.

At a vertical load of 3000N or higher when the inflation pressure is not greater than 200kPa, the contact width reaches the shoulder of the tyre which leads to a contact shape different from the elliptical form.

4.5 Summary and conclusions

In this chapter, analysis of static properties of the tire has been presented. Inflation pressure analysis was conducted using 2D tire model. The 3D tire model was obtained by revolving the 2D axisymmetric tire model, and static stiffness and footprint were predicted using the 3D model.

Inflation pressure analysis was presented by comparing the tire cross-section shape variation at different inflation pressures. Since it was difficult to find the variation of the cross section shapes clearly, the specified tread node and sidewall node were taken to analyse the displacements of tire tread and sidewall at different inflation pressures.

In order to obtain accurate values for static stiffness and footprint, fine meshes were adopted on the contact region of the tire. Validation of vertical stiffness was carried out, and results show that the model is capable of predicting vertical stiffness at different operating conditions.

The footprint areas as well as the footprint shapes at different operating conditions were validated, and satisfactory results were obtained in the comparison between simulations and experiments.

Since the model is capable of prediction of static properties of the tire, it is deemed ready for the further analyses at steady-state rolling conditions and transient dynamic conditions.

Chapter 5 NUMERICAL ANALYSIS FOR STEADY-STATE ROLLING TIRES

5.1 Introduction

The cornering force characteristics of a tire have a significant effect on the directional control and handling stability of the vehicle, making it one of the most influential factors in full vehicle dynamics simulation.

Experimental tests for cornering properties were conducted at different operation conditions, such as different inflation pressures and different vertical loads. However, the effect of geometry and material properties of the tire on cornering properties in different conditions could not be carried out as many different tyres will have to be made to reflect the different geometries and material properties. ABAQUS™/Standard program is applied to meet the requirements which experimental tests cannot conduct. In this chapter, with numerical simulation using FE program, tire properties at steady-state rolling condition can be predicted efficiently. Parametric studies were also carried out to determine the factors affecting cornering force characteristics using FE analysis of the tire model.

5.2 Cornering simulation and validation

For the steady-state rolling simulation in ABAQUS™/Standard, the rigid body rotation is described in an Eularian approach, while the deformation of the tire measured relative to the rotating rigid body is described in Lagrangian approach. With this kinematic description, the steady-state rolling contact problem is converted to a purely spatially dependent contact simulation [118]. Therefore, the mesh needed to be refined only in the contact region, and the 3D model for steady-state rolling analysis is shown in Figure 5.1.

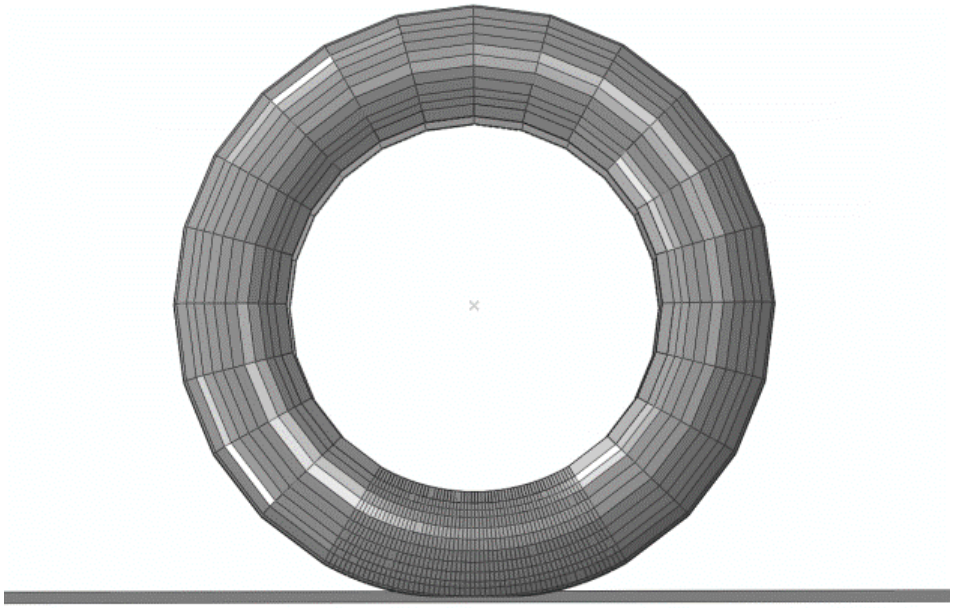

Figure 5.1 3D tire model for steady state analysis

Before the cornering simulation is carried out, tire braking and traction simulation is conducted in order to acquire the straight line free rolling solutions at a 0° slip angle, at which state no longitudinal force occurs. With the angular velocity variation from 6.5 rad/s to 8.5 rad/s, corresponding to full braking condition and full traction condition respectively, the angular velocity on the condition of free rolling is obtained as shown in Figure 5.2. By applying the free rolling angular velocity 7.66rad/s in cornering simulation, the cornering forces and aligning moments are calculated with the slip angle increasing from 0 to 7 degrees gradually by steering the tire on the flat road.

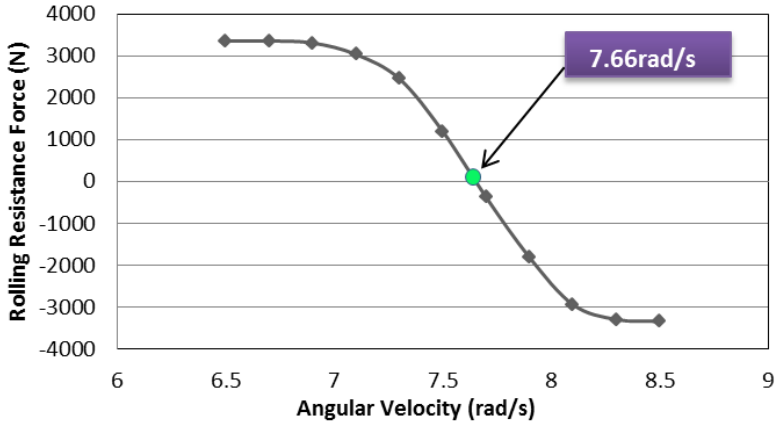

Figure 5.2 Rolling resistance forces at different angular velocities

In order to validate the results obtained using Finite Element method, cornering test of the tire 235/60 R18 was performed with an initial drum-road velocity of 10km/h. Pre-conditioning of the tire was carried out to make the tire warm up with a 0° slip angle, from which the test rig could reach a steady state condition. Before steering input was applied in the cornering behaviour test, a vertical load of 3000N and an inflation pressure of 200kPa were applied to the tire. The tire/road contact in the cornering simulation and measurement and schematic representation of cornering test rig are illustrated in Figure 5.3. Tire rolling test results were obtained beginning with the cornering force at 0° slip angle, and then the tire was steered gradually from 0° to 7° to obtain the cornering characteristics in terms of cornering forces.

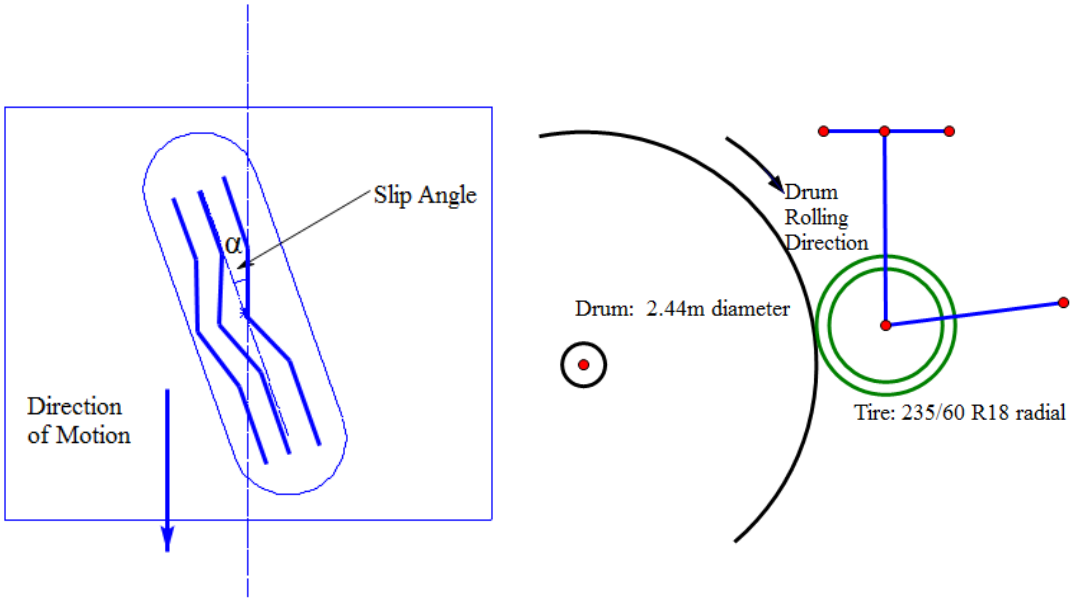

Figure 5.3 (a) Tire/road contact for cornering simulation and measurement, (b) Schematic representation of tire rolling

Each test result is recorded for 30s and the average values of test data measured in the experiments represents the cornering forces used for comparison with the FE modelling results. Tire rolling speed, vertical load and inflation pressure were varied in the tire rolling test in order that tire cornering properties at different conditions and parameters could be analysed. The simulation results of cornering stiffness of the tire model and the corresponding experiment results are compared with each other, which are shown in Figure 5.4. Particularly, in order to reflect reasonable tire/road contact situation, the frictional

coefficient applied in the tire, with relation to the cornering test, was set as 1.0. From the comparison between simulation results and measurement results, it can be seen that the predicted cornering forces agree well with the test data at both vertical load of 3000N and 2000N conditions.

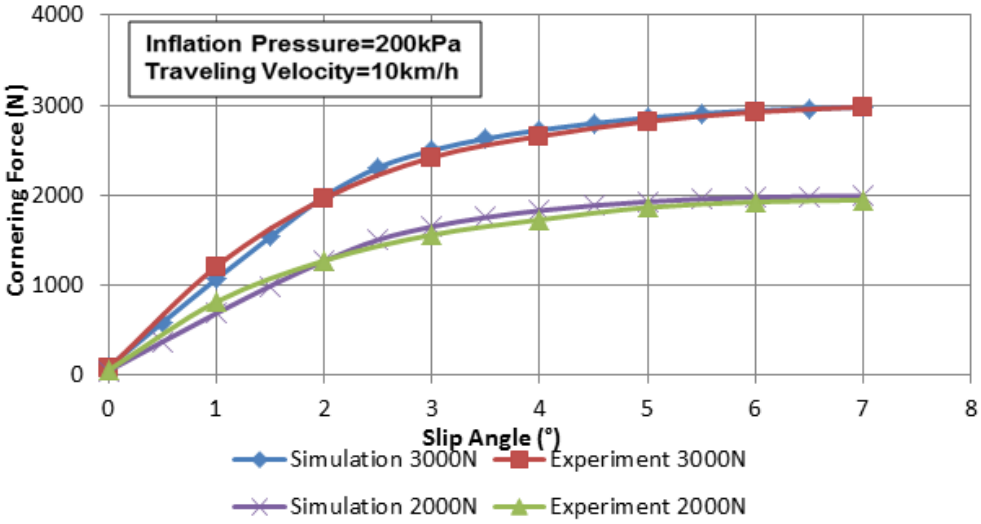

Figure 5.4 Tire cornering forces at different slip angles

5.3 Parametric investigation

In order to investigate the influence of tire parameters on the cornering behaviour, different tire models with different parameters are simulated and analysed. The parametric studies are performed by using FE tire modelling and analysis, in which the parameters are varied and cornering properties of the tire are compared with the magnitude of variations of the parameters. Normally, most of the studies are concentrated on the effect of vertical load (radial load) and inflation pressure, while the frictional coefficient, geometry properties (layup structures) and material properties are usually ignored in cornering behaviour research studies. In this study, these parameters are considered and analysed as potential factors influencing the cornering properties. The cornering properties are calculated and analysed with different conditions and parameters, which can be divided into two categories. The vertical load, inflation pressure, frictional coefficient are classified as external operating

conditions, while the geometry and material properties of the tire could be considered as internal design characteristics of the tire.

5.3.1 Effect of vertical load

The effect of vertical (radial) load on the cornering behaviour was investigated in terms of cornering force and aligning moment. Figure 5.5 shows the simulated cornering forces at four different vertical loads (2000N, 3000N, 4000N, 5000N) under an inflation pressure of 200kPa and a travel speed of 10km/h, while Figure 5.6 shows the simulated aligning moment at the four different vertical loads with the same inflation pressure and travel velocity. With the increasing slip angle, the cornering forces increase linearly till the slip angle of 2.5 °, and then the growth of cornering force tends to slow down. For the cornering stiffness and aligning moment variation with different vertical loads, it can be concluded that higher vertical load produces higher cornering stiffness and higher peak of aligning moment.

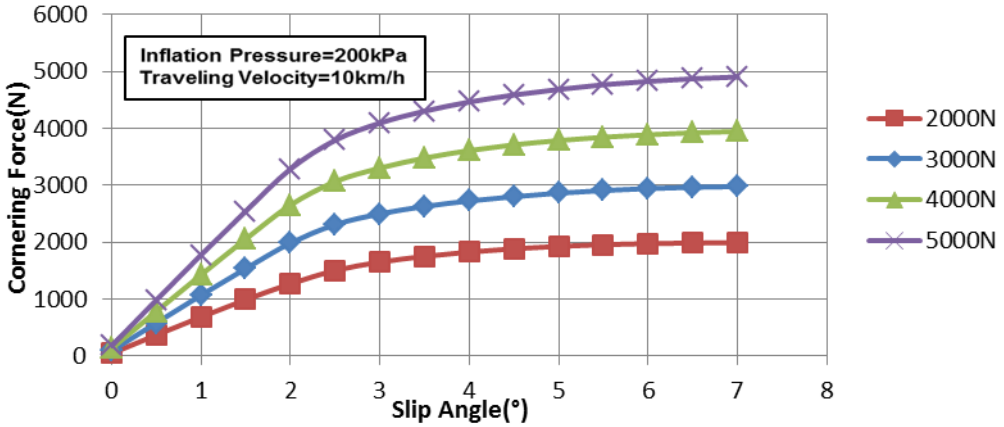

Figure 5.5 Cornering Forces at different vertical loads

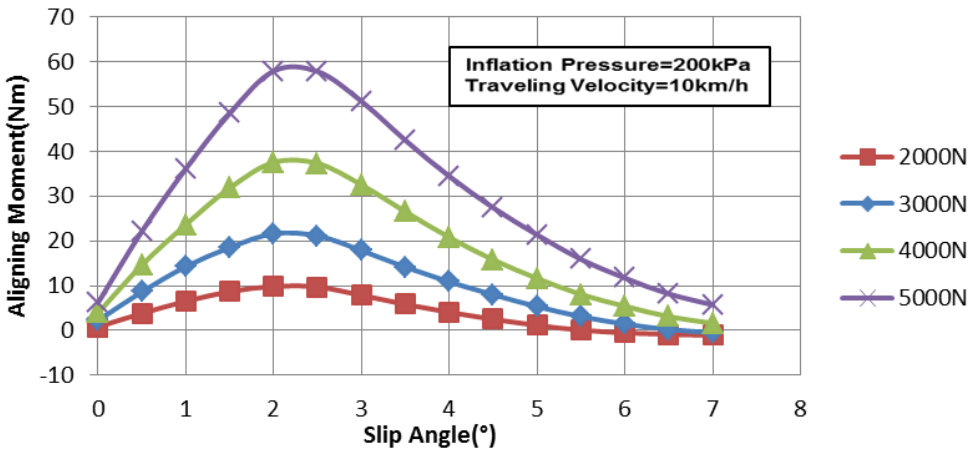

Figure 5.6 Aligning Moment at different vertical loads

The relationship between cornering properties and tire/road contact patch was investigated. As shown in Figure 5.7, where d represents the deformation of the tire in vertical direction, R_0 is the radius of the tire, and L is the contact length in the rolling direction. It is no difficulty to acquire L_c , which is as follows

$$L_c = 2\sqrt{R_0^{\,2} - (R_0 - d)^2} \qquad (5\text{-}1)$$

Table 5.1 shows the effect of the length of contact patch on cornering behaviour, from which it can be seen that with the increase of the tire/road contact length, the computed cornering stiffness is becoming larger.

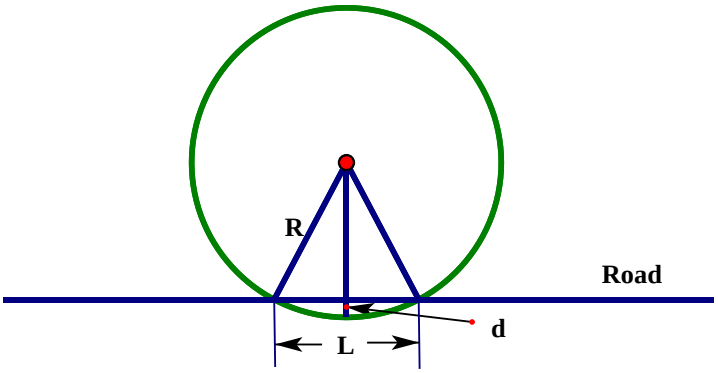

Figure 5.7 Tire/Road deformation and contact length

Table 5.1 Contact lengths and cornering properties under different vertical loads

Vertical Load	Contact Length	Cornering Stiffness	Peak of Aligning Moment
2000N	170.7mm	0.6284kN/deg	9.87Nm
3000N	201.4mm	0.9633kN/deg	21.62Nm
4000N	227.8mm	1.2801kN/deg	37.55Nm
5000N	251.1mm	1.5765kN/deg	57.94Nm

5.3.2 Effect of inflation pressure

Figure 5.8 shows the simulation results of the effect of inflation pressure on cornering stiffness and aligning moment, at the constant vertical load of 3000N and road speed of 10km/h. By investigating the cornering behaviour of the rolling tire with the increase of slip angle, the simulation results of cornering force and aligning moment from FE tire model and

experimental test show the same trend, which are illustrated in Figure 5.8 and Figure 5.9. With the increasing inflation pressure, the cornering stiffness decreases, and the divergence of cornering forces at different inflation pressure is more evident when the slip angle is between 2 ° and 4 °, compared with the divergence at a slip angle of less than 2 ° or greater than 4 °. In addition, as seen in

Figure **5.10**, higher inflation pressure leads to lower aligning moment.

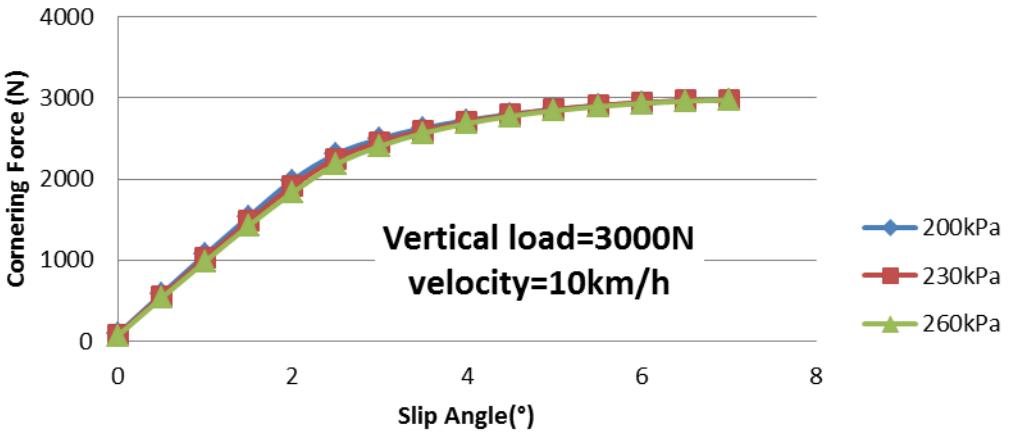

Figure 5.8 Cornering forces at different inflation pressures (Simulation)

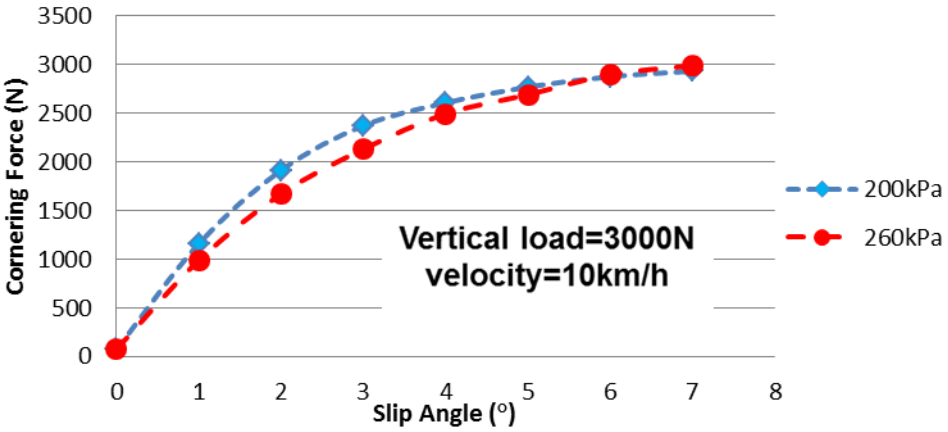

Figure 5.9 Cornering forces at different inflation pressures (Physical Testing)

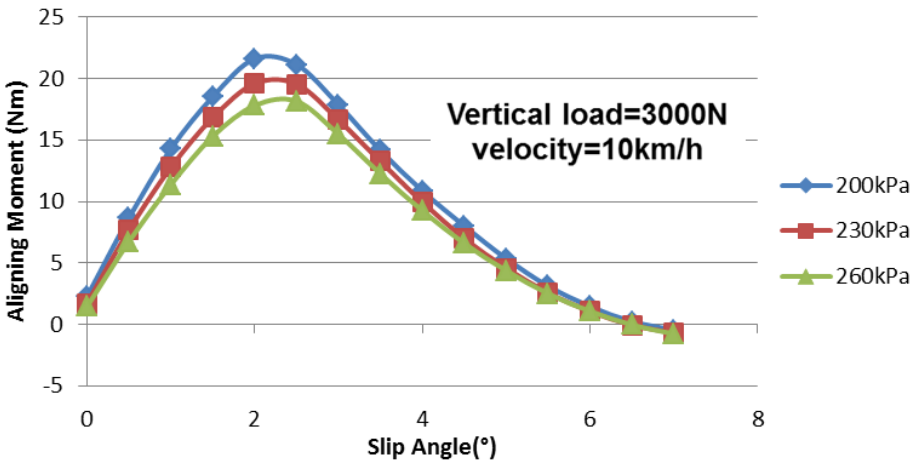

Figure 5.10 Aligning moment of with different inflation pressure (simulation)

Due to the decrease of the inflation pressure, the length of the contact patch tends to increase, which is shown in Table 5.2. Therefore, the increase of the cornering stiffness and peak of aligning moment can be attributed to the increase of the tire/road contact length.

Table 5.2 Contact length and cornering properties under different inflation pressure

Inflation Pressure	Contact Length	Cornering Stiffness	Peak of Aligning Moment
200kPa	201.4mm	0.9663kN/deg	21.6192Nm
230kPa	191.4mm	0.9338kN/deg	19.5990Nm
260kPa	182.9mm	0.9042kN/deg	17.8064Nm

5.3.3 Effect of tire velocity

The effect of tire travelling velocity on cornering properties was investigated by FE analysis and experimental test. By applying different travelling velocities of 10km/h, 15km/h and 20km/h in the FE tire model, the cornering stiffness show slight sensitivity at these three conditions of different rolling velocities (Table 5.3).

Table 5.3 Cornering forces under different travelling velocities

slip Angle	*velocity of 10km/h* Corn. Forces	*velocity of 15km/h* Corn. Forces	*velocity of 20km/h* Corn. Forces
0	90.9268	94.8726	84.2678
1	1068.47	1066.21	1064.27
2	1984.22	1978.80	1985.19
3	2497.97	2502.10	2495.23
4	2724.71	2723.67	2724.02
5	2861.51	2858.34	2852.48
6	2942.62	2936.72	2932.21
7	2977.35	2970.50	2970.74
Corn. Stiffness (kN/deg)	**0.963**	**0.963**	**0.963**

5.3.4 Effect of tire-road friction

In the FE tire model, a friction coefficient of 1.0 was used for simulation of the tire cornering behaviour. As one of the important parameters in tire rolling simulation, the effect of friction on cornering force and aligning moment was investigated. From Figure 5.11 and Figure 5.12, it can be seen that higher friction coefficient leads to higher cornering force. In addition, with the increase of the friction coefficient, the peak of aligning moment increases from 9.61Nm to 21.62Nm.

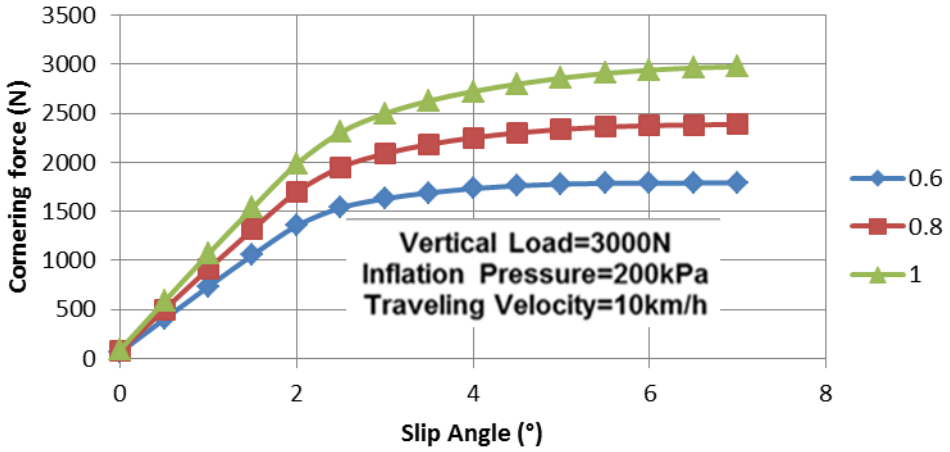

Figure 5.11 Cornering force at the condition with different friction coefficient

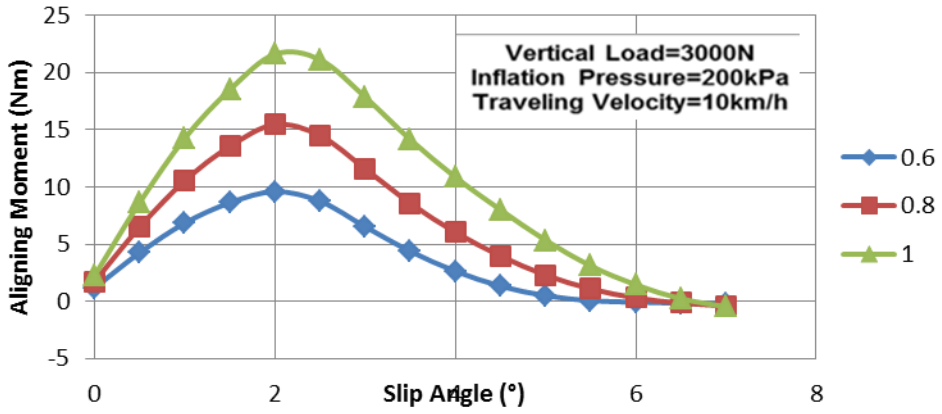

Figure 5.12 Aligning moment at the condition with different friction coefficient

5.3.5 Effect of internal tire design characteristics: geometry and material properties

FE tire model is very efficient and effective in simulating the effect of tire geometry and material properties on cornering characteristics; characteristics which could not be conveniently determined by experimental testing because many tires will have to be made to reflect the different geometries and material properties. As mentioned, the geometry and

material properties of the tire could be considered as internal component characteristics of the tire.

5.3.5.1 Different Steel Belt Angle

By modifying the steel belt angle in the tire construction, the cornering stiffness is modified as well. Under an inflation pressure of 200kPa, a vertical load of 3000N, and a road speed of 10km/h, the cornering stiffness values obtained are 0.9123kN /deg, 0.9466kN/deg and 0.9511kN /deg when the corresponding belt angles are 10deg, 20deg, and 30deg, respectively (Figure 5.13). In addition, the sensitivity of aligning moment to belt angle is shown in Figure 5.14. The peak value of aligning moment with a belt angle of 10 degrees is observed to be a little higher than that with a belt angle of 20 degrees and 30 degrees.

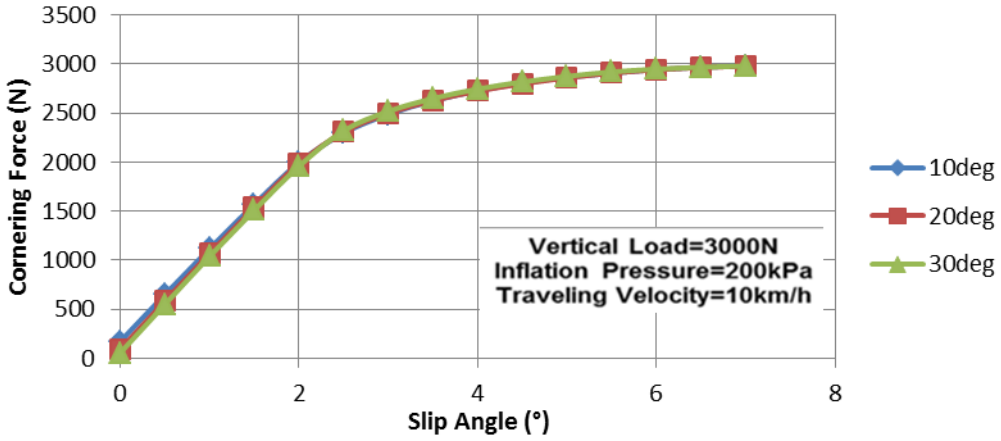

Figure 5.13 Cornering forces with different belt angles

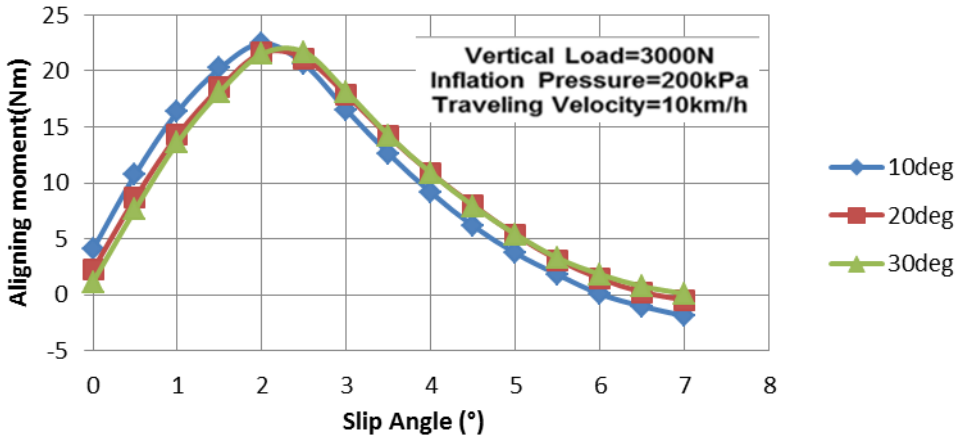

Figure 5.14 Aligning moment with different belt angles

5.3.5.2 Different Steel Belt Spacing

By modifying the spacing of adjacent bundles of steel belt, the computed cornering force and aligning moment show very small sensitivity, which are described in Table 5.4 and Figure 5.15. In addition, the cornering stiffness of the tire model with broader belt space has a 0.6750% difference compared with that of the tire model with narrower belt space.

Table 5.4 Cornering force at the condition with different steel belt space

Slip Angle	*Space= 1.8882mm* Corn. Force	*Space=2.8882mm* Corn. Force	Deviation of Corn. Forces (%)
0	90.9309	85.9608	-5.4658
1	1068.47	1057.77	-1.00143
2	1984.22	1962.92	-1.07347
3	2497.97	2500.65	0.107287
4	2724.71	2736.02	0.41509
5	2861.51	2870.17	0.302637
6	2942.62	2945.23	0.088696
7	2977.35	2979.67	0.077922
Corn. Stiffness (kN/deg)	**0.963**	**0.9568**	**0.6750**

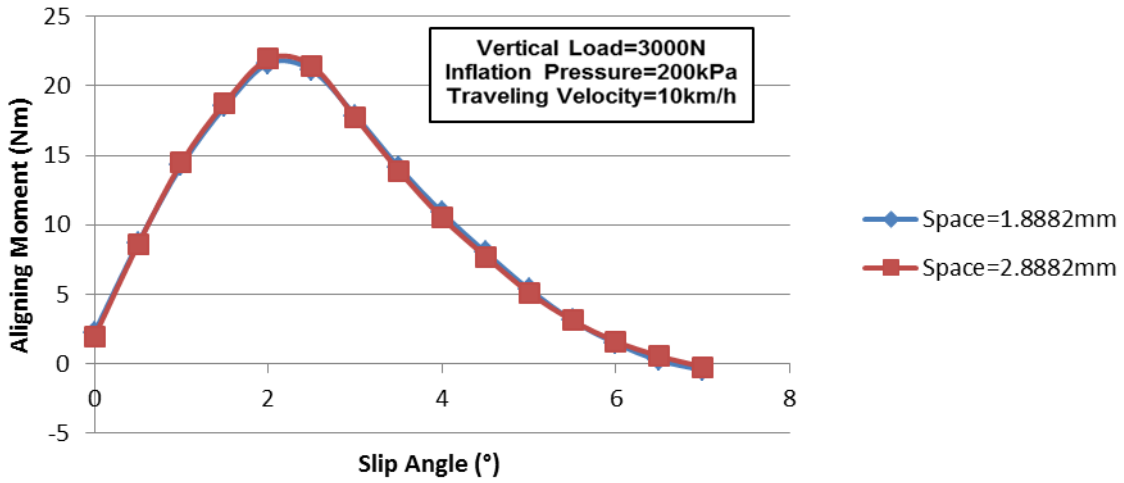

Figure 5.15 Aligning moment with different steel belt space

5.3.5.3 Different rubber densities

Table 5.5 shows the effect of rubber density of the tire on cornering force. From the deviation of cornering forces from the tire models with different rubber material properties, there is small sensitivity of cornering force when different kinds of rubber density are applied on the

tire model. As shown in Table 5.5, the difference of cornering stiffness of the tire models with different rubber density is only 0.0311%. In addition, the difference between the aligning moments at the two conditions with different values of rubber density is considerably small, which is shown in Figure 5.16.

Table 5.5 Cornering forces at the condition with different rubber densities

Slip Angle	*Rubber density =1200kg/m^3* Corn. Force	*Rubber density =2400kg/m^3* Corn. Force	Deviation of Corn. Forces (%)
0	90.9268	86.7006	4.647915
1	1068.47	1061.37	0.664502
2	1984.22	1977.23	0.352279
3	2497.97	2494.22	0.150122
4	2724.71	2718.88	0.213968
5	2861.51	2858.40	0.108684
6	2942.62	2939.50	0.106028
7	2977.35	2974.03	0.111509
Corn. Stiffness (kN/deg)	**0.9633**	**0.9630**	**0.0311**

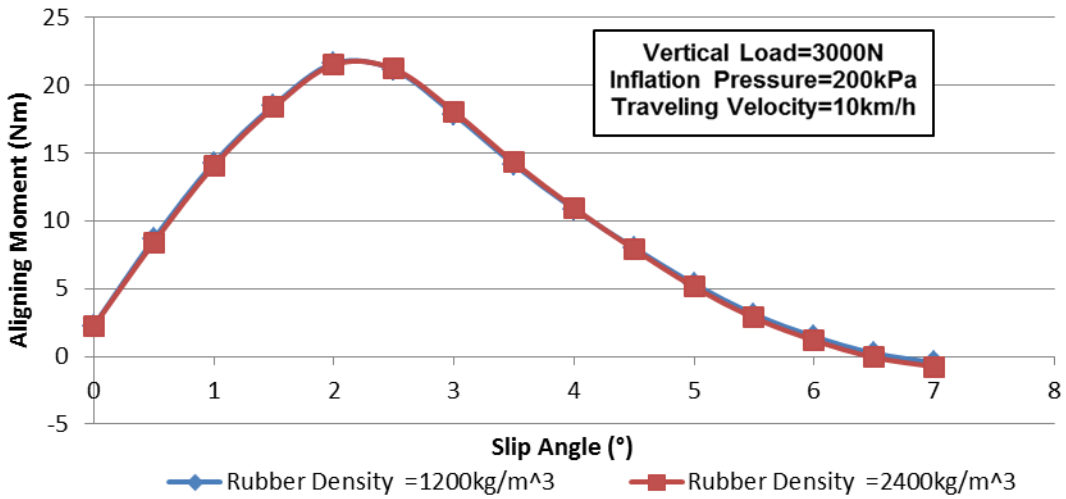

Figure 5.16 Aligning moment at the condition with different rubber densities

5.3.5.4 Different carcass densities

In order to investigate the effect of carcass density on tire cornering properties, cornering force and aligning moment were computed in the conditions with different carcass densities of the tire. It can be seen in Table 5.6 that the predicted cornering forces in the two conditions

with different slip angles generate a maximum deviation up to 4.95%, and the difference of the cornering stiffness between the tire models with different carcass densities is only 0.2595%, which shows very small sensitivity. What's more, the tire model with higher carcass density leads to a higher cornering stiffness, as well as the peak of aligning moment, which is shown in Figure 5.17.

Table 5.6 Cornering forces at the condition with different carcass densities

Slip Angle	*Carcass density =1500kg/m^3* Corn. Force	*Carcass density =2000kg/m^3* Corn. Force	Deviation of Corn. Forces (%)
0	90.9268	86.4297	4.945846549
1	1068.47	1065.09	0.316340187
2	1984.22	1984.5	-0.014111338
3	2497.97	2498.84	-0.034828281
4	2724.71	2723.62	0.040004257
5	2861.51	2852.77	0.305433145
6	2942.62	2935.21	0.251816409
7	2977.35	2971.48	0.197155188
Corn. Stiffness (kN/deg)	**0.9633**	**0.9658**	**0.2595**

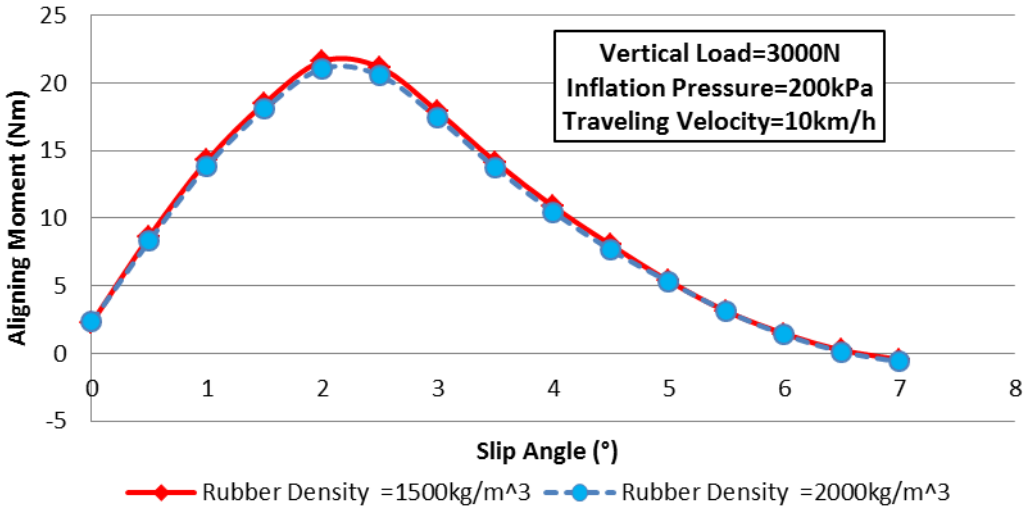

Figure 5.17 Aligning moment at the condition with different carcass densities

5.3.5.5 Different Hyperelastic properties of tread rubber

Three different rubber materials were used for tire cornering behaviour modelling, the properties of the rubber components were defined in terms of hyperelastic and viscoelastic properties. Hyperelatic properties of the sidewall and tread were selected to compare the

cornering properties of the tire models with different rubber characteristics. The test data and rubber material models of the two different hyperelastic properties are illustrated in Figure 5.18, from which it can be seen that for the same strain of 0.9, the corresponding stress for tread rubber is higher than that of the sidewall rubber.

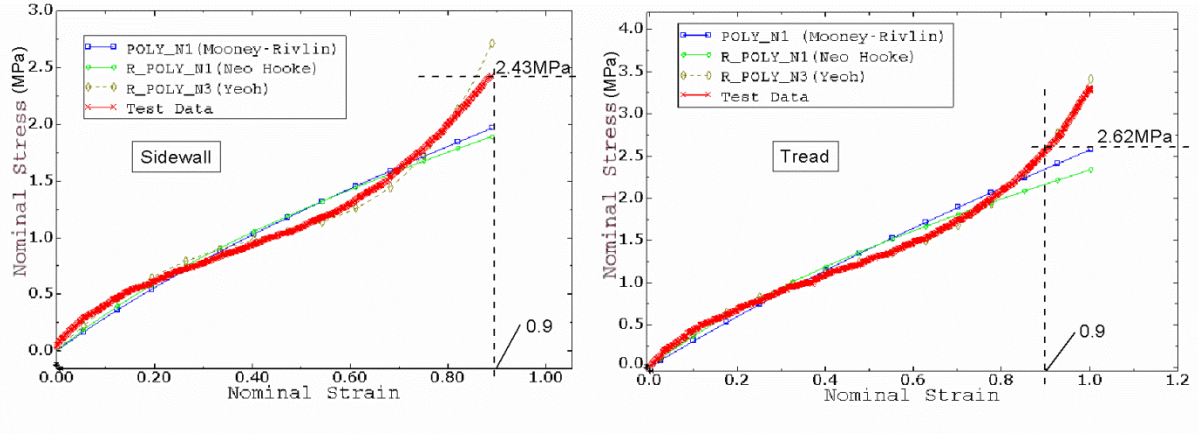

Figure 5.18 Relationship between strain and stress for the sidewall rubber and tread rubber

In Table 5.7, hyperelastic#1 represents the hyperelastic property of the sidewall, while the tread hyperelastic property was specified as hyperelastic#2. The hyperelastic data of the sidewall was applied on the tread section to have a comparison with the original tire model, in which hyperelastic property of tread rubber was applied on the tread section. Results in Table 5.7 show that there is a great difference between the cornering forces obtained from the simulation applying the two different hyperelastic properties on the tread section. The difference of the cornering stiffness for the two cases is up to 10.97%, and the peak value of aligning moment applying hyperelastic#2 is much higher than that using hyperelastic#1 property, which is shown in Figure 5.19.

Table 5.7 Cornering forces at the conditions with different hyperelastic properties on tread

Slip Angle	*Hyperelastic#1 on tread* Corn. Force	*Hyperelastic#2 on tread* Corn. Force	Deviation of Corn. Forces (%)
0	58.9329	90.9268	35.18644
1	929.002	1068.47	13.05306
2	1742.62	1984.22	12.17607
3	2304.43	2497.97	7.747891
4	2578.04	2724.71	5.382958
5	2743.78	2861.51	4.114261
6	2844.63	2942.62	3.330026

7	2908.87	2977.35	2.300032
Corn. Stiffness (kN/deg)	**0.8576**	**0.9633**	**10.9727**

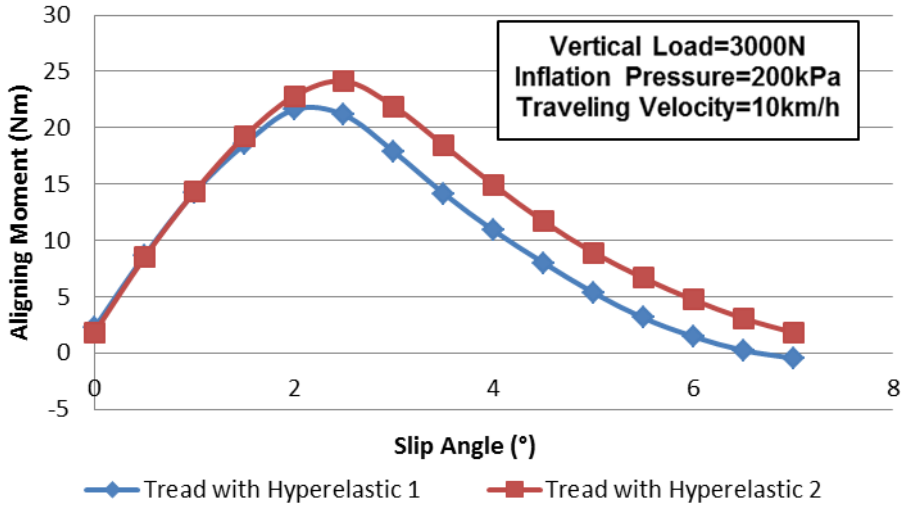

Figure 5.19 Aligning moment at the condition with different hyperelastic properties on tread

5.4 Summary and conclusions

Based on the detailed FE tire model with had been validated using tire static properties, cornering simulation was carried out using steady-state rolling analysis. Braking and traction simulation was conducted initially in order to acquire free rolling velocity of the running tire. Cornering forces and aligning moment were obtained by steering the tire from 0° to 7° gradually. Meanwhile, the physical cornering tests were conducted in order that cornering forces at different inflation pressures and vertical loads were obtained. Cornering stiffness was derived in terms of the relationship between cornering forces and slip angles. Validation of the cornering properties at different vertical loads and inflation pressures show that the cornering stiffness agrees well with the experimental results under the operating conditions.

Parametric studies were carried out to determine the factors affecting cornering force characteristics using FE analysis of the tire model. Results show that higher vertical load and higher friction coefficient lead to higher cornering force, producing higher cornering stiffness

and higher peak of aligning moment, but higher inflation pressure leads to lower cornering stiffness. In addition, the sensitivity of cornering stiffness to tire travelling velocity is very slight.

For the sensitivity of cornering performance to tire material properties and structural layup, the results show that the steel belt angle of 30 degree gives bigger cornering stiffness than that of 10 degree and 20 degree, and other parameters such as steel belt spacing, tread rubber density and carcass reinforcement density have very little effect on cornering properties. However, the hyperelastic property of the tread section shows great sensitivity on the cornering properties.

Chapter 6 TRANSIENT DYNAMIC ANALYSIS OF ROLLING TIRE

6.1 Introduction

In this chapter, transient dynamic analysis is presented in section 6.2 for tire traversing obstacles with different heights using ABAQUS^{TM}/Explicit. It is also noted that the initial inputs (rolling velocity, tire vertical deflection, etc.) of the tire model is generated using ABAQUS/Standard. Experimental procedure is given to validate the transient tire model. Parametric studies of transient dynamic responses at different traveling velocities and different road obstacles are also presented.

In addition, prediction of rolling resistance generated on the uneven road is presented in section 6.3. In this study, only the energy dissipation generated by the longitudinal forces against motion because of road unevenness is considered in the study. Therefore, the rolling resistance can be obtained based on the transient dynamic responses.

6.2 Transient dynamic performance validation for tire rolling obstacles

6.2.1 Experimental test

In order to examine the transient dynamic responses of a tire rolling over road obstacles and identify the capability and accuracy of the FE tire model in transient dynamic analysis, experimental tests were carried out for a tire traversing obstacles. The tests were carried out under laboratory conditions on the experimental test rig whose schematic representation is illustrated in Figure 6.1.

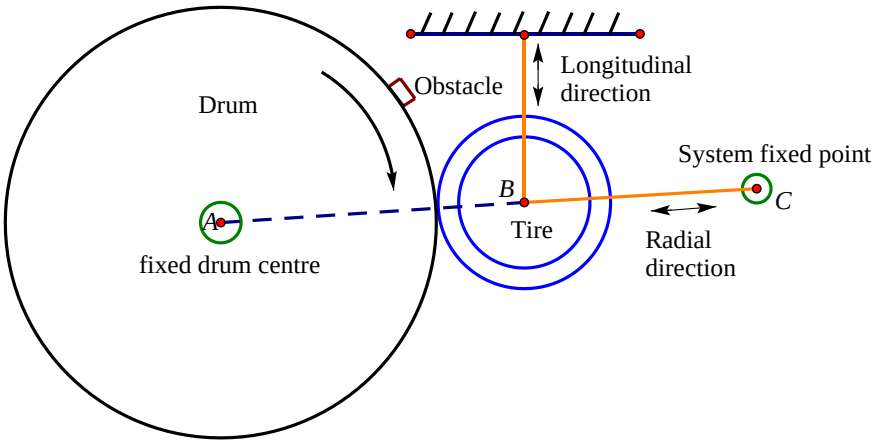

Figure 6.1 Schematic transient dynamic test rig for tire rolling over obstacles

The characteristics and conditions of the test rig are as follows:

- A large drum with a diameter of 2.44m was used to represent the flat road. The large diameter of the drum ensures that there is only slight difference between the road and the large drum for tire/road contact. The error in contact length is less than 0.1%.
- The position of the tire in the longitudinal direction and radial direction is flexible, but for this study, the displacement of the tire centre is fixed in the tire rolling tests.
- The fixed drum centre A, tire centre B and the system fixed point C should be adjusted to be in the same line in order that accurate responses data can be obtained.
- The cleat is made of stiff metal material to make sure no deformation occurs on the cleat when the tire rolls over the obstacle. Also, the cleat is attached to the

circumference of the drum, and positioned perpendicular to the circumferential direction of the rolling drum in order to avoid tire/road contact at an oblique angle.

- The drum rotation is controlled precisely using digital control equipment and the tire moves with the rotation of the drum when they are in contact with each other. The velocity of the tire rotation can be controlled by adjusting the rotational velocity of the drum.
- Two strain gauge based load cells are used in the experiments, which can measure the longitudinal and radial forces generated at the hub of the tire. The frequency responses of the transducers are 0 to 2 kHz. A time domain system was used to record the response data at a rate of 1000 samples per second.

The tire 235/60 R18 was inflated to 200kPa initially, and then the tire was pushed against the static drum until a radial force of 3000N was achieved. The radial displacement of the tire was recorded, which would be used after the drum started to rotate. The tire was then retracted so that no contact force was generated between tire and the drum and then the drum was set to rotate to reach a specified constant velocity, after which the tire was pushed toward the flywheel to achieve the displacement previously recorded, and the tire hub position was fixed in order to make the tire radial height constant when the tire rolls over an obstacle. Sufficient time was allowed for the tire to warm up and attain a constant rolling velocity. The transient dynamic responses in terms of longitudinal and radial forces at different operating conditions were captured and recorded by using a data acquisition system.

6.2.2 Numerical dynamic simulations

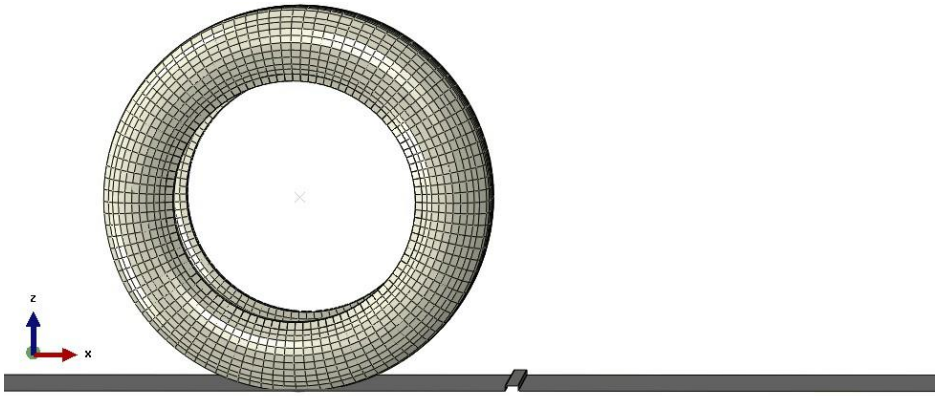

Figure 6.2 tire/road contact model in FE program

As mentioned above, in order to carry out explicit dynamic analysis for tire rolling over obstacles, ABAQUS/Standard is firstly applied to derive the free rolling velocity and tire deformation, which is taken as the initial condition for explicit dynamic simulation. In the tire rolling simulation, the road was modelled as an analytical rigid flat surface, which is illustrated in Figure 6.2. In addition, the tire-rim assembly was simplified and a rigid body was created between the rim reference node and tire-rim interface nodes using the tie function in ABAQUS™. The numerical dynamic simulations of tire rolling over obstacles were conducted in the following manner. First, quasi-static analysis was carried out in ABAQUS™/Standard by inflating the tire to 200kPa and pushing the road surface toward the hub of the tire with a deformation to achieve a vertical load of 3000N, the results of which would be used for an initial condition for steady-state simulation. The second part of the simulations is steady-state analysis of the rolling tire, in which braking and traction simulation was conducted to obtain the free rolling condition, which was taken as initial conditions in the transient dynamic analysis. Figure 6.3 shows a braking and traction process to derive the angular velocity at free rolling condition with a traveling velocity of 10km/h, and the desired angular velocity is determined from the free rolling velocity of the tire. In order to obtain the free rolling angular velocity, the *TRANSPORT VELOCITY was used to define the angular velocity variation. In this study, the angular velocity was set from 6.5 rad/s to 8.5 rad/s when the travelling velocity was 10km/h. The results derived in steady-state

dynamic rolling analysis (free rolling velocity, tire/road contact situation, etc.) were imported to simulate tire transient rolling from ABAQUS™/standard to ABAQUS™/Explicit.

ABAQUS™/Explicit is particularly well-suited for simulate transient dynamic events. One of the important abilities of ABAQUS™/Explicit is to effectively handle severely nonlinear behaviour such as contact. ABAQUS/Explicit can readily analyse problems involving complex rolling contact interaction between independent bodies [118]. The tire rolling over an obstacle is a complex transient dynamic event and suitable for be carried out using ABAQUS™/Explicit program. In the transient dynamic model using explicit integration, the road was adjusted to an appropriate position in order that the preload of 3000N was achieved, and the cleat was positioned ahead of the tire to make sure the rolling tire can reach a steady state condition before it impacts the cleat. In addition, the tire was allowed to roll for some time after passing the cleat in order for steady state to be reached after dissipation of the transient dynamic responses. In the transient dynamic simulation using ABAQUS™/Explicit program, the simulation time was set as 0.5 seconds, and a High Performance Computing (HPC) cluster with 16 CPUs was used for this simulation. Because of the computing power of the HPC system, the simulation was completed in a CPU time of 3 hours and 42 minutes.

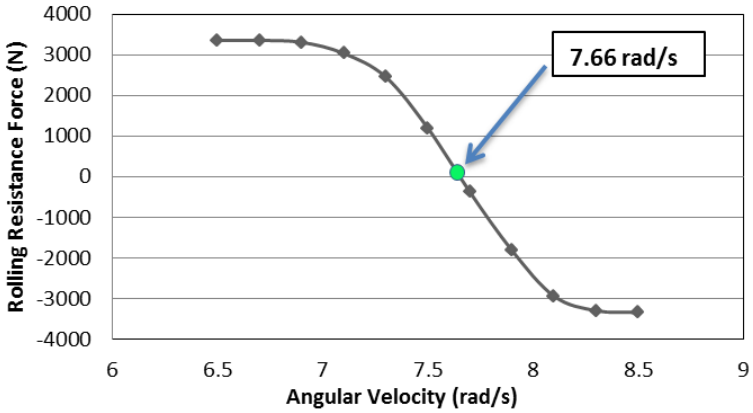

Figure 6.3 Rolling resistance force at different angular velocities

Rectangular cleats with different height values in accordance with the experimental conditions were adopted in the simulations. Besides, the height of the hub was fixed in the

process of tire rolling so that the tire hub could not move in the vertical direction. Three different cleats of 25mm × 10mm, 25mm × 20mm and 25mm × 25mm were selected to represent road obstacles, which are shown in Figure 6.4. Figure 6.5 to Figure 6.6 describe the transient dynamic responses of tire rolling over these three obstacles with traveling velocities of 10km/h, 20km/h and 30km/h. The inflation pressure and initial vertical load were set as 200kPa and 3000N respectively in both experiment and simulation. The transient dynamic responses were expressed in terms of longitudinal and vertical spindle forces. By comparison between the experimental test data and simulation results, the variations of dynamic responses of the spindle forces show good agreement between the numerical simulations and experimental tests, which give confidence that the model well represents the tire behaviour in various transient conditions. However, for the responses after impacting obstacles, the numerical predicted values are shown to be higher than the experimental results. This demonstrates that the artificial proportional damping used for the numerical stability purposes is somewhat underestimated. On the other hand, for lower rolling velocity (10km/h), the vertical impact loads are a little lower than the experimental values. This may be attributed to inaccuracy in predicting the bending stiffness of the belts.

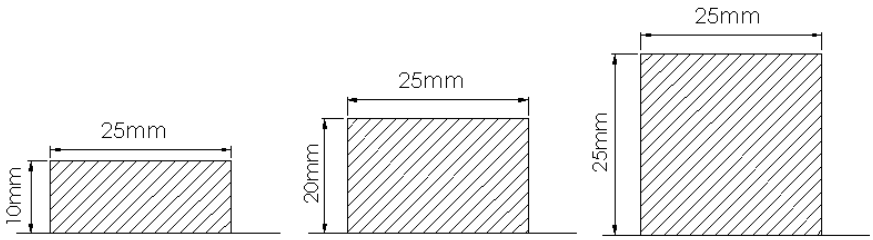

Figure 6.4 Road obstacles used for transient dynamic simulations

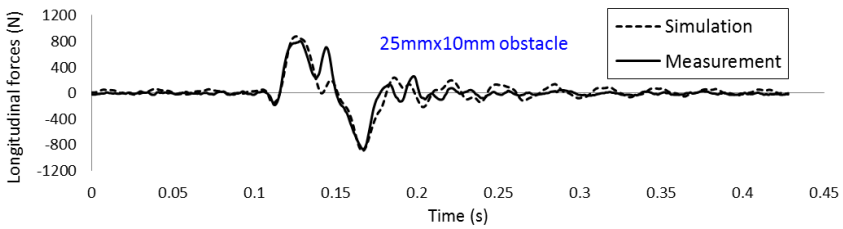

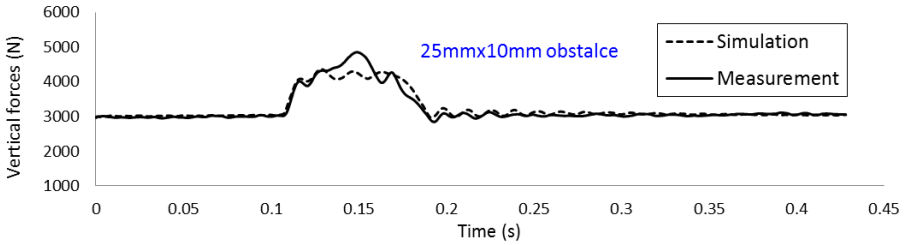

(a)

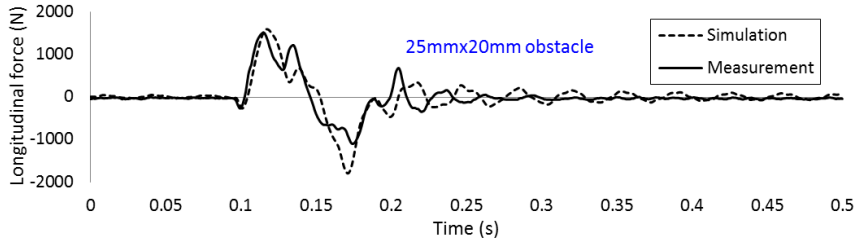

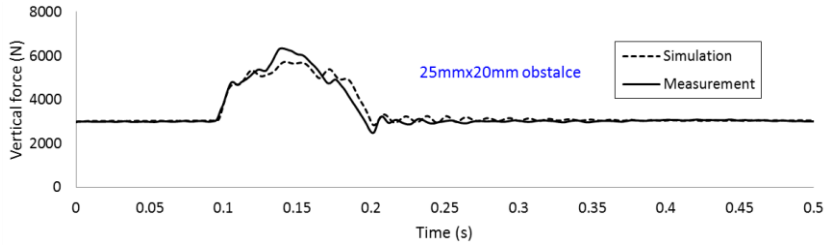

(b)

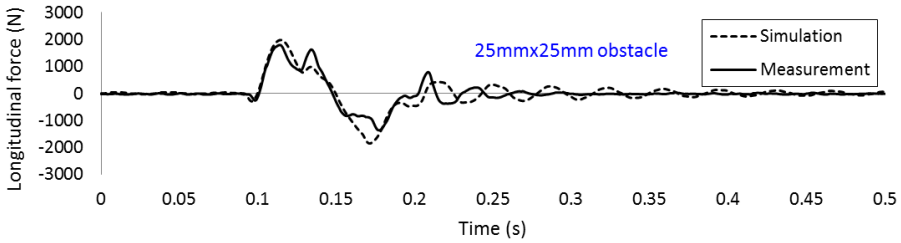

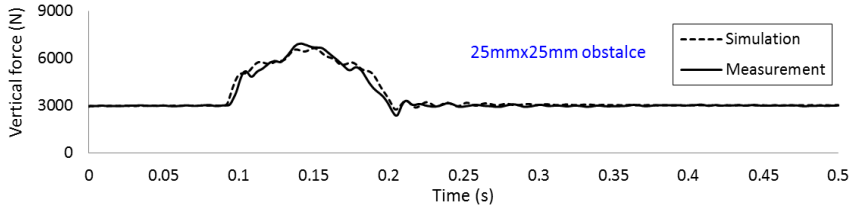

(c)

Figure 6.5 Spindle responses for tire rolling velocity of 10km/h (a) longitudinal and vertical responses for obstacle 25mm×10mm, (b) longitudinal and vertical responses for obstacle 25mm×20mm, (c) longitudinal and vertical responses for obstacle 25mm×25mm. The inflation pressure was 200kPa and the vertical pre-load was set as 3000N.

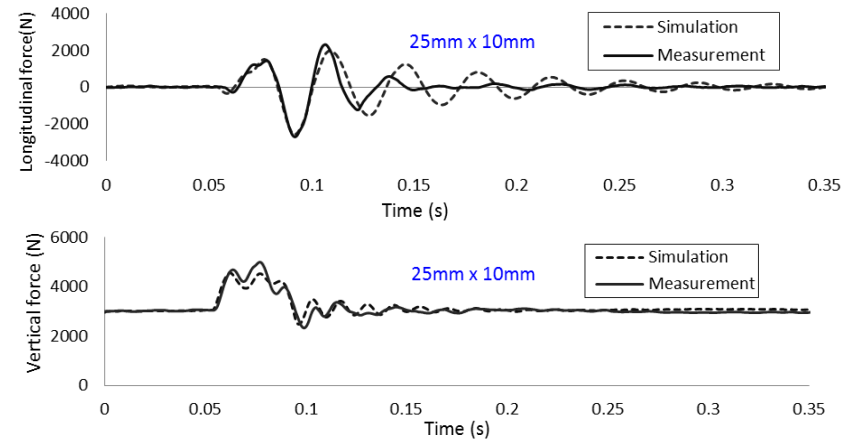

(a)

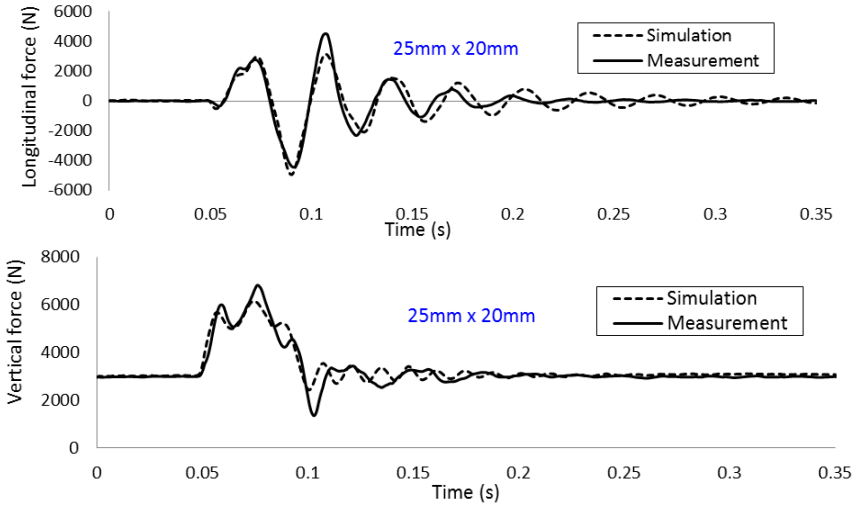

(b)

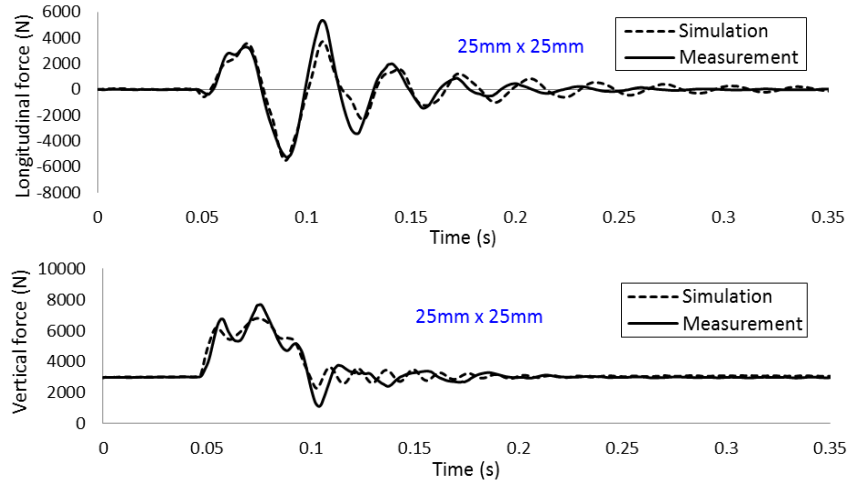

(c)

Figure 6.6 Spindle responses for tire rolling velocity of 20km/h (a) longitudinal and vertical responses for obstacle 25mm×10mm, (b) longitudinal and vertical responses for obstacle 25mm×20mm, (c) longitudinal and vertical responses for obstacle 25mm×25mm. The inflation pressure was 200kPa and the vertical pre-load was set as 3000N.

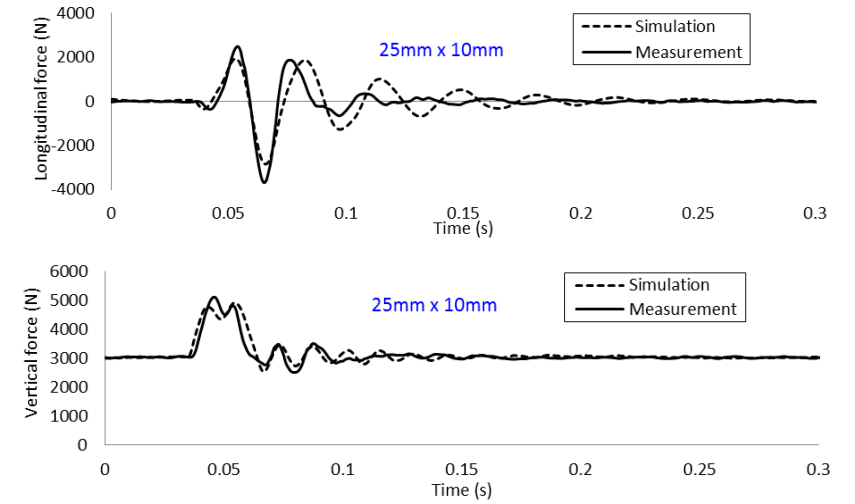

(a)

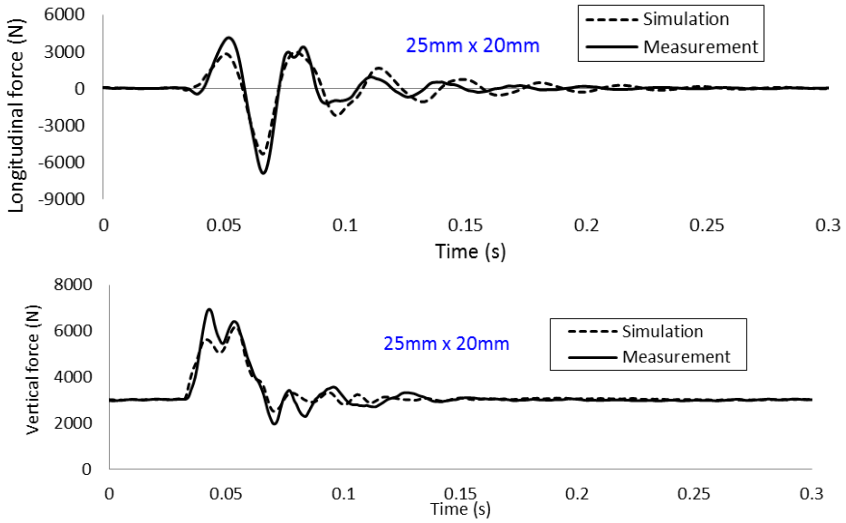

(b)

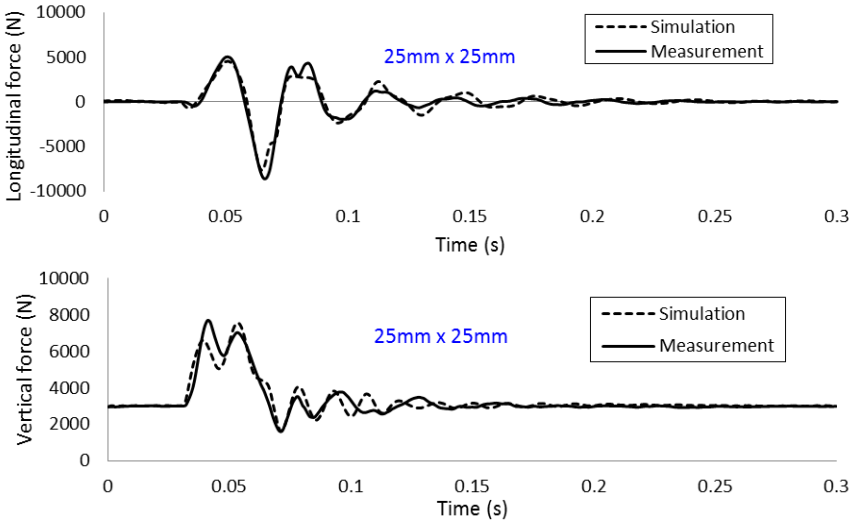

(c)

Figure 6.7 Spindle responses for tire rolling velocity of 30km/h (a) longitudinal and vertical responses for obstacle 25mm x 10mm, (b) longitudinal and vertical responses for obstacle 25mm x 20mm, (c) longitudinal and vertical responses for obstacle 25mm x 25mm. The inflation pressure was 200kPa and the vertical pre-load was set as 3000N.

6.2.3 Sensitivity of transient dynamic responses to traveling velocity

In order to investigate the effect of traveling velocity of rolling tire on the spindle forces when the tire traverses obstacles, transient dynamic simulation was carried out on the tire at three traveling velocities of 20km/h, 30km/h and 40km/h in which an obstacle with the width of 25mm and height of 20mm was attached to the rigid flat road. The sensitivity of the dynamic forces to traveling velocity can be derived from the comparison of responses. Figure 6.8(a) and (b) show the transient dynamic spindle forces for different traveling velocities of the tire in frequency domain in longitudinal and vertical directions respectively. The first resonant frequencies of the longitudinal spindle forces at different traveling velocities are approximately the same. With the increase of traveling velocity, the corresponding resonant amplitude of the longitudinal force decreases from 644.78N to 458.53N, and the resonant amplitudes for different tire velocities are shown in Figure 6.9. The result can be explained that the spindle forces in longitudinal direction are reduced as a result of the decease of rotation resistance with the increase of tire traveling velocity. On the other hand, higher traveling velocity of the tire leads to higher resonant amplitude of spindle forces in the vertical direction. For this response, it is worth noting that higher traveling velocity of the tire leads to shorter period of tire/obstacle impact, which results in increase of the impact force on the tire hub in the vertical direction.

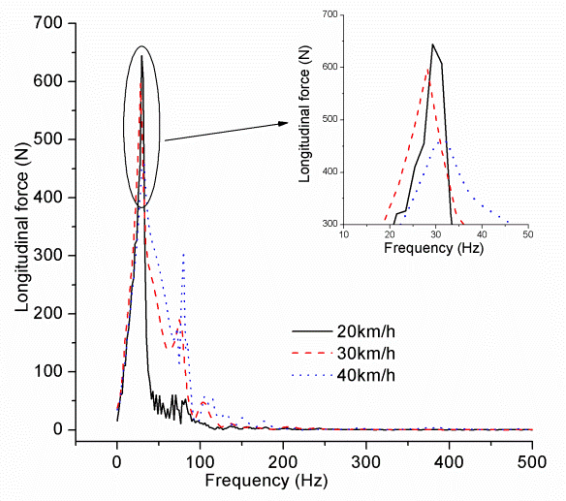

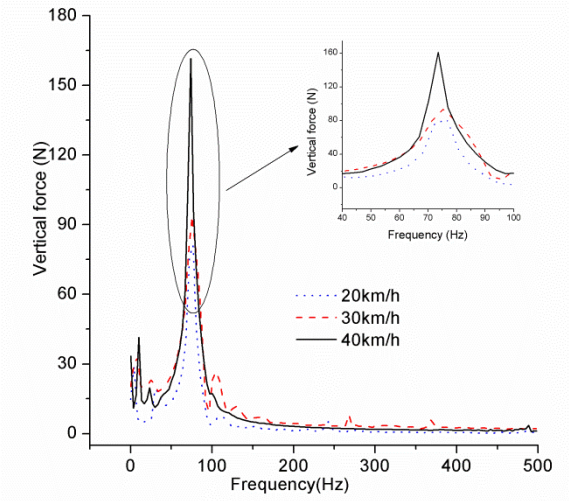

(a) (b)

Figure 6.8 (a) Simulated longitudinal dynamic forces for different traveling velocities in frequency domain (b) Simulated vertical dynamic forces for different traveling velocities in frequency domain.

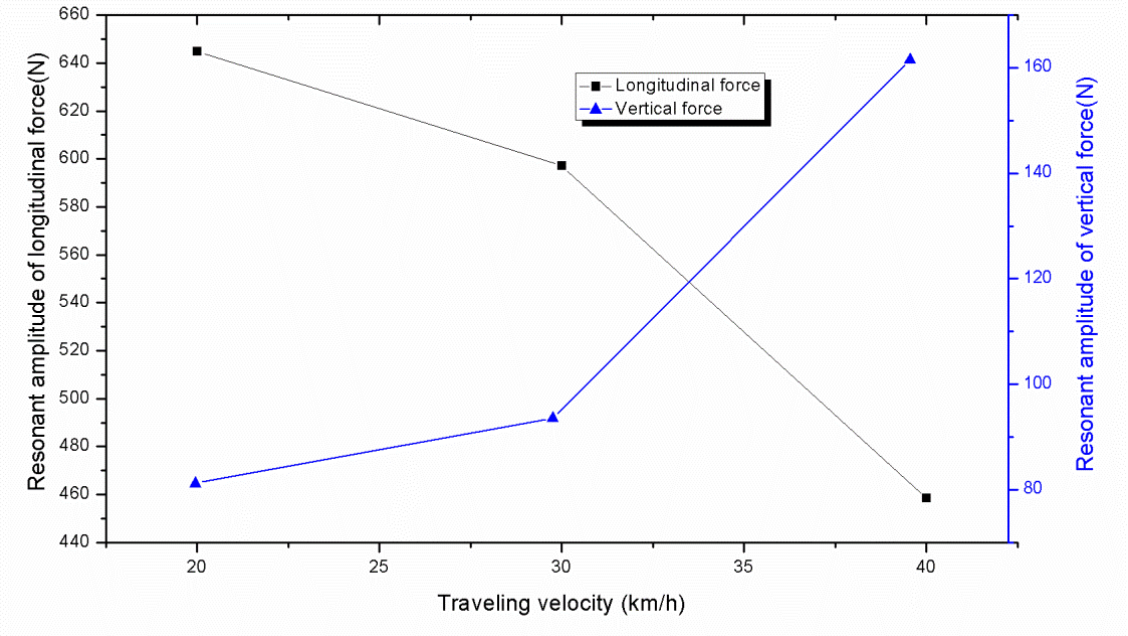

Figure 6.9 Resonant amplitude of longitudinal and vertical spindle force for different tire traveling velocities.

6.2.4 Sensitivity of transient dynamic responses to height of road obstacle

As mentioned above, different obstacles were applied for the transient numerical simulation, the objective of which is to investigate the effect of the height of obstacle on transient dynamic responses. The numerical simulation of the transient dynamic model was carried out at a traveling velocity of 30km/h for the rolling tire inflation pressure of 200kPa and vertical pre-load of 3000N. Figure 6.10 (a) and (b) respectively illustrate the transient responses of the longitudinal and vertical spindle forces in the time domain. With the increase of height of obstacle, both the longitudinal spindle force and vertical force display higher peak values when the tire traverses the obstacle. The reason can be attributed to the deformation of the tire when enveloping the obstacles. As the operating condition is that the height of rolling tire is fixed in vertical direction, larger deformation in the vertical direction will occur when the tire impacts a higher obstacle, which leads to the increase of spindle force in the vertical

direction. On the other hand, increase of the height of the obstacle will generate higher rotation resistance of the rolling tire, which leads to the increase of peak value of longitudinal spindle forces as the tire traverses the obstacles.

Using the FFT technique, the transient dynamic responses of longitudinal forces and vertical forces were transformed into the frequency domain and illustrated in Figure 6.11(a) and (b) respectively. The resonant frequencies of oscillation show similar values for different heights of obstacles in both longitudinal direction and vertical direction. The 32 Hz oscillation corresponds to the resonant frequency for longitudinal response, while the 73 Hz oscillation represents the resonant frequency for vertical response. In addition, with the increase of height of the rectangular obstacle, the longitudinal force displays higher value of amplitude, and the variation of resonant amplitude of the longitudinal force for different road obstacles is illustrated in Figure 6.12. Similarly, the spindle force in the vertical direction shows a trend similar to that of the spindle force in the longitudinal direction, and with the increase of height of road obstacle, the growth of resonant amplitude of spindle forces becomes larger in both longitudinal direction and vertical direction.

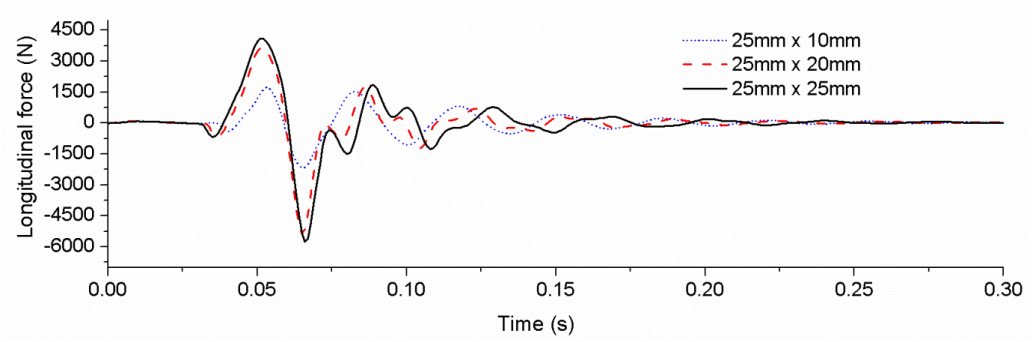

(a)

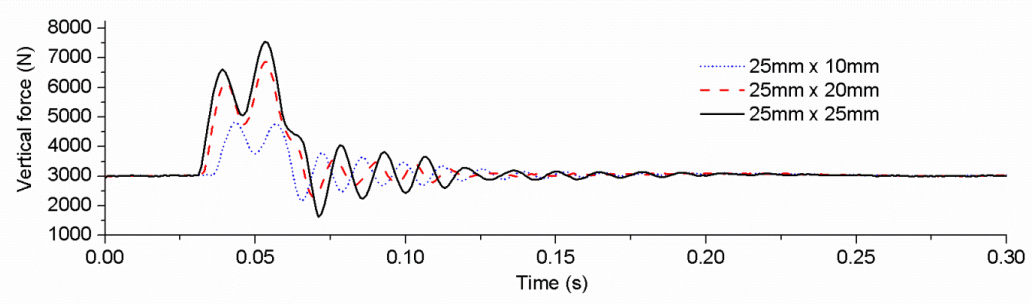

(b)

Figure 6.10 (a) Simulated longitudinal forces for the tire traversing a 25mm high and 25mm wide obstacle on a rigid flat surface at 30km/h in time domain (b) Simulated vertical forces for the tire traversing a 25mm high and 25mm wide obstacle on a rigid flat surface at 30km/h in time domain

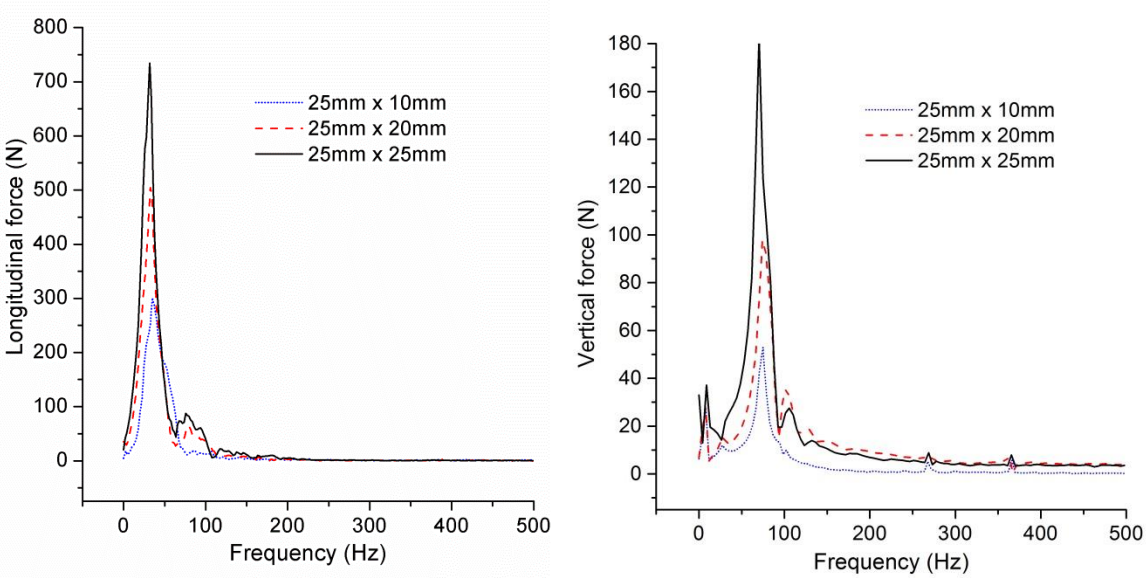

Figure 6.11 (a) Simulated longitudinal forces for the tire traversing a 25mm high and 25mm wide obstacle on a rigid flat surface at 30km/h in frequency domain (b) Simulated vertical forces for the tire traversing a 25mm high and 25mm wide obstacle on a rigid flat surface at 30km/h in frequency domain

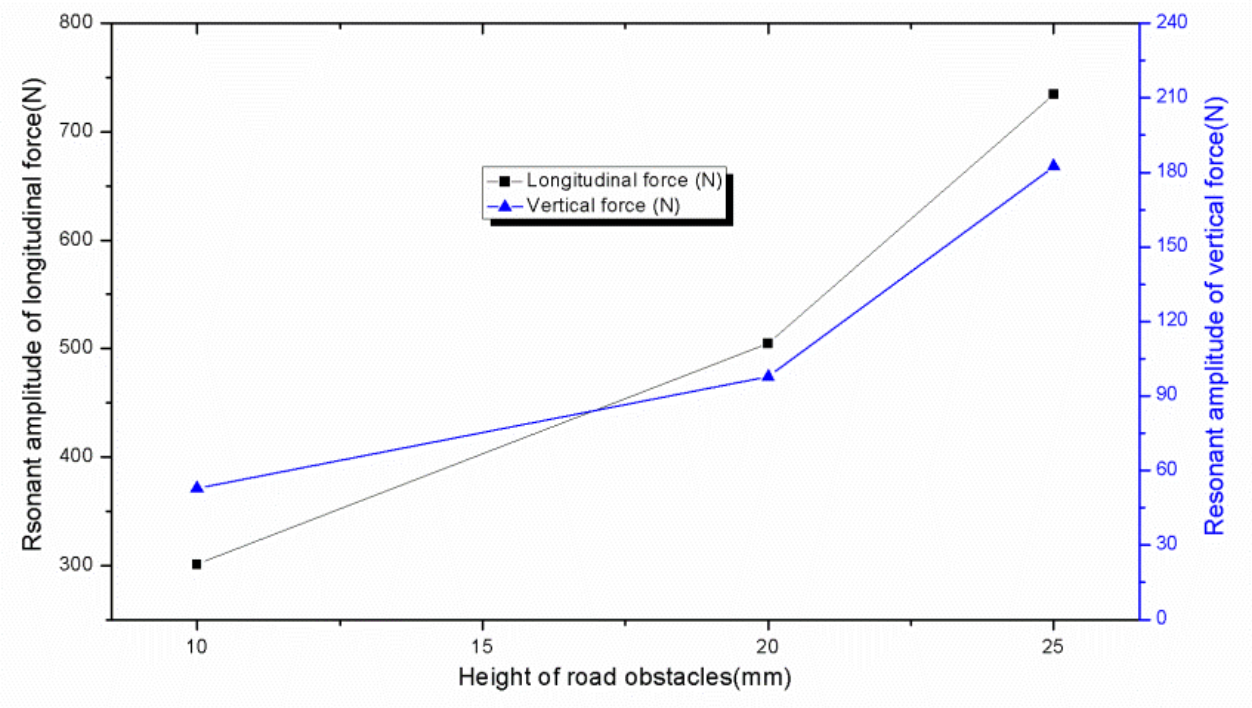

Figure 6.12 Resonant amplitude of longitudinal and vertical forces for different heights of road obstacles

6.2.5 Tire deformation when impacting obstacles

Another important property of tires is their capability to sustain severe impact loads. Some researchers attempted to use different methods to investigate tire impacting property. Neves et al. [122] conducted a series of impact tests, in which an impact mass with a round indenter was adopted to hit the tires with different impact velocities. Their study provided important tire impacting results for engineers to improve the performance of wheels comprising rim and tire. Reid et al. [123] developed a detailed FE tire model to perform tire compression simulations. Both single-sided compression and double-sided compression tests were carried out using the tire model. With the development of the tire model, tire deformation when impacting a curb can be predicted. In this study, tire deformations when the tire impacts different obstacles are predicted.

Figure 6.13 (a), (b) and (c) show the deformed configurations of the tire model when the tire impacts on different rectangular obstacles at a rolling speed of 20km/h. It can be seen that with the increase of the height of road obstacle, the deformation of the tire in the contact area becomes greater. For the tire rolling over the 25mm x 10mm obstacle, the tire almost envelopes the obstacle, while for the tire rolling over the obstacles with the heights of 20mm and 25mm, the tire cannot envelope the obstacles completely since carcass and steel belt are much stiffer in the circumferential direction. In addition, the deformation in the sidewall section for tire rolling over 25mm x 25mm is more significant compared to the other two conditions(25mm x 10mm, 25mmx20mm). For the tire rolling over the same obstacle with different travelling velocities, however, little sensitivity of the tire deformation to travelling velocity is observed. As an example, Figure 6.14 shows the deformed configurations for the tire rolling over the 25mm x 10mm obstacle with the velocities of 10km/h, 20km/h and 30km/h.

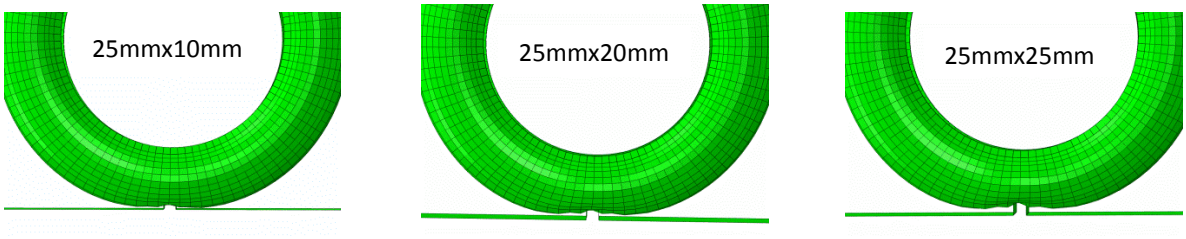

(a) (b) (c)

Figure 6.13 Deformed shapes of the tire rolling over an obstacle (at 20km/h) of (a) 25mm x 10mm, (b) 25mm x 20mm, (c) 25mm x 25mm.

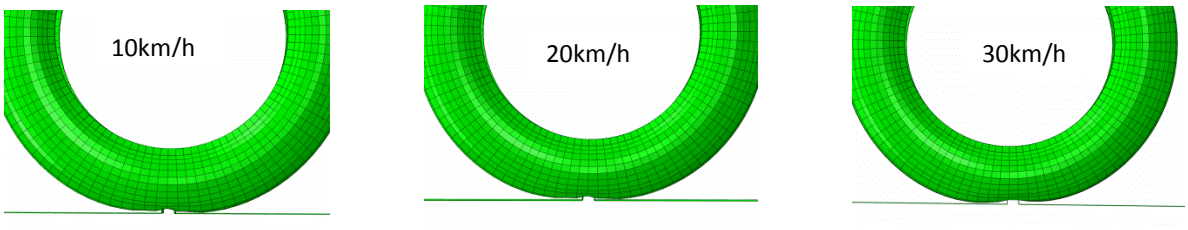

(a) (b) (c)

Figure 6.14 Deformed shapes of the tire rolling over the 25mm x 10mm obstacle with a velocity of (a) 10km/h, (b) 20km/h, (c) 30km/h.

6.2.6 Natural frequencies at different conditions

The variation of natural frequencies with the traveling velocities of the tire and height of road obstacles are illustrated in Table 6.1. From the table, it is obvious that the natural frequency determined from the spindle force responses in the vertical direction ranged from 73.62Hz to 74.07Hz, which means that the natural frequency has small sensitivity to the height of obstacle when the tire rolls at a speed of 20km/h. For the traveling velocity of 30km/h, the natural frequency also shows little difference for different rectangular obstacles with different height.

With regard to the transient dynamic responses in the longitudinal direction, the natural frequencies are between 28.29Hz and 34.91Hz. For the tire rolling on the road at a velocity of 20km/h, with the increase of height of rectangular obstacle, the natural frequency decreases from 33.18Hz to 28.19Hz. When the tire traveling velocity becomes 30km/h, the results also show that higher road obstacle leads to lower natural frequency, which is from 34.91Hz to 31.94Hz.

Table 6.1 Natural frequencies for different operating conditions

Velocity\obstacle	25mm x 10mm (Hz)	25mm x 20mm (Hz)	25mm x 25mm (Hz)
	Vertical		
20km/h	74.07	73.85	73.62
30km/h	73.33	73.28	73.33
	Longitudinal		
20km/h	33.28	29.95	28.29
30km/h	34.91	32.67	31.94

6.2.7 Dynamic stiffness derivation

The dynamic stiffness of tires is one of the crucial factors affecting vehicle ride comfort. To analyse the effects of traveling velocity and shape of obstacles on dynamic stiffness of tires, a derivation method was developed according to the transient dynamic responses to achieve the dynamic stiffness at resonance [124]. The peak of the mobility function was considered in calculating the dynamic stiffness at the natural frequency. The modulus of motion mobility $\dot{Y} / F$ is given by the expression

$$\left|\frac{\dot{Y}}{F}\right| = \frac{\omega}{\sqrt{(k_r - \omega^2 m)^2 + \omega^2 c^2}} \tag{6.1}$$

in which k_r and c represent the dynamic stiffness and damping ratio of the tire respectively, ω is natural frequency and m is the mass of the tire, and the peak of the modulus of motion mobility plot occurs at the condition

$$\frac{d}{d\omega}\left|\frac{\dot{Y}}{F}\right| = \frac{d}{d\omega}\left(\frac{\omega}{\sqrt{(k_r - \omega^2 m)^2 + \omega^2 c^2}}\right) = 0 \tag{6.2}$$

from which it can be derived that

$$\frac{(k_r - \omega^2 m)(k_r + \omega^2 m)}{\sqrt{(k_r - \omega^2 m)^2 + \omega^2 c^2}\,((k_r - \omega^2 m)^2 + \omega^2 c^2)} = 0 \tag{6.3}$$

Hence the dynamic stiffness can be obtained by

$$k_r = \omega^2 m \qquad (6.4)$$

From eq. 6.4, we may conclude that for a tire with constant mass, the dynamic stiffness is determined by the natural frequency. By analysing the natural frequencies obtained by prediction of transient dynamic responses for the tire traversing different obstacles in the previous section, the natural frequency obtained from the vertical spindle responses show very small sensitivity to the height of rectangular obstacles, which means the vertical dynamic stiffness has a small sensitivity to the height of obstacles. On the other hand, with the increase of height of road obstacle, the natural frequency of spindle responses in longitudinal direction becomes smaller, which implies that the dynamic stiffness in the longitudinal direction decreases.

6.3 Prediction of rolling resistance generated on the uneven road of quarter car

As an important factor in vehicle fuel consumption, the rolling resistance has been paid more and more attention by researchers, since the energy dissipation due to tire rolling resistance is a major component of vehicle energy loss. Rolling resistance is caused by tire deflection and deformation during rolling on the road, and the material hysteresis of tire rubber and tire structure is the primary contribution to energy dissipation. When the tire is loaded on a flat surface, energy losses occur due to the contact patch being deformed from the original shape in the unloaded condition according to the property and flexibility of internal tire structure, rubber, sidewall and tread. On the other hand, for the tire rolling on an uneven road, the tread element is deflected in the horizontal direction, and rolling resistance will be generated by the longitudinal force against motion because of the road unevenness. During the last decades, most of the researches were concentrated on the rolling resistance of the tire at steady state

conditions. In this study, special attention is paid to the energy loss generated in the tire due to the equivalent longitudinal force when the tire is rolling on an uneven road.

Finite element analysis is a useful method for predicting tire properties and parameters instead of tire testing, since test rigs in the laboratory could not meet the requirements in some extreme or special operating conditions, particularly for the tire rolling on the uneven road or large obstacles. Over the last twenty years, there have been many researchers using finite element analysis to study the prediction of temperature distribution and rolling resistance of tires and energy dissipation. Ebbott et al. [125] demonstrated a semi-coupled finite element-based method to predict rolling resistance and temperature distribution, in which particular attention is paid to the constitutive models and material properties of the tire. Shida et al. [126] proposed a simulation method using static finite element analysis to estimate the energy dissipation based on the relationship between the variation of stresses and strains approximated by Fourier series and the viscoelastic phase lag. In order to achieve adequate accuracy of the rolling resistance prediction, the anisotropic loss factor in fiber-reinforced rubbers was appropriately considered in the tire model. More recently, Ghosh [127] evaluated rolling resistance of a passenger car radial tyre with nanocomposite based tread compounds by using finite element (FE) analysis, in which energy dissipation was obtained through steady state rolling simulation. Cho et al. [71, 128] constructed a detailed periodic patterned tire model to predict the hysteretic loss and rolling resistance making use of the 3-D static tire contact analysis. However, the prediction of rolling resistance from these models was conducted at static or steady-state rolling condition, but the transient rolling resistance of tires was ignored. In the research of Luchini and Popio [129], an analytical transient tire model was used to predict rolling resistance, in which the model parameters were derived using equilibrium test data. From the comparison of the prediction of rolling resistance from the tire model and test data, it could be observed that different test protocols would have an

effect on the difference between the simulation results and the test data. In this study, the detailed FE model developed before is used for prediction of transient dynamic responses. Finally, the rolling resistance generated by the equivalent longitudinal force during the tire rolling on an uneven road is predicted using transient dynamic simulation.

In this study, the FE tire model associated with the simple suspension is used for predicting rolling resistance. In addition, a mathematical method for prediction of rolling resistance generated by the longitudinal forces between the tire and uneven road was developed.

6.3.1 Steps for calculation of rolling resistance

The procedure for calculating rolling resistance generated is as follows:

(1) Construct a random uneven road for definition of the road roughness

(2) Define the traveling distance (L) of the tire on the uneven road.

(3) Extract longitudinal forces ($F_x(i)$) against the motion in every time increment during simulation.

(4) Extract tire traveling displacement ($U_x(i)$) in x direction in every time increment.

(5) Calculate energy loss (E_d) from external work in the traveling direction.

(6) Calculate rolling resistance (RR) generated by the longitudinal forces.

(7) Extract the effective rolling resistance ($RR\big|_e$) from rolling resistance variation, which is the objective of this study.

Energy loss in a tire, because of road unevenness, results from external work against tire motion in the longitudinal direction. The difference between rolling velocity and traveling velocity leads to the generation of a longitudinal force. The energy loss from external work can be considered as work done against tire motion in every time increment. Hence the

energy loss due to the uneven road is given by the work done by the longitudinal force opposing motion:

$$E_d = \sum |F_x(i)| \cdot U_x(i) \tag{6.5}$$

In the process of a tire rolling at a constant traveling velocity v on the uneven road and the tire loses the state of free rolling, the situation where $\omega \cdot r < v$ (where ω is the angular velocity and r is the rolling radius) results in a negative longitudinal force, while the situation where $\omega \cdot r > v$ results in a positive longitudinal force. However, both the negative and positive longitudinal forces have the effect of disturbing tire rolling from the free rolling state, which means both the longitudinal forces in positive x direction and negative x direction generate energy dissipation.

The rolling resistance force can be defined as the energy dissipated in unit distance travelled, which can be presented as follows

$$RR = E_d / L = E_d / \sum U_x(i) \tag{6.6}$$

6.3.2 Road unevenness derivation

Road unevenness has been created to investigate the deformation, dynamic response and enveloping properties in terms of obstacles and steps [68, 69, 71, 73]. As a source of excitation for rolling tires, road unevenness is the primary contribution to tire vibration as well as vehicle vibration. In the full vehicle simulation, road unevenness is one of the important input parameters for vehicle dynamic simulation. Road unevenness is the main factor to disturb the tire from the free rolling state, and rolling loss generated by longitudinal forces are attributed to the unbalanced state. Figure 6.15 illustrates the schematic representation of the contact between the tire and the uneven road. The generated road unevenness data was imported into the FE model for tire rolling analysis.

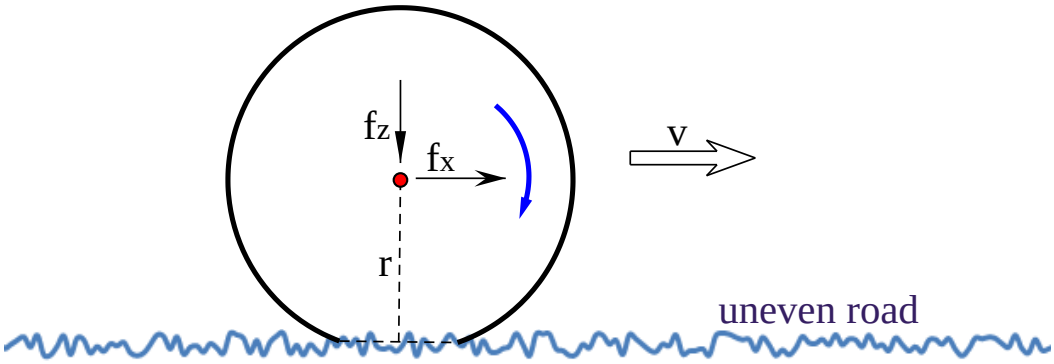

Figure 6.15 Representation of tire rolling on uneven road

6.3.2.1 Power spectral density of road unevenness

In early studies on vehicle ride performance, the road unevenness was used in the form of sine waves, triangular waves and step functions. However, this simple form of road profiles could not serve as a valid basis for studying vehicle dynamic performance. Later, random functions were introduced to realistically describe the road profiles [130]. When the road profile is recognized as a random function, it can be characterized by a power spectral density function. It has been found that the road unevenness related to the power spectral density for the road profiles can be approximated by [130]

$$S_x(\Omega) = C_{sp}\Omega^{-N_b} \tag{6.7}$$

in which Ω is the spatial frequency, $S_x(\Omega)$ ($\mathrm{m}^2/\mathrm{cycle}/\mathrm{m}$)is the power spectral density function of the elevation of the road profile, C_{sp} and N_b are dimensionless road profile constants to determine the road unevenness. In order to carry out time domain conversion for road profiles, the power spectral density is expressed in terms of time frequency, which is given by

$$S_x(f) = C_{sp}v^{N_b-1}f^{-N_b} \tag{6.8}$$

Where v is the travelling velocity of the vehicle, f is the time frequency, and the unit of the power spectral density function $S_x(f)$ is m^2/Hz.

Different road surfaces with different road profile constants are given in Table 6.2, and the power spectral density for different road surfaces is illustrated in Figure 6.16.

Table 6.2 Values of N and C_{sp} for different PSD functions for various road surfaces [130]

Road surfaces	N_b	C_{sp}
Smooth runway	3.8	4.3×10^{-11}
Rough runway	2.1	8.1×10^{-6}
Smooth highway	2.1	4.8×10^{-7}
Highway with gravel	2.1	4.4×10^{-6}

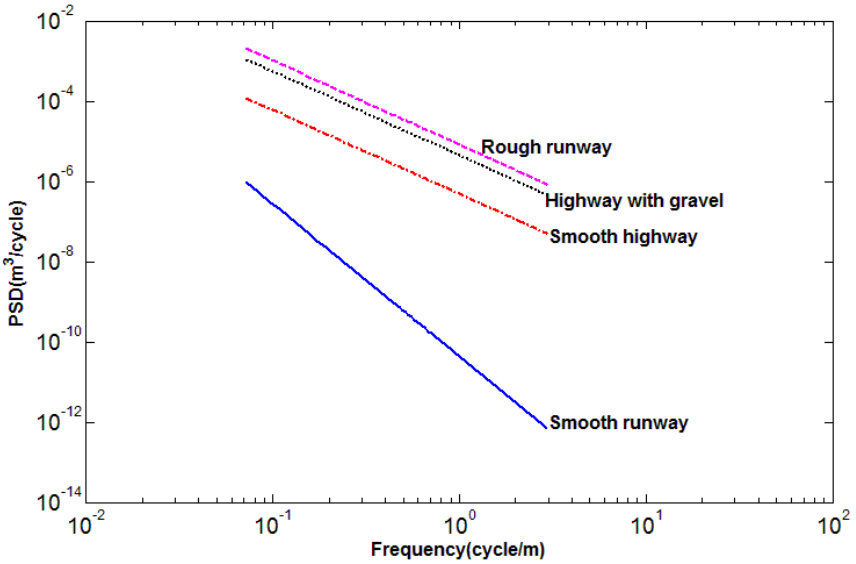

Figure 6.16 Power spectral density as a function of spatial frequency for various types of road surfaces

6.3.2.2 Discrete Fourier Transform Method

The objective of Discrete Fourier Transform (DFT) is to build the relationship between the time sequence $x(n)$ and the frequency sequence $X(k)$ [26], which can be given by

$$\text{DFT} \qquad X(k) = DFT[x(n)] = \sum_{n=0}^{N-1} x(n) e^{-j\frac{2\pi}{N}nk} \qquad k = 0,1,2,...,N-1 \qquad (6.9)$$

$$\text{IDFT} \qquad x(n) = \frac{1}{N}\sum_{k=0}^{N-1} X(k) e^{j\frac{2\pi}{N}nk} \qquad k = 0,1,2,...,N-1 \qquad (6.10)$$

in which N represents the length of the two sequences.

Generally, the definition of power spectral density for road file is limited in $[0,+\infty)$ in the DFT process, the one-sided PSD $S_x(f)$ needs to be transformed to the two-sided PSD $G_x(f)$. Based on the characteristics of real even function $G_x(f)$, the power spectral density, the relationship between $S_x(f)$ and $G_x(f)$ can be given by

$$S_x(f)=\begin{cases}2G_x(f) & f\geq 0\\ 0 & f<0\end{cases} \qquad (6.11)$$

and according to the definition of power spectral density, $S_x(f)$ can be expressed by

$$S_x(f)=\lim_{T\to\infty}\frac{2}{T}\left|X(f)\right|^2=\lim_{T\to\infty}\frac{2}{T}\left|\int_{-\infty}^{+\infty}x(t)e^{-j2\pi ft}dt\right|^2 \qquad (6.12)$$

in which t is the simulation time, T is the period, $x(t)$ is the time sequence, and $X(f)$ is the corresponding sequence in terms of frequency. When $t>0$ and the period T is limited, the Equation (6.12) can be written as

$$S_x(f)=\frac{2}{T}\left|X(f)\right|^2=\frac{2}{T}\left|\int_0^T x(t)e^{-j2\pi ft}dt\right|^2 \qquad (6.13)$$

By applying DFT on the above equation, associated with eq. 6.9 and eq. 6.10, the power spectral density can be derived as

$$S_x(f_k)=\frac{2}{N\Delta t}\left|\sum_{n=0}^{N-1}x(n)e^{-j2\pi f_k n\Delta t}\Delta t\right|^2=\frac{2\Delta t}{N}\left|X(k)\right|^2=\frac{2T}{N^2}\left|X(k)\right|^2=\frac{2}{\Delta fN^2}\left|X(k)\right|^2 \qquad (6.14)$$

in which Δt is the time increment, $N=T/\Delta t$, $\Delta f=1/N\Delta t$ and $f_k=k\Delta f$. Therefore, according to the relationship between power spectral density and the time sequence, the frequency sequence can be obtained by

$$\left|X(k)\right|=\left|DFT\left[x(n)\right]\right|=N\sqrt{S_x(f_k)\Delta f/2}=N\sqrt{S_x(f=k\Delta f)\Delta f/2} \qquad (k=0,1,...,N_r-1) \qquad (6.15)$$

The time sequence can be obtained by taking the inverse discrete Fourier transform function (eq. 6.10) on the above frequency sequence. Based on the above method, the road surface elevations for various types of road surfaces are obtained (Figure 6.17), in which the travelling velocity was set as 20km/h, and frequency range within [0.5Hz, 25Hz] was adopted for the simulation.

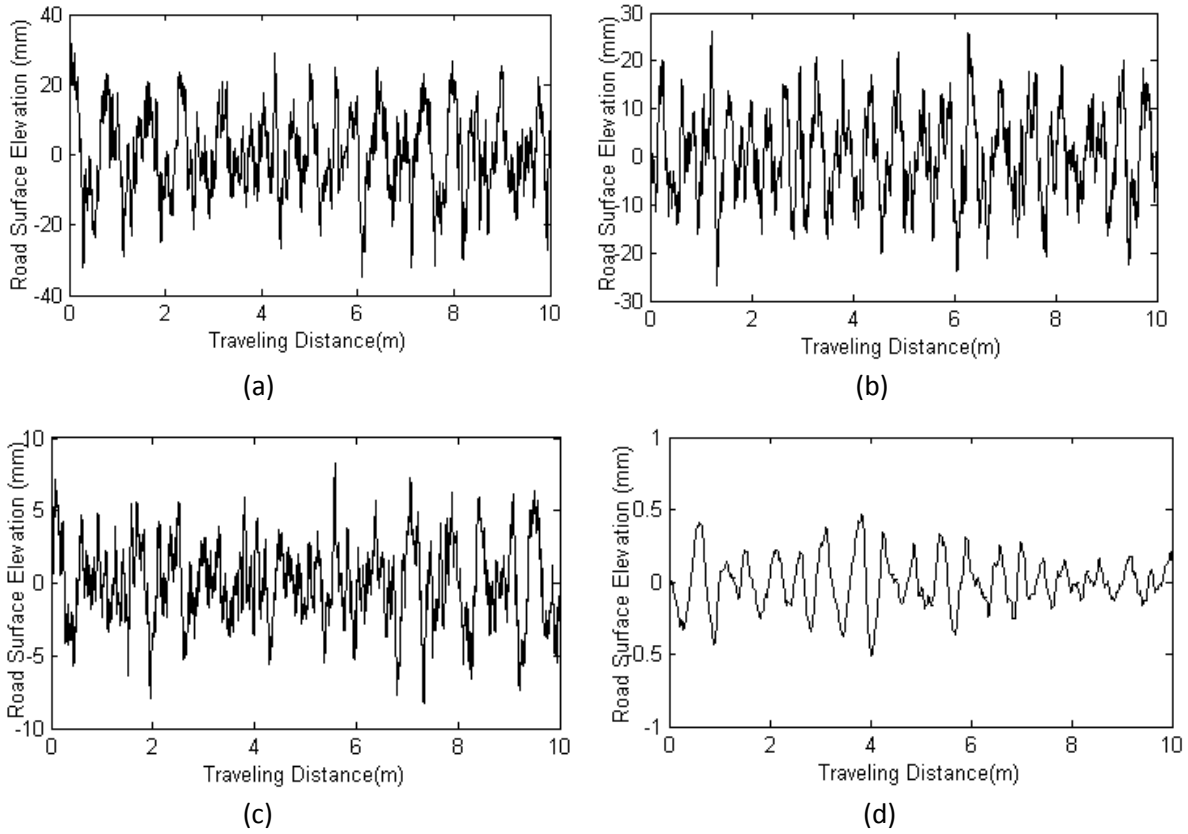

Figure 6.17 Road unevenness in time domain (a) Rough runway (b) Highway with gravel (c) Smooth highway (d) Smooth runway

The road profiles represented in Figure 10 are 2-D profiles based on the "average" PSD contained in the road unevenness. The 3-D real road profile is randomly uneven, not only in the longitudinal direction but also in the transverse direction. However, the longitudinal force generated over the tyre/road contact patch width is calculated, using the 2-D longitudinal profile, by integrating over small elements of track width across the width of the contact patch. For each track element the longitudinal force is determined from the local longitudinal force per unit width. Hence the total longitudinal force over the tyre/road contact patch is obtained by summing over small elements of track width across the width of the tyre.

6.3.3 Quarter car model

The importance of improving dynamic behaviour is growing in vehicle research and development, particularly for the prediction of tire and suspension dynamics properties in rolling over road irregularities, which is important for evaluation of ride comfort in the real

driving conditions [131]. Besides, the quarter car model has been used for investigation of chaotic vibration excited by road unevenness [132]. In this study, a quarter car model consisting of a Finite Element tire and suspension system was built to predict the tire dynamic properties for tire rolling on an uneven road, with a view to deriving the rolling resistance generated by the longitudinal dynamic responses on the uneven road. The quarter car model consists of three components: a tire with an initial condition of contact with the flat road, a chassis which is located above the tire, a suspension composed of spring and dashpot in parallel connecting the chassis and the centre of the tire. In this study, the weight of the chassis in the finite element model is set as 306kg, and the acceleration due to gravity is set as 9.8 m/s^2, in which way the initial vertical load can be set as 3000N. The schematic representation of the quarter car system is illustrated in Figure 6.18.

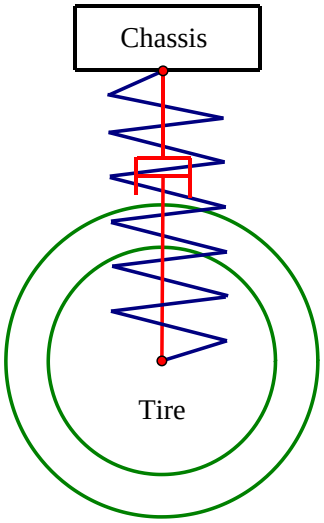

Figure 6.18 Schematic representation of the quarter car model

6.3.4 Road length

The total length of the road for tire rolling is constructed in three sections: the flat length where the road is assumed to be flat (no excitation), the transition length where there is a transition from no excitation to excitation by the road roughness and the calculation length over which the effective rolling resistance is predicted, as shown in Figure 6.19. The flat length is created in order that the chassis of the quarter-car can reach an equilibrium position

before the tire moves on the uneven road. As different rolling velocities will generate different travelling distances over which the chassis achieves an equilibrium position, the flat length is calculated based on the travelling velocities.

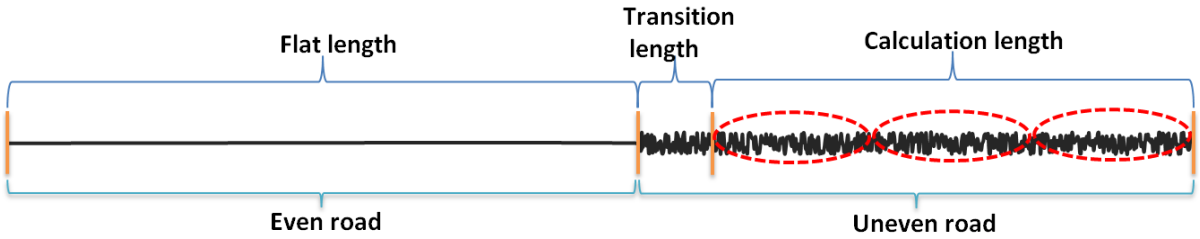

Figure 6.19 Road length composed of different sections

As mentioned above, the determination of the length of flat road is based on the travelling velocities. Thus, it is important to calculate the equilibrium settling point in the longitudinal direction with different travelling velocities in order that the quarter car system achieves steady state. The travelling time or distance for the tire to achieve a settled state is determined by how long it takes for the system to reach a tolerance band around the final value of vertical displacement [133]. In this study, the permissible zone is set as less than 5% of preload displacement. Figure 6.20 illustrates the chassis vibration history for the tire travelling at a velocity of 30km/h. The chassis preloading process can be considered as a damped vibration, and the equilibrium position displacement can be estimated as:

$$d = m_c g / k_c \qquad (6.16)$$

with m_c, g, k_c being the mass of the chassis, gravity acceleration, and suspension stiffness respectively.

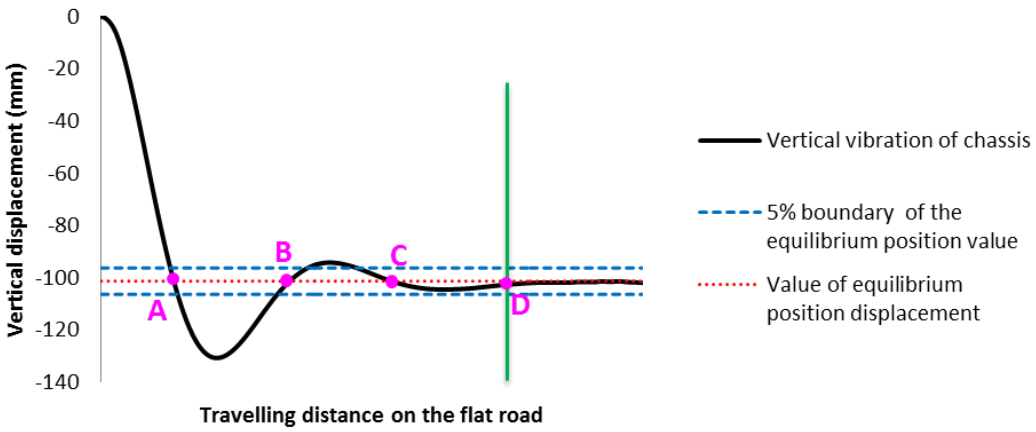

Figure 6.20 Preloading history of the chassis to get stability for the quarter car model

As shown in Figure 6.20, the chassis vibration system achieves stability before the D point, which is the fourth crossing point of the vertical displacement curve and the axis of equilibrium. The settling travelling distance at point D meets the requirement of the permissible zone of the vertical displacement. Therefore, the flat length for tire rolling can be determined between the beginning of the road and the perpendicular shown in Figure 6.20. The lengths of flat road for travelling velocities of 60km/h and 90km/h are defined by using the same approach as that of 30km/h, and the relationship between the flat length and travelling velocity is illustrated in Figure 6.21, from which it can be observed that the flat length and the travelling velocity have a nearly linear relationship with each other.

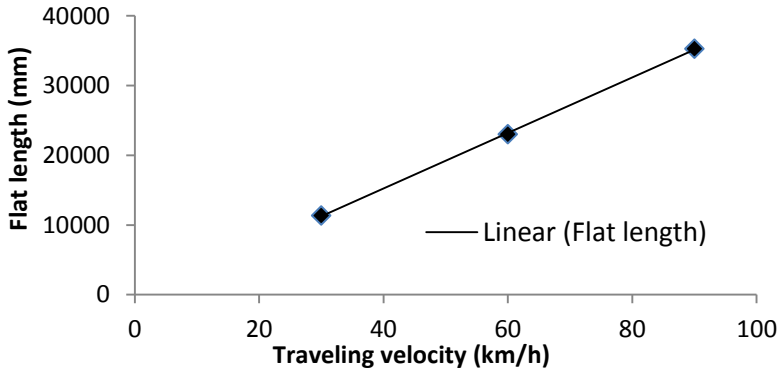

Figure 6.21 Flat length variation for different travel velocities

With regard to the transition length, it is a required section of uneven road for dissipating the transient response of the system before the rolling resistance is measured, to ensure accurate rolling resistance results. Figure **6.22** illustrates the relationship between rolling resistance

and distance travelled by the tire on one of the uneven roads at 90km/h. The objective of defining transition length is to determine the starting position for calculation of rolling resistance accurately. As shown in Figure **6.22**, the initial values of rolling resistance is much lower than that in the latter rolling distances, the reason being that the model needs to build up the rolling resistance when the tire moves on to the uneven road, and then rolling resistance reaches a fairly steady value. The perpendicular is the point at which the transient response has dissipated enough for the rolling resistance to be calculated accurately over the calculation length.

As the most important length of the three parts of road length, the calculation length is applied for derivation of rolling resistance, which is the objective of this study. In order to improve the accuracy of rolling resistance calculation on the uneven road associated with requirement of covering different characteristics of the random road, the rolling resistance is calculated over a minimum of three revolutions of rolling tire on the uneven road. The total distance of the tire rolling over three revolutions was applied for the rolling resistance calculation, which is illustrated in both Figure 6.19 and Figure 6.22, and the calculation length can be considered as the effective length.

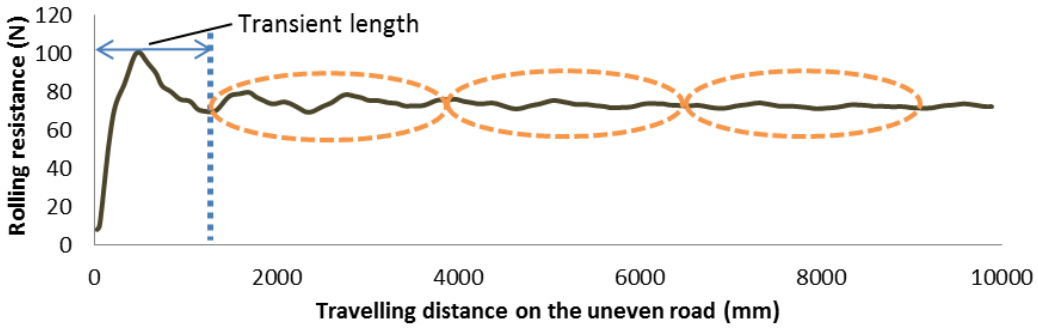

Figure 6.22 Rolling resistance variation for the tire rolling on the uneven road at 90km/h

6.3.5 Rolling resistance calculation

As mentioned, the calculation length is applied for the derivation of effective rolling resistance. However, the starting point for rolling resistance calculation is the beginning of

the uneven road, which consists of the transition length plus the calculation length. As described in eq. 6.6, for a tire rolling over a distance L of the uneven road, the rolling resistance for this part of the uneven road is calculated in terms of

$$RR\big|_{0\to L} = \frac{E_d}{L} = \frac{E_d}{\sum U_x(i)} \tag{6.17}$$

in which the $RR|_{0\to L}$ represents the average rolling resistance for the tire traversing a distance L of the uneven road. Figure **6.22** illustrates the rolling resistance variation of the whole uneven road. However, the effective rolling resistance is obtained by extracting the rolling resistance in the distance covered in three revolutions of the tire and calculating the average value of the rolling resistance for this distance, the function of the effective rolling resistance $RR|_e$ is defined by

$$RR\big|_e = \frac{RR_1 + RR_2 + RR_3}{3} \tag{6.18}$$

where RR_1 , RR_2 , RR_3 represent the rolling resistance for revolution 1, revolution 2 and revolution 3, respectively.

6.3.6 Results and Discussion

6.3.6.1 Sensitivity of rolling resistance to travelling velocity

As the transition distances for different travelling velocities are different from each other, the definition of the transition length used for the study of comparison of rolling resistance for different travelling velocities was derived by the longest transition length in order that the effective rolling resistance derivation is based on the same road unevenness and the same calculation length. The rolling resistance variations for different travelling velocities are shown in Figure 6.23, in which the perpendicular represents the dividing line between transition length and calculation length. Three revolutions behind the perpendicular were selected as the calculation length to evaluate the effective rolling resistance.

The calculation of the end position of the third revolution of rolling tire is determined by the rotational displacement of the tire rim. Figure 6.24 describes the corresponding rotational displacement variation with the increase of travelling distance of the tire rolling on the uneven road for the travelling velocity of 30km/h. With the relationship between rotational displacement of the rim and the tire travelling distance on the uneven road, in which the perpendicular illustrated is applied for determining the corresponding position with the starting position of the calculation length, the calculation length can be conveniently determined by extracting the section between the two positions. Although different travelling velocities were applied in the simulation, the methods of applying rotational displacement to evaluate the three revolutions section for the three travelling velocities were consistent with each other. Hence the end position of the third revolution of the rolling tire is the same for the other two different travelling velocities.

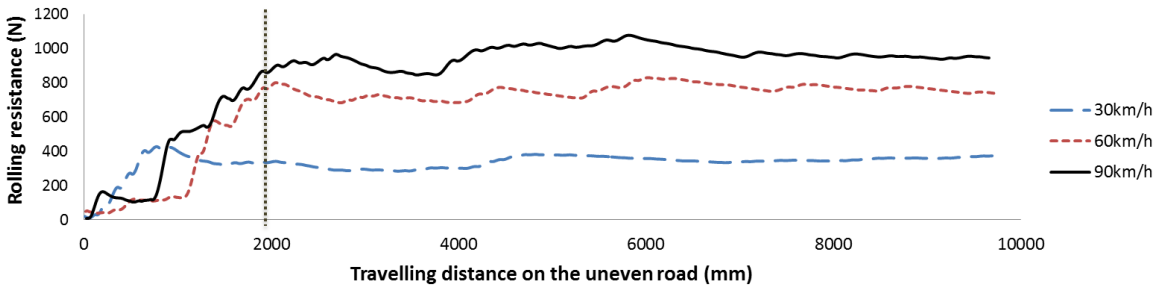

Figure 6.23 Rolling resistance variation with the increase of travelling distance of the uneven road

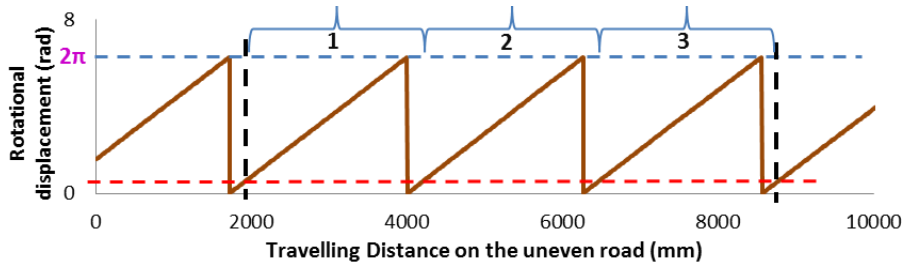

Figure 6.24 The corresponding rotational displacement variation with the increase of travelling distance of the uneven road for the travelling velocity of 30km/h

The effective rolling resistances for different travelling velocities can be derived according to eq. 6.18, the relationship between rolling resistance and travelling velocities were derived and

illustrated in Figure 6.25. Different travelling velocities of 30km/h, 60km, and 90km/h associated with an inflation pressure of 200kPa were set as operating conditions and applied for rolling simulation for investigation of the influence of travelling velocities on rolling resistance. From the results represented in Figure 6.25, it can be observed that higher travelling velocity leads to higher rolling resistance.

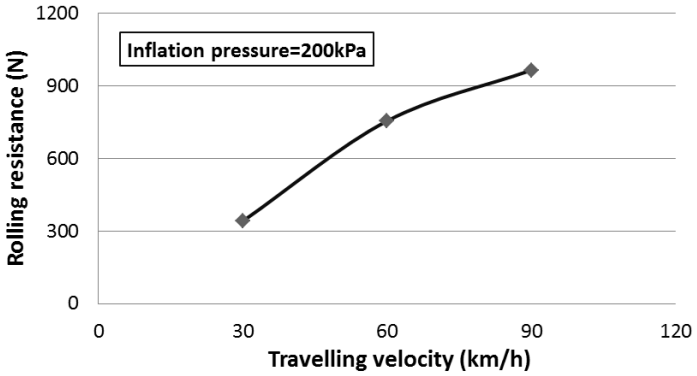

Figure 6.25 Effective rolling resistance variations for the quarter car model at different travelling velocities

6.3.6.2 Sensitivity of rolling resistance to road surface level

In order to investigate the effect of road roughness on rolling resistance, two typical road surfaces the smooth runway and rough runway mentioned in the previous section were chosen for rolling resistance analysis. In this study, coefficient of rolling resistance is applied to make the comparison between different road surfaces. The coefficient of rolling resistance is the standard way of expressing rolling loss of the rolling tire and is defined as the ratio of the rolling resistance to the normal load. Various empirical formulas have been developed based on experimental results for calculating the rolling resistance of tires on hard surfaces. Rolling resistance coefficient for a radial-ply tire may be expressed as [130]:

$$f_r = 0.0136 + 0.40 \times 10^{-7} V^2 \qquad (6.19)$$

where V is the vehicle speed in km/h.

The rolling resistance coefficient of a tire on a hard surface is due mainly to the hysteresis loss in the tire due to deformation as it rolls. Here, the rolling resistance coefficients from

numerical simulation for the two kinds of road surfaces are compared to that for a hard surface in Figure 6.26 for different travelling velocities. It can be observed that the rolling resistance coefficient for the uneven surface is much higher than that of the smooth surface (calculated from eq. 6.19), indicating that the rolling resistance for an uneven surface is mainly due to the transient longitudinal contact forces generated at the tire-pavement interface.

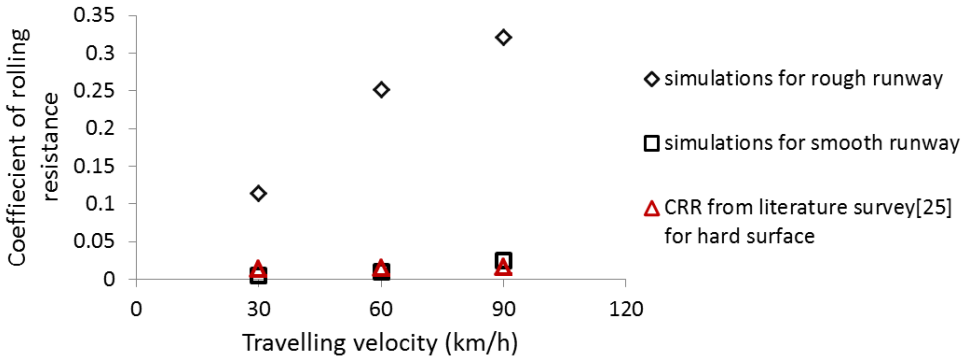

Figure 6.26 Variation of Coefficient of rolling resistance with the increase of travelling velocities for the two conditions in comparison to smooth road.

In the BOSCH automotive handbook [134], the average measured values of the coefficient of rolling resistance for various types of road surfaces are shown in Table 6.3. The average measured values of rolling resistance coefficient confirm that the rolling resistance for the uneven road is much higher than that for the smooth road surfaces.

Table 6.3 Coefficient of rolling resistance for different road surfaces [134]

Road Surface	Coefficient of Rolling resistance
Pneumatic Car tires on	
Large sett pavement	0.015
Small sett pavement	0.015
Concrete, asphalt	0.013
Rolled gravel	0.02
Tarmacadam	0.025
Unpaved road	0.05
Field	0.1-0.35
Pneumatic truck tires on	
Concrete, asphalt	0.006-0.01

6.4 Summary and conclusions

Transient dynamic simulations for the tire traversing different road obstacles were carried out using finite element method. Satisfactory results were obtained from the comparison of transient responses between the tire model and experimental tests, which means that the FE tire model is capable of predicting spindle forces for tire traversing different road obstacles.

The tire rolling over different heights of rectangular cleat at different traveling velocities was simulated and results showed that both speed and height of road obstacle had significant influence on the resonant amplitude of reaction forces. With the increase of traveling velocity, the corresponding resonant amplitude of the longitudinal force decreases from 644.78N to 458.53N, while the resonant amplitude of vertical force increases from 81.20N to 161.47N. Furthermore, with the increase of height of road obstacle, the resonant amplitude of spindle force response becomes larger in both longitudinal and vertical directions.

The resonant frequency of vertical responses showed very small sensitivity to the height of road obstacle, which means very small change in vertical dynamic stiffness when the tire traversed obstacles with different heights. However, it was predicted that the dynamic stiffness in the longitudinal direction decreased when the tire traversed a higher obstacle.

In addition, with the increase of height of road obstacle, tire deformation became greater when the tire impacted the road obstacle. Particularly, the sidewall of the tire has a significant deflection when the tire impacts large obstacles (more than 20 mm high). However, due to the increase of stiffness of carcass when the tire rolls over an obstacle, the tire could not envelop the whole obstacle. On the other hand, the deformation has slight sensitivity to travelling velocity of the tire, which may be attributed to the slight deformation of the carcass component for different velocities.

The processes of calculation of rolling resistance generated by the longitudinal dynamic responses on the uneven road were described, where the rolling resistance was defined as energy dissipation per unit distance travelled. In order to predict the effective rolling resistance for this study, a quarter-car model was used, consisting of a tire and a chassis, with suspension in the form of a parallel spring-damper combination connecting the centre of the tire and the chassis. Road length for the effective rolling resistance generation was defined in order to satisfy the requirement of the rolling tire, in which the chassis of the quarter car needs to reach an equilibrium position before it arrived on the uneven road. In addition, transition section and calculation section of the whole road were developed separately, and the effective rolling resistance was derived by calculating the average rolling resistance over the calculation section, which was generated by three revolutions of the rolling tire.

In this study, the simulation was concentrated on rolling resistance generated by the unevenness of the road, and did not account for the rolling resistance generated in the steady state condition (flat road). However, based on the rolling resistance investigation by other researchers [126-130, 134, 135], the material hysteresis is the main contributor to tire rolling resistance in the steady state condition, and it is much smaller when compared to the rolling resistance generated on the uneven road. Thus it can be concluded that the rolling resistance due to transient longitudinal contact forces is the most significant factor for a rolling tire on the uneven road.

Chapter 7 CHARACTERISATION OF FTIRE AND MULTI-BODY DYNAMICS SIMULATION

7.1 Introduction

With the experimental and numerical simulation data including static, steady-state and transient dynamic analysis, different FTire models can be derived using different data. FTire/fit is such software to derive FTire model through parameterization based on the test or simulation data. In this chapter, the procedure of characterisation of FTire model is presented in section 7.2. After the procedure for generating FTire, the derived FTire models are used for Multi-body dynamic analysis, which is given in section 7.3. In order to create an equivalent scenario with that in FE analysis, a simple tire/wheel model is developed using SIMPACK, and the same boundary conditions have been defined.

In order to identify the influence of different characteristics of FTire models derived at different operation conditions, three FTire models have been derived for multi-body dynamic analysis. One is from experimental data, while the other two are from numerical simulation data obtained at different road condition ranges. Dynamic analysis using the three different FTire models is presented in section 7.3, in which the dynamic analysis at non-extended conditions and extended conditions are compared. It is noted that the transient dynamic analysis at the non-extended conditions can be carried out using experimental tests. However, the extended conditions can be considered as severe conditions where transient dynamic experiments cannot be carried out because of laboratory rig limitations.

7.2 Procedure of Characterisation of FTire

FTire parameter identification and validation are conducted using FTire/fit, which is the parameters identification and validation toolbox for FTire. The following kinds of experimental data or simulation data are used in FTire/fit:

- Static tire properties (cross-section shape, radial, longitudinal, lateral stiffness)
- Footprint shapes
- tire properties in steady-state rolling conditions (cornering stiffness)
- time-domain spindle responses for cleat tests or simulations (radial forces, longitudinal forces)

7.2.1 Tire geometry data

The tire size, speed symbol, rim width mass and initial inflation pressures are to be defined by entering the data in the window shown in Figure 7.1 and Figure 7.2. Based on the size and inflation pressure of the tire, FTire/fit can use the input data file to roughly estimate the basic stiffness, damping and some other basic data of the new FTire file.

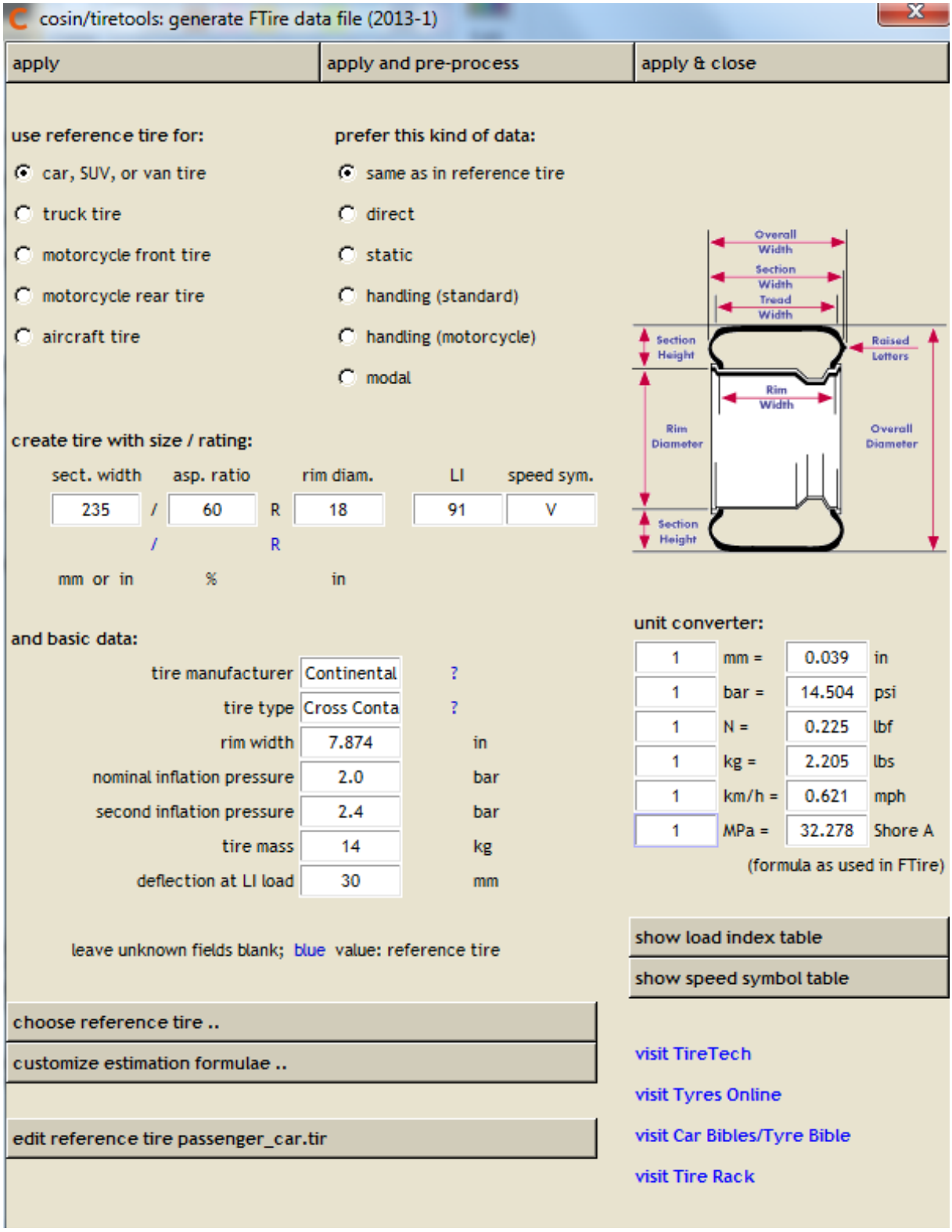

Figure 7.1 Tire geometry property definition to generate initial FTire data file

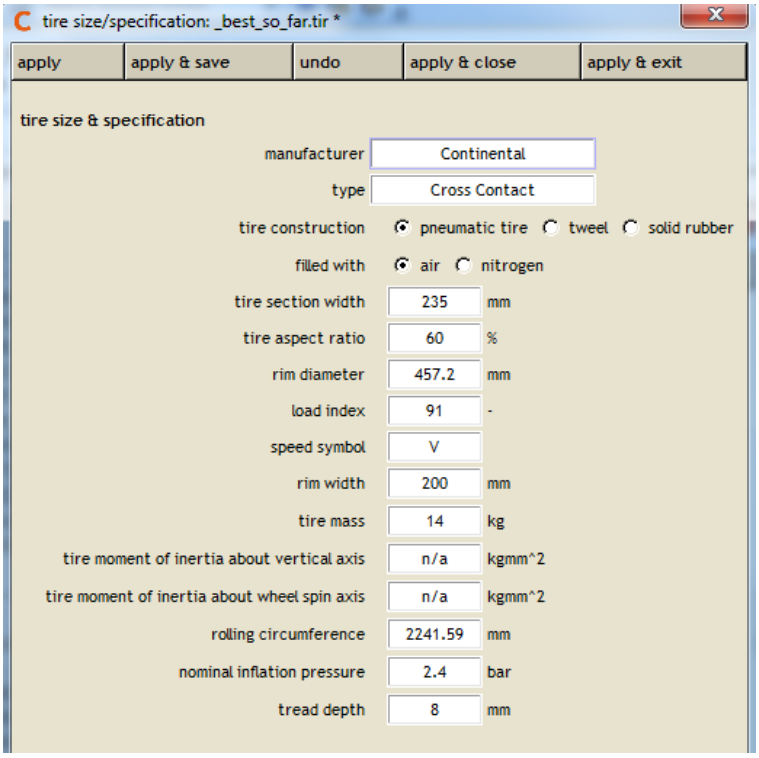

Figure 7.2 Tire size specification

According to the size of the tire model defined by users, FTire/fit will generate a rough tire cross section, in which the sidewall and the tread are included (Figure 7.3). However, the tire cross section is not exactly the same with the real tire cross section. Based on the difference, the real tire cross section image was imported into FTire/fit for identification. Figure 7.4 shows the real tire cross section image, in which the yellow points and the red points are marked to represent the tread surface and reinforcements respectively. In this way, the tread surface and reinforcements can be recognized by FTire/fit, and the geometry parameters can be tuned.

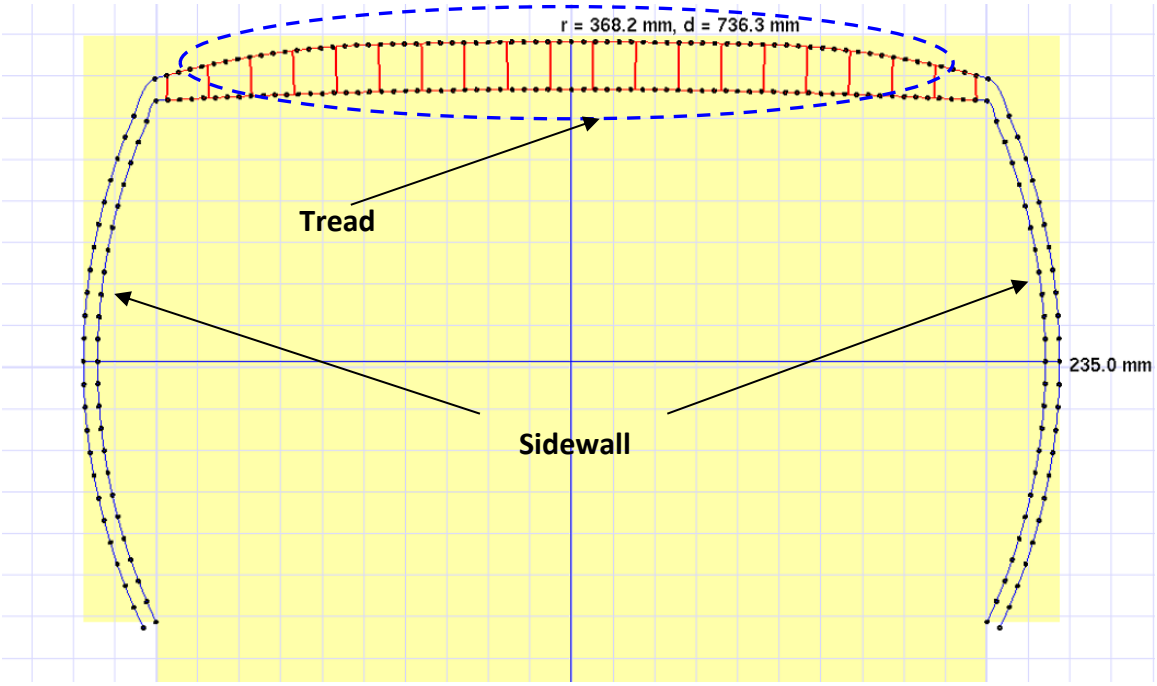

Figure 7.3 The rough tire cross-section generated by FTire/fit

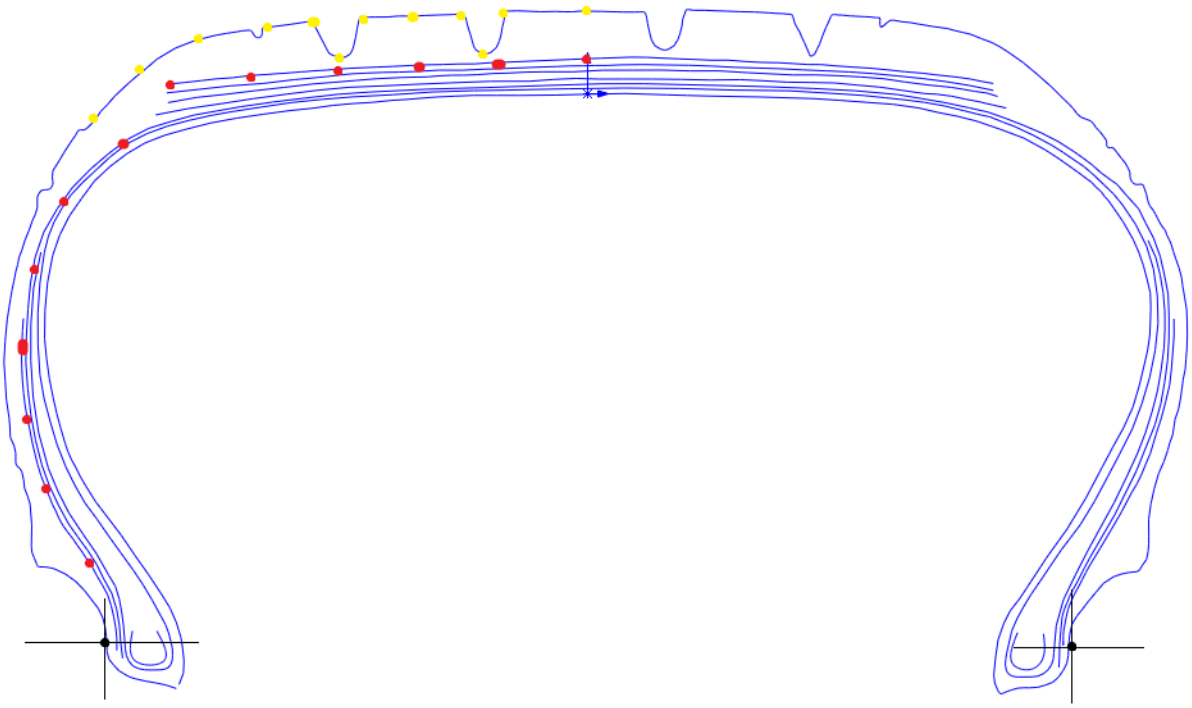

Figure 7.4 Tire cross section image extracted from a real tire

7.2.2 Footprint shapes

As discussed before, footprint images are an important part of experimental or simulation data, used for tire model identification in further steps.

The tread pattern is extracted from tire footprint figure (Figure 7.5), and the tire tread can be constructed by repeating the extracted pattern.

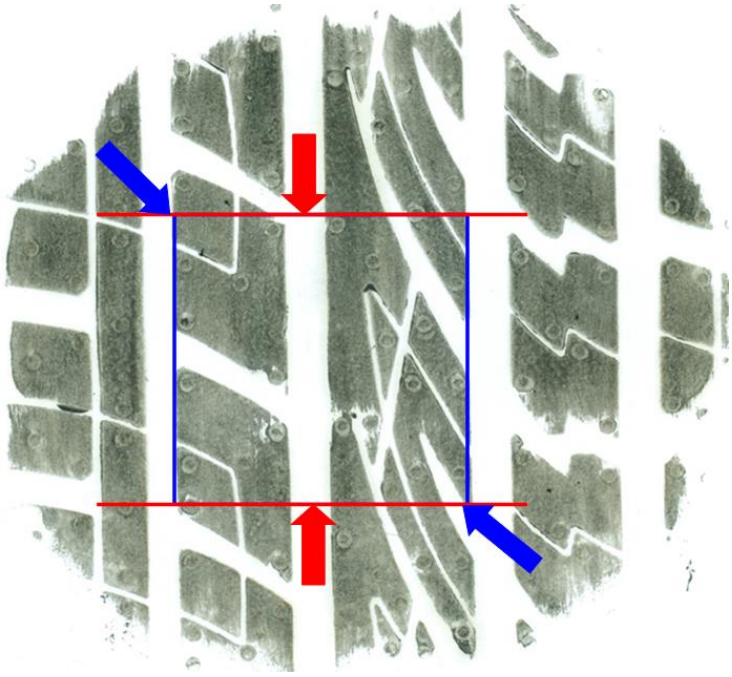

Figure 7.5 Tread pattern extraction

Tire footprint shapes can also be easily imported into FTire database using FTire/fit. The footprint image was scaled exactly by scanning the footprint image including a red line with known length, which can be entered in the data entry field in FTire/fit (Figure 7.6). In this study, the red line needs to be oriented perpendicular to the rolling direction. Tire footprints images for different vertical loads (1000N, 2000N, 3000N,4000N) and different inflation pressures (120kPa, 160kPa, 200kPa) were imported into FTire/fit using the same method, in which way the contact patch of FTire model can be validated and identified by FTire/fit (Figure 7.7).

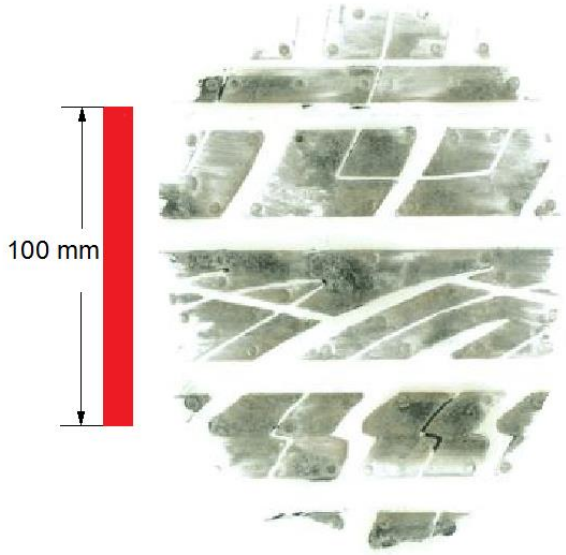

Figure 7.6 Image of footprint

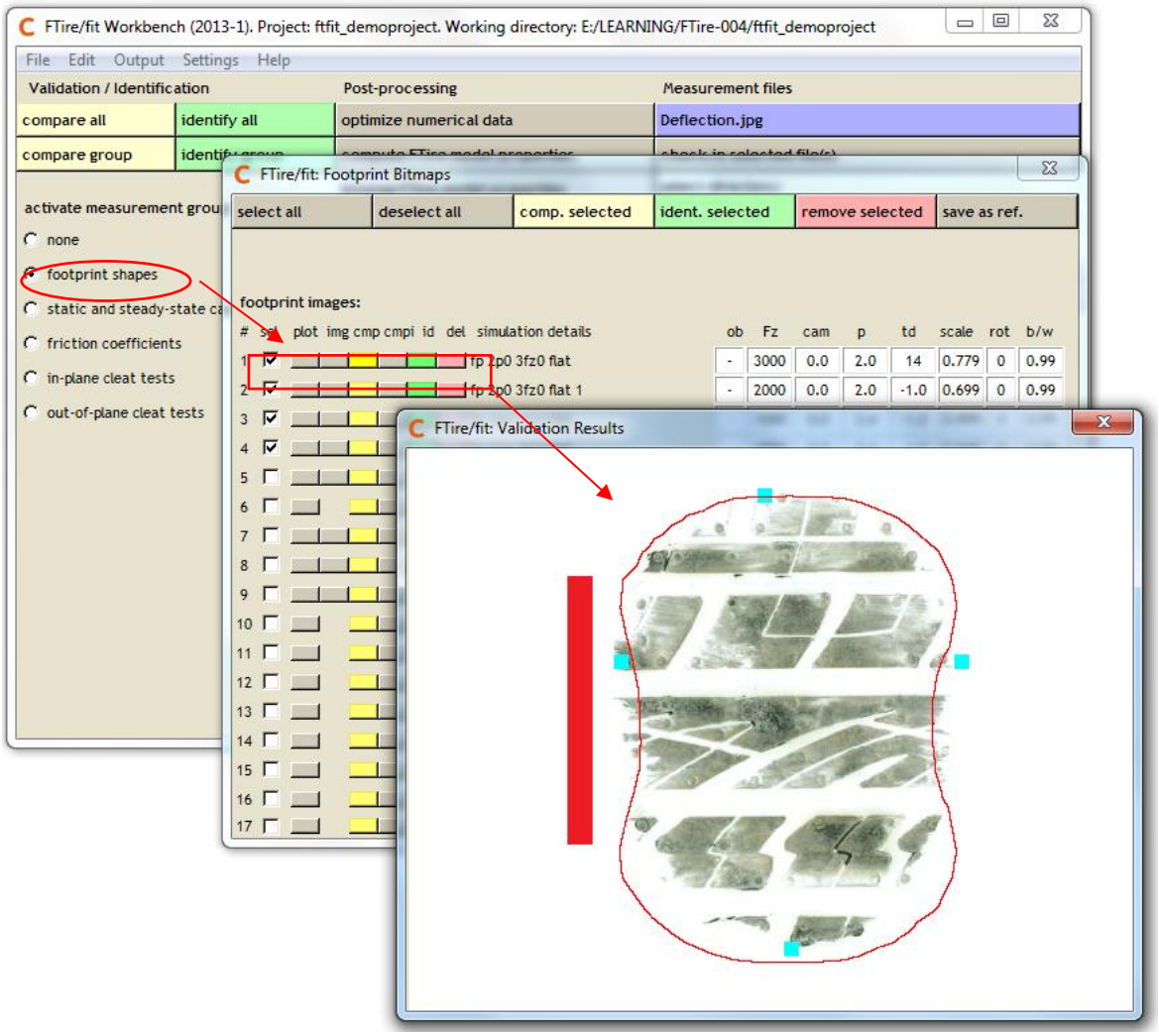

Figure 7.7 Validation of size of footprint

7.2.3 Static and steady-state test/simulation data

As very important parameters, tire static stiffness data like radial, longitudinal and lateral stiffness from experimental tests or simulations are imported into FTire database for validation and identification.

Two methods are available for importing the radial stiffness data into FTire/fit. The first one is marking the points with single red pixels on the tire stiffness curve, which is illustrated in Figure 7.8. These important points can be recognized in the FTire/fit software. In order to exactly calibrate and straighten out the image, the origin position as well as axis end points were marked using blue pixels. With regard to the second method, FTire/fit user can directly input the data using ASCII file. The measured data or simulated data are used for validation and identification of the original FTire model as illustrated in Figure 7.9.

Similarly, tire longitudinal stiffness, lateral stiffness, together with cornering stiffness can be imported into FTire/fit using the same method as with radial stiffness. Different from static stiffness, cornering stiffness describes the relationship between slip angles and cornering forces.

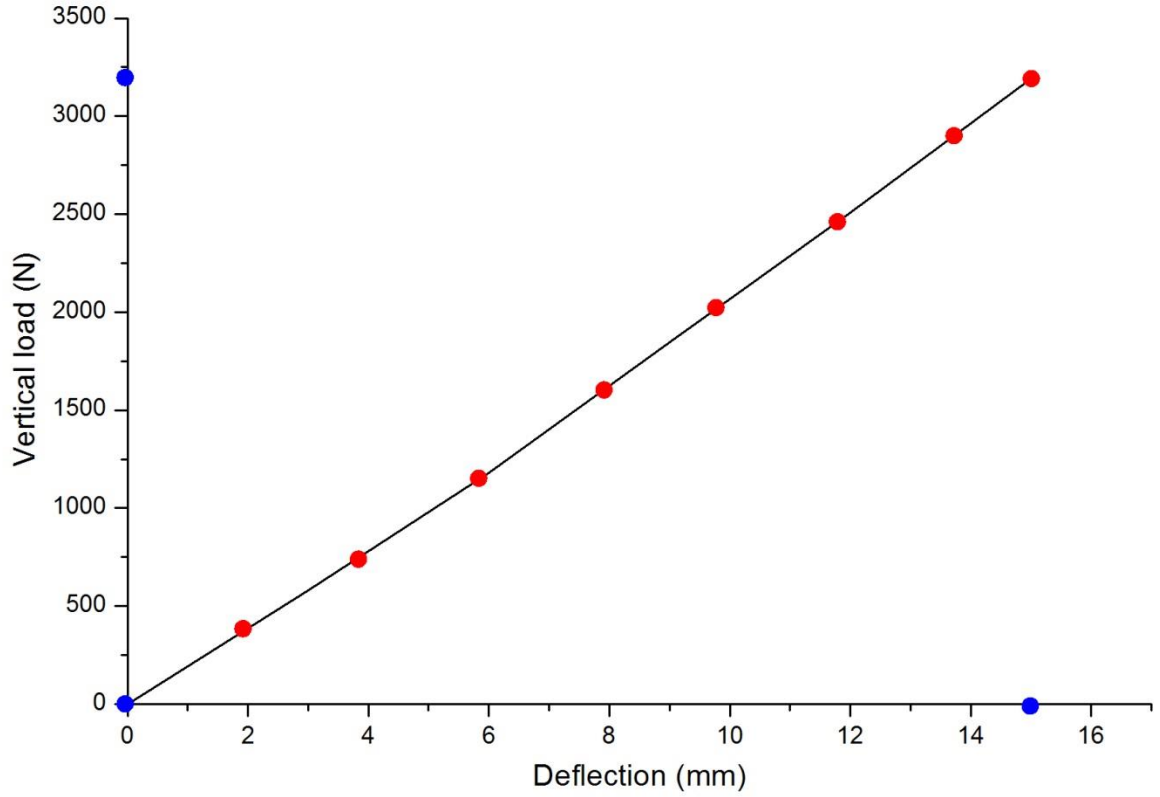

Figure 7.8 Image processing for static stiffness

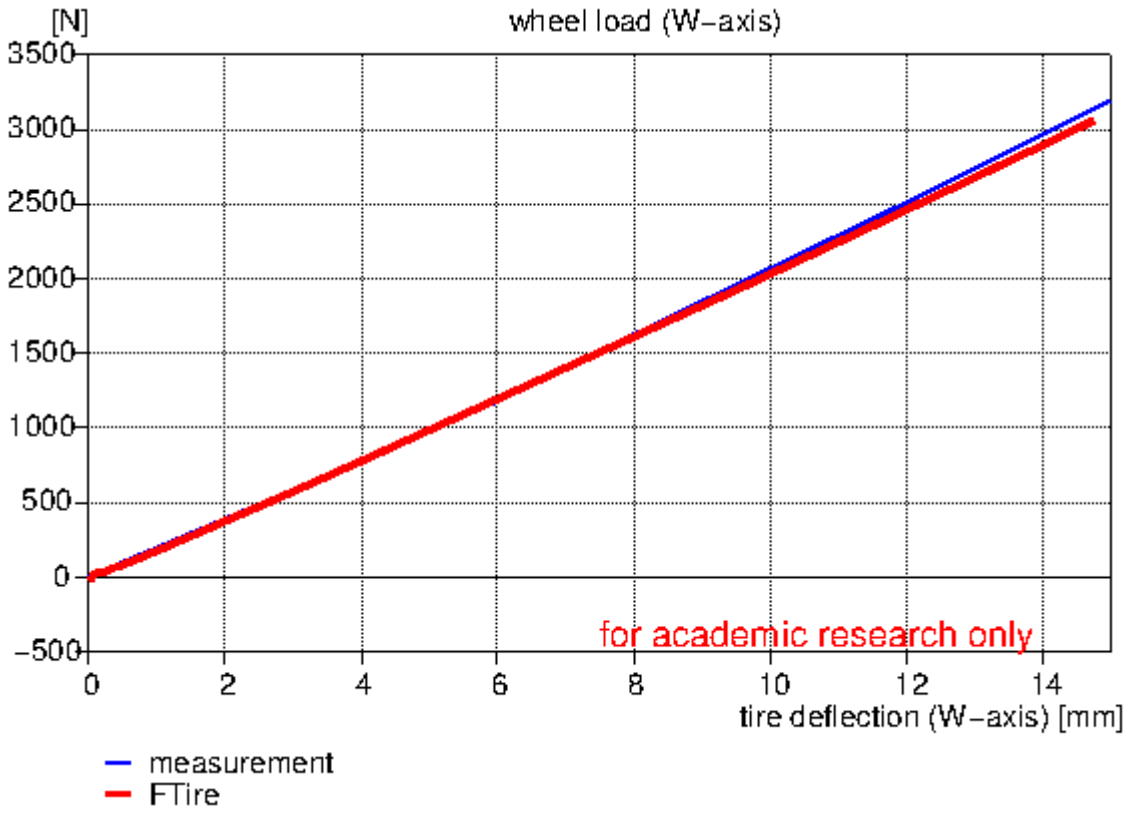

Figure 7.9 Validation of static stiffness

7.2.4 In-plane cleat test/simulation data

Cleat definition was conducted using the contr.clt file, in which different types of cleats can be defined according to the requirements of users. In this study, 25mm x 10mm, 25mmx 20mm, 25mmx 25mm, 25mm x 30mm, 25mm x 40mm cleats were defined to represent the road obstacles.

Tire transient dynamic responses for tire traversing obstacles were imported in FTire/fit in terms of in-plane cleat test/simulation data. Take the tire rolling over a 25mm × 20mm cleat at 30km/h as an example, the longitudinal responses validation in both time domain and frequency domain are given in Figure 7.10, while Figure 7.11 shows the radial forces validation. FTire/fit identification was also carried out based on the differences between measurement/simulation data and FTire data in order to tune the existing FTire model.

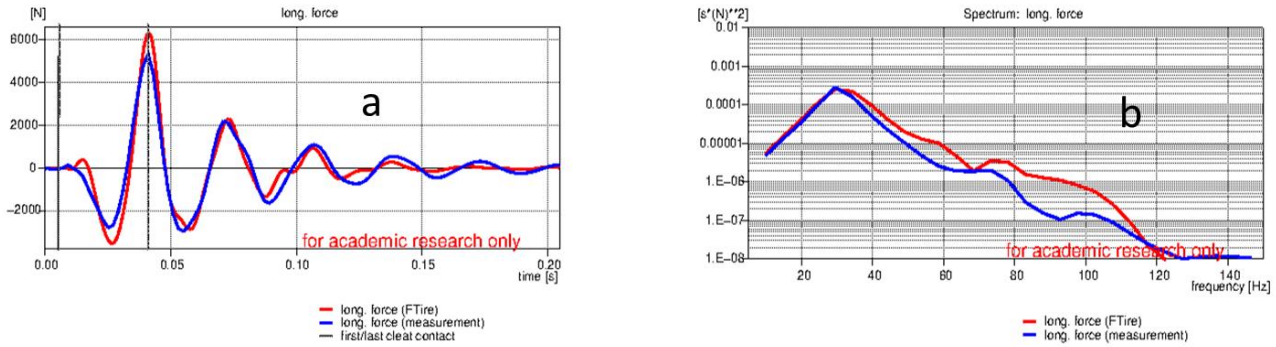

Figure 7.10 Validation results of tire longitudinal forces for tire rolling over 25mm × 20mm cleat at 30km/h (a) in time domain (b) in frequency domain

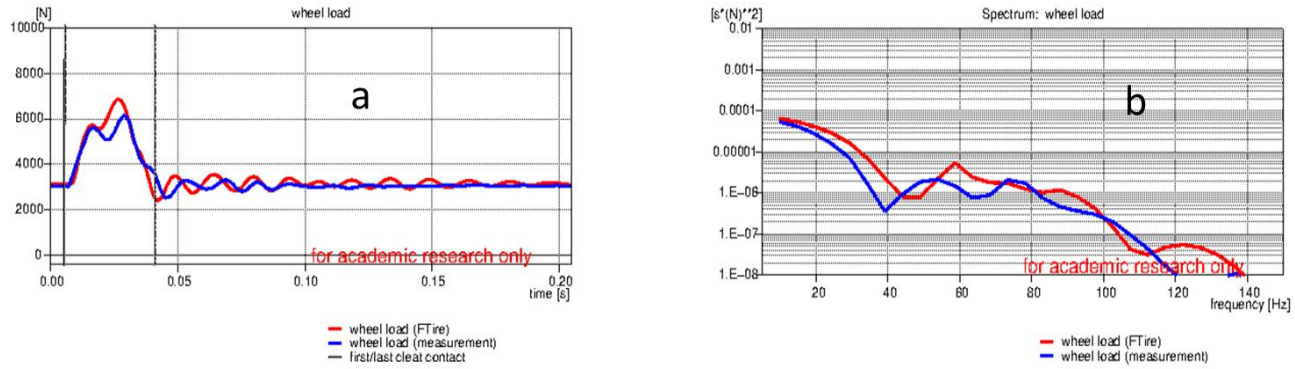

Figure 7.11 Validation results of tire longitudinal forces for tire rolling over 25mm × 20mm cleat at 30km/h (a) in time domain (b) in frequency domain

7.3 Multi-body dynamic simulation with FTire models

According the requirement of the research together with the derivation method described in the previous section, different FTire models are derived using the measurement and simulation data.

In this study, three kinds of FTire models are obtained and described in the following:

FTire derived by Mearsurement data (FTire#a)

- Footprint shapes
- Static and steady-state case
- In-plane cleat test data (25mm x 10mm, 25mmx 20mm, 25mm x 25mm)

FTire derived by FE simulation data for normal road obstacles (FTire#b)

- Footprint shapes
- Static and steady-state case
- In-plane cleat simulation data (25mm x 10mm, 25mmx 20mm, 25mm x 25mm)

FTire derived by FE simulation data including large road obstacles (FTire#c)

- Footprint shapes
- Static and steady-state case
- In-plane cleat simulation data (25mm x 10mm, 25mmx 20mm, 25mm x 25mm, 25mm x 30mm, 25mm x 40mm)

It can be found from the three models that FTire#c was derived at a wider operating condition, which covers much higher road obstacles. FTire#a and FTire#b were derived under the same operating conditions, and this is also convenient to identify the accuracy of FTire model derived using FE methods.

7.3.1 Multi-body dynamic model for tire rolling analysis

A simple tire/wheel model was built in SIMPACK. This model is composed of a tire, an axle, and a rim, which can be seen in Figure 7.12. Figure 7.13 shows the topology structure of the tire/wheel model. In this model, the axle is allowed to travel at a constant velocity in the longitudinal direction, the rim can only rotate relative to the axle, and all the freedoms of the tire relative to the rim are fixed.

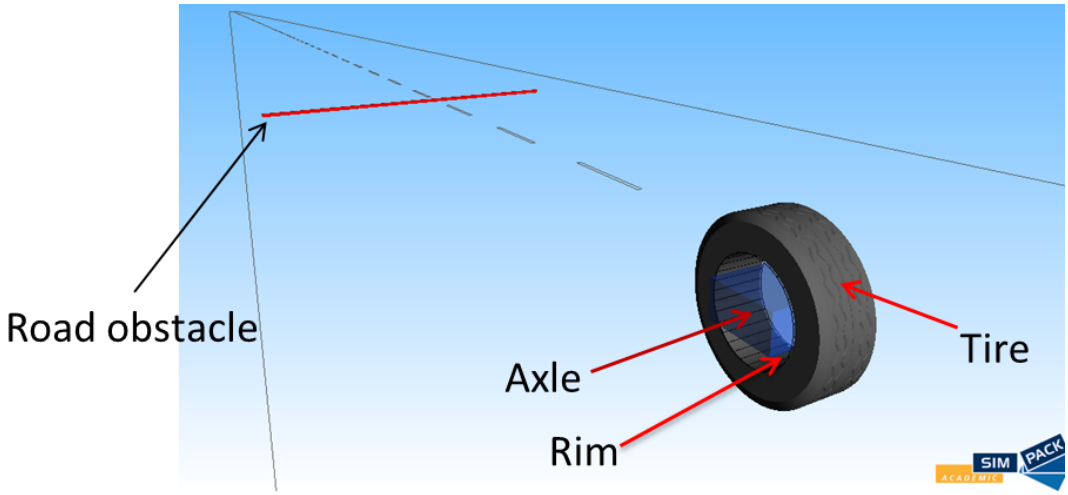

Figure 7.12 3D tire/wheel model in SIMPACK

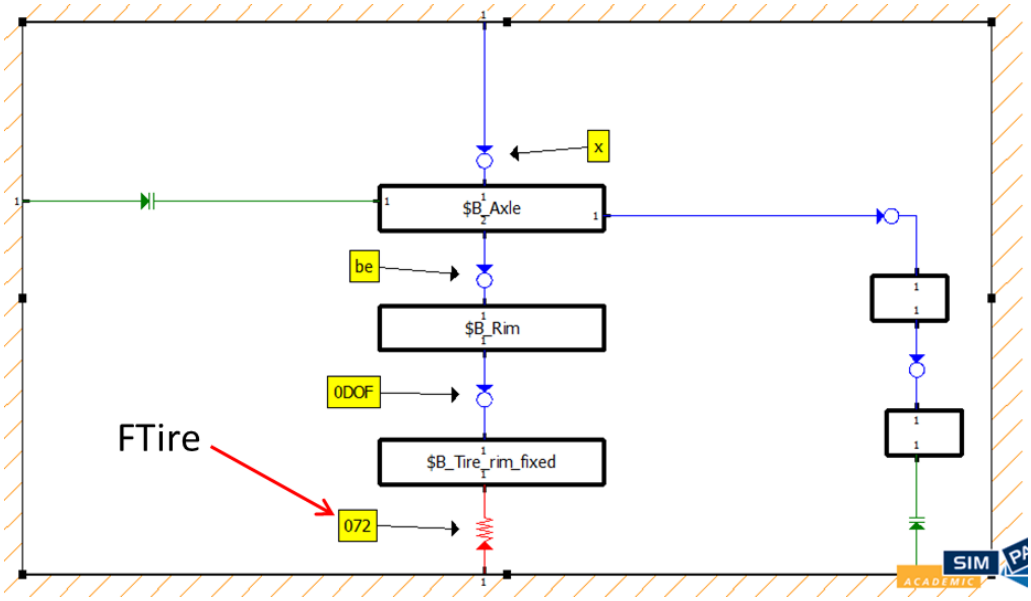

Figure 7.13 Topology Structure of the tire/wheel model

7.3.2 Multi-body simulation for tire rolling over obstacles (lower than 25mm)

These three different FTire models (FTire#a, FTire#b, FTire#c) were applied on the multi-body dynamic system for tire rolling analysis. Two different cleats (25mm x 10mm, 25mm x 20mm) were created for modelling of road obstacles using FTire/road file. As mentioned above, FTire#a was derived by measurement data, in which only obstacles not higher than 25mm were adopted. Hence, multi-body dynamic simulations are firstly carried out under an available condition in order that the accuracy of the three FTire models can be examined. It is worthy to note that the available condition means that it can be conducted with physical tests. Meanwhile, comparisons between these three kinds of FTire models are carried out. The difference between FTire#b and FTire#c is that FTire#c was derived by more simulation data, which means it can cover road conditions with higher obstacles. In this study, the road condition defined by road obstacles lower than 25mm is considered as non-extended condition, while the road condition defined by road obstacles higher than 25mm is considered as extended condition.

Figure 7.14 shows tire dynamic responses when it rolls over 25mm x 10mm obstacle in SIMPACK. Figure 7.14(a) describes the longitudinal spindle force variation, and the process is recorded from when the tire starts rolling until the tire traverses the obstacle. It is needed to mention that the travelling velocity in the simulations is 30km/h. Tire longitudinal dynamic responses simulated using the three different FTire models agree well with each other. However, the peak value of longitudinal forces obtained by FTire#b is smaller than the other two models. The reason for this can be attributed to the FE simulation results for tire rolling over the 10mm high obstacle, which can also be found in Figure 6.7. With regard to the tire rolling over 25mm x 20mm obstacle, the same difference can be found between tire dynamic responses using FTire#a and FTire#b in Figure 7.15(a). It is noted that the peak value of longitudinal forces predicted using FTire#c is much closer to that predicted using FTire#a for

both 10mm and 20mm high obstacles. Since FTire#c model is derived from tire dynamic responses with a wider range of road obstacles, the FTire/fit system may attempt to tune the model, which make the results be closer to the results predicted using FTire#a.

Figure 7.14(b) and Figure 7.15(b) show the vertical force variation for tire traversing 25mm x 10mm and 25mm x 20mm obstacles. It can be seen the vertical dynamic responses predicted using the three different FTire models agree well with each other, particularly for the peak value of the vertical forces.

With the comparison between the transient dynamic responses using the three FTire models, the following conclusions may be drawn:

- FTire models (e.g. FTire#b) derived using the dynamic responses obtained by FE simulations at non-extended condition is capable of predicting tire dynamic responses at non-extended conditions using Multi-body dynamic simulations.
- There are slight differences between transient dynamic responses predicted using FTire#c and FTire#b. Therefore, The FTire model (e.g. FTire#c) derived using the dynamic responses at both non-extended and extended conditions obtained by FE simulations is also capable of predicting tire dynamic responses at non-extended conditions using Multi-body dynamic simulations.

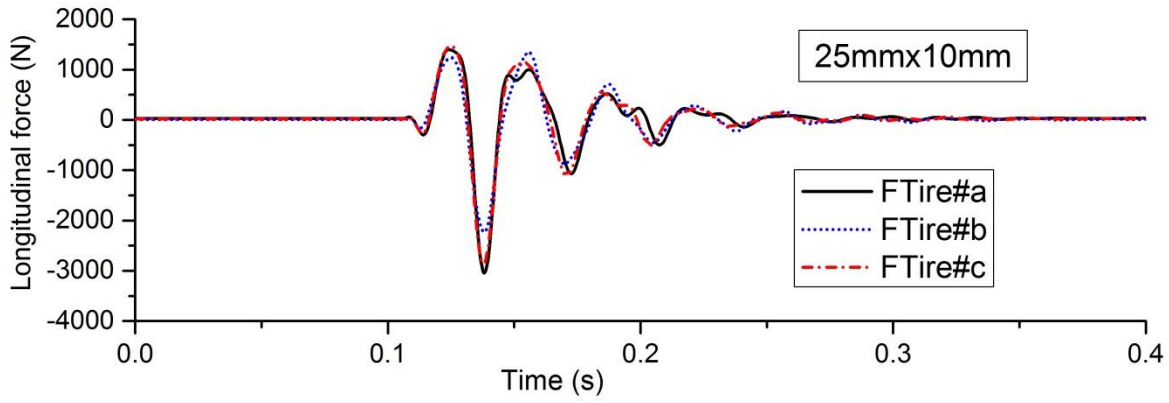

(a)

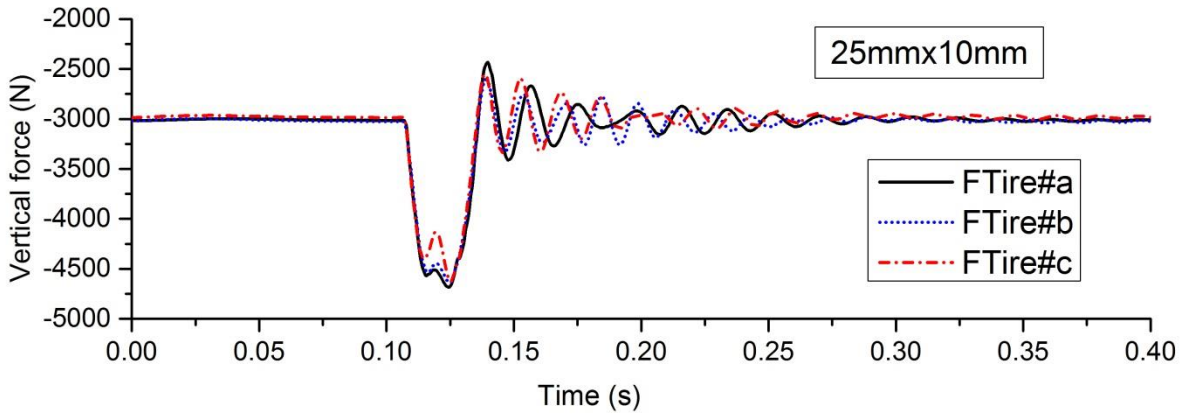

(b)

Figure 7.14 Tire transient dynamic responses for tire traversing 25mmx10mm cleat. (a) Longitudinal force, (b) Vertical force.

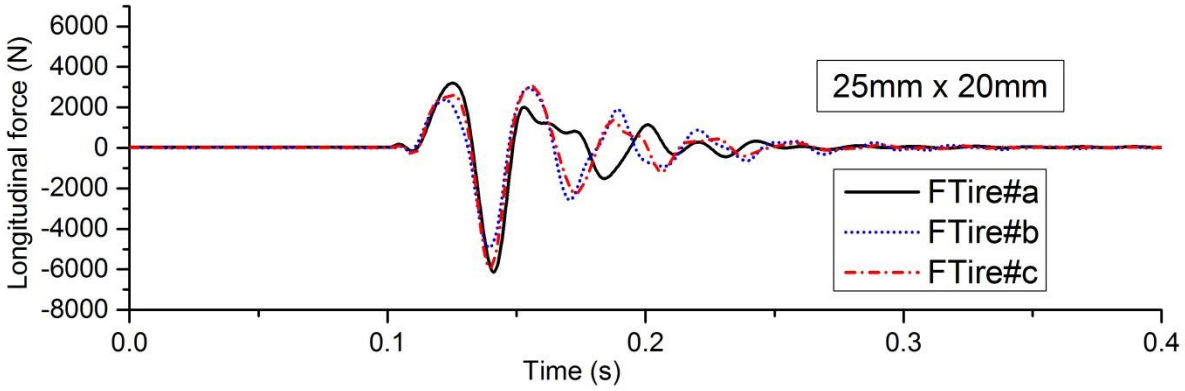

(a)

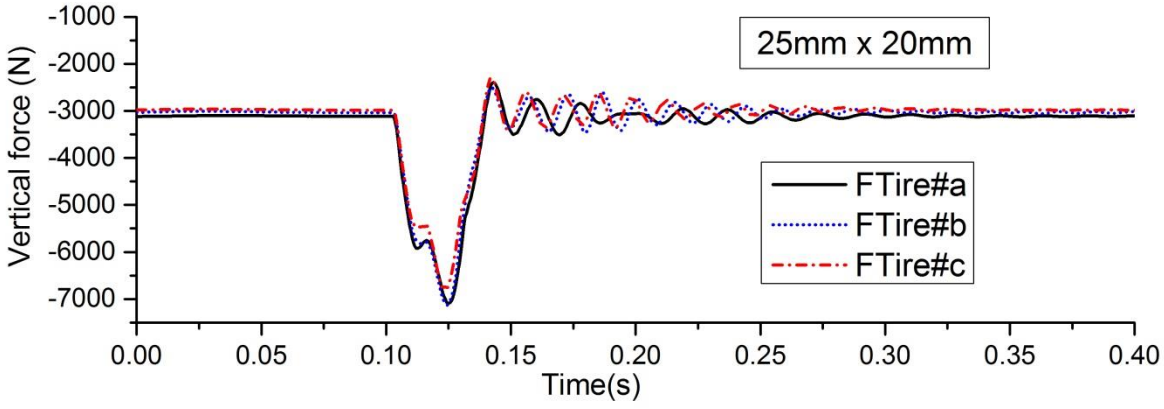

(b)

Figure 7.15 Tire transient dynamic responses for tire traversing 25mmx20mm cleat. (a) Longitudinal force, (b) Vertical force.

7.3.3 Multi-body simulation for tire rolling over obstacles (higher than 25mm)

In order to investigate the influence of FTire model's difference on multibody dynamic responses at severe conditions, the two kinds of FTire models (FTire#b, FTire#c) together

with the original FE simulation results were considered to make comparisons. FTire#b model was derived by limited FE simulation data, which means the transient dynamic responses did not include the simulation data at extended conditions (cleat higher than 25mm). FTire#c, however, was derived using full simulation data which covered both smaller obstacles (lower than 25mm) conditions and extended conditions (obstacle higher than 25mm). And also the FE simulation results are taken to identify the accuracy of the two FTire models.

In terms of tire rolling over 25mm x 30mm obstacle, it can be found in Figure 7.16 (a) that the longitudinal responses predicted using FTire#c agrees well with that predicted using FE code ABAQUS. The peak value of the longitudinal forces predicted using FTire#b is smaller than that predicted using the other two methods. On the other hand, Figure 7.16 (b) shows the vertical responses predicted by FE codes and Multi-body Simulation (MBS) using FTire#b and FTire#c. The general variations of vertical responses for the three cases are similar. However, the peak value predicted using FTire#b is much bigger than that predicted using the other two methods (FE simulation and MBS with FTire#c).

For tire rolling over 25mmx 40mm obstacle, the longitudinal dynamic forces predicted using FTire#b and FTire#c have similar characteristics with that predicted using pure FE method. However, the peak value of longitudinal forces obtained by MBS using FTire#c model is closer to the FE simulation result when compared with that obtained by simulation using FTire#b model. The vertical dynamic forces generated when the tire rolls over 25mm x 40mm obstacle are shown in Figure 7.17 (b). The peak value of the vertical forces obtained using FTire#b is much higher than the value obtained for the other two cases.

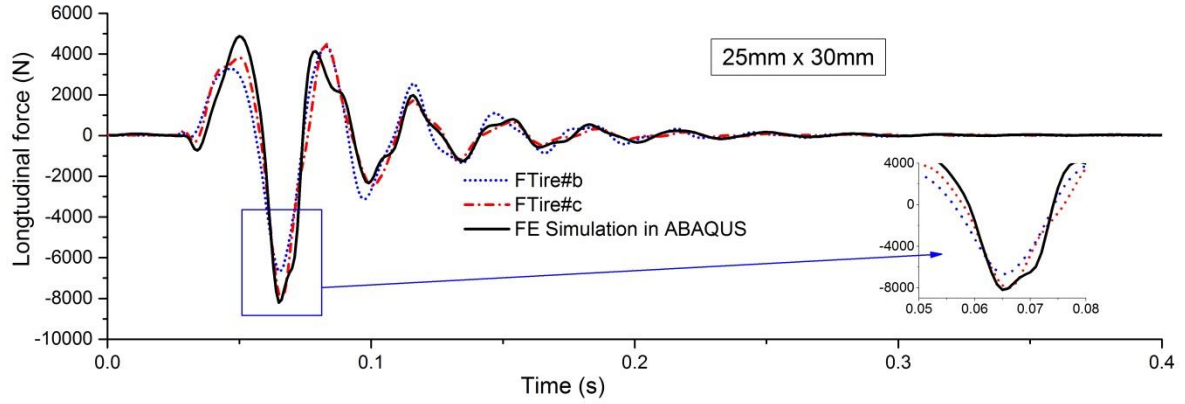

(a)

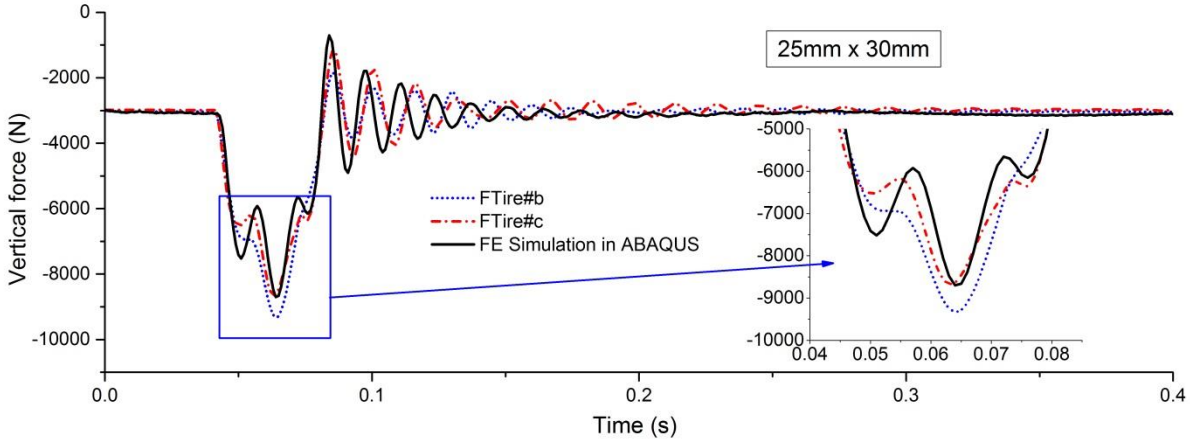

(b)

Figure 7.16 Tire transient dynamic responses for tire traversing 25mmx30mm cleat. (a) Longitudinal force, (b) Vertical force.

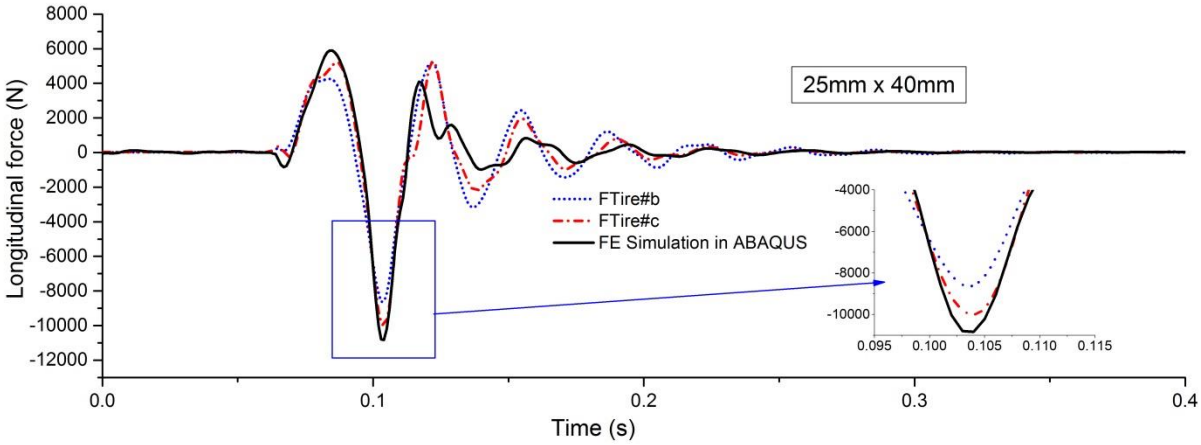

(a)

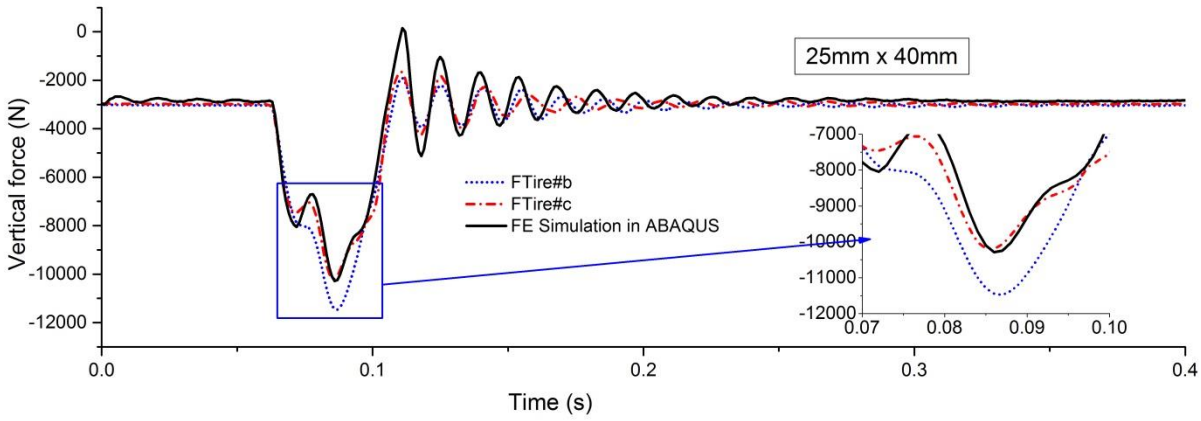

(b)

Figure 7.17 Tire transient dynamic responses for tire traversing 25mmx40mm cleat. (a) Longitudinal force, (b) Vertical force.

7.4 Summary and Conclusions

In this chapter, FTire model derivation procedure was presented. The geometry information, static and steady-state property, together with transient dynamic property data were used to validate and identify FTire parameters. Three kinds of FTire models were derived based on the experimental data and numerical simulation data.

Multi-body dynamic software SIMPACK was adopted to build a tire/wheel model, the boundary condition of which was set the same as that in numerical simulations. The three different FTire models FTire#a, FTire#b and FTire#c were imported into multi-body dynamic model through an interface.

With the comparison of transient dynamic responses among the FTire models under non-extended conditions and extended conditions, the following conclusions can be obtained:

1. Both FTire#b and FTire#c are able to be used for predicting tire dynamic responses for tire rolling over obstacles lower than 25mm in SIMPACK. Particularly, the peak value of transient dynamic forces have slight difference between FTire#a, FTire#b and FTire#c.

2. With regard to multi-body simulations under extended conditions, FTire#b is not accurate enough for prediction of transient dynamic responses, particularly for tire impacting on the obstacles. Nevertheless, transient dynamic responses obtained using FTire#c showed very satisfactory results in comparison with FE simulation data.
3. Multi-body dynamic tire/wheel model associated with FTire model can be more efficient to predict transient dynamic properties of rolling tires. The satisfactory results obtained using appropriate FTire model within SIMPACK agree well with results obtained from FE analysis.
4. The FTire model tuned using FE simulation including both non-extended and extended condition can be used for simulation of tire impacting on large obstacles. It also gives multi-body dynamic software users confidence to conduct tire impacting road unevenness simulations using quarter-vehicle and whole vehicle simulations under severe conditions.

Chapter 8 CONCLUSION AND FUTURE WORKS

8.1 Conclusion

In order to derive FTire parameters for extended range of operating conditions, a detailed finite element tire model was developed for static and dynamic analysis. Based on the literature surveys, it was found that most of the analytical tire models cannot predict tire transient dynamic responses under high-frequency road excitations. In addition, measurements of tire dynamic properties for tire rolling over large obstacles are also unavailable because of limitations in laboratory facilities.

A detailed method for the determination of geometry and material properties of tires has been developed for tire modelling. An image processing method was adopted to capture the tire cross-section geometry data. Hyperelastic and viscoelastic properties were determined by fitting experimental data using Yeoh model and Prony series respectively.

The analysis procedure consists firstly of developing a 2D FE tire model followed by inflation pressure analysis conducted based on the 2D model. The 3D tire model was then obtained by revolving the 2D axisymmetric tire model. Inflated tire shapes, tire static stiffness and footprints under different operating conditions have been predicted using the 3D tire model and validated by physical tests and satisfactory results were obtained.

As part of the study to validate the tire model, steady-state dynamic analysis has also been carried out in predicting cornering behaviour. The cornering forces predicted using FE tire model under different vertical loads and inflation pressures agree well with those measured in physical tests. Parametric studies were carried out to investigate the effect of operating conditions and material properties on the cornering behaviour. In terms of operating

conditions, it was found that higher vertical load and higher friction coefficient produce higher cornering stiffness and higher peak of aligning moment, but the higher inflation pressure produces lower cornering stiffness. In terms of design parameters, it was shown that the steel belt angle has the most significant effect on cornering stiffness with a steel belt angle of 30° producing significantly higher cornering stiffness than that of 10° and 20°. Other parameters such as steel belt spacing, tread rubber densities and carcass reinforcement density have much less significant effect on cornering properties.

Based on the FE tire model developed, transient dynamic analysis was carried out for tire rolling over different road obstacles. Validation of tire dynamic responses when rolling over 25mmx10mm, 25mmx20mm, 25mmx25mm obstacles was carried out. The spindle responses in terms of longitudinal and vertical forces predicted using FE tire model agreed well with experimental data. Therefore, the tire model was deemed capable of predicting tire transient dynamic responses for tire impacting road obstacles.

Three FTire models were derived for the tire using footprint shape, static test and steady state rolling test data in conjuction with in-plane cleat test data. FTire#a was obtained using physically measured data for cleats up to 25mm x 25mm (width x height). FTire#b was obtained using FE model derived data for cleats up to 25mm x 25mm while FTire#c was derived using FE model derived data for cleats up to 25mm x 40mm. When these FTire models were implemented in a multi-body dynamics (MBD) model, the FTire#c model performed well in terms of tire transient dynamic responses under extended conditions for prediction of both longitudinal spindle forces and vertical spindle forces. Particularly, the peak value of longitudinal forces obtained using FTire#c is much closer to full scale FE simulation results than using FTire#b. Also, the peak value of vertical forces predicted using

FTire#b is much higher than the original FE simulation result, while the peak value obtained using FTire#c shows satisfactory result when compared the FE simulation value.

Since MBS simulation using FTire model is much more efficient in carrying out vehicle dynamic analysis, numerical simulation in terms of FEA can be chosen to develop accurate and suitable FTire models, and then tire and vehicle dynamic responses can be accurately predicted using the tuned FTire models.

Therefore, FEA can be effectively used to derive FTire paramters at extended conditions which experimental tests cannot carry out.

8.2 Future works

A detailed Finite Element model was developed and used for derivation of FTire parameters. However, some numerical simulation data are also needed so that more accurate FTire model can be derived. Longitudinal and lateral stiffness under different operating conditions need to be measured in future. In addition, because of the limitations in laboratory facilities, experiments of camber behaviour could not be carried out. The current test rig's configuration has to be changed whenever a cornering test needs to be carried out. A re-design of the rig to enable different tests to be carried out without having to change the rig configuration would facilitate easier determination of FTire parameter determination since tire natural frequencies under different conditions are important for tire dynamic analysis.

For the transient dynamic properties prediction using FE tire model, it can be seen that some results when the tire rolls over obstacles are not very satisfactory compared with the experimental data. The reason can be attributed to the damping model used in this study. A more accurate structural damping model or material model needs to be developed in future. In addition, the accuracy of predicting longitudinal dynamic forces can be improved since

only a simple friction model was used in this study. A new friction model could be developed based on rubber-pavement force measurements.

All the transient dynamic analysis done in this study was concentrated on tire rolling over obstacles normal to the road track line. Only a few simulations or measurements focusing on the cleat inclined at an angle with the road track line (Figure 8.1) can be found in the literature. This would apply in the case of the tire traversing an obstacle while cornering or the tire traversing an obstacle inclined to the road track. In the future study, this case should be considered in order that a more comprehensive FTire model can be derived.

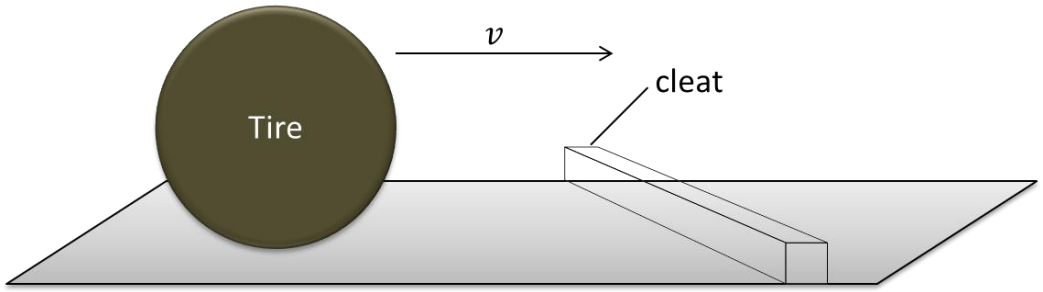

Figure 8.1 Tire rolls over an inclined cleat

For the boundary conditions used in measurements and simulations, the height of the rolling tire has been fixed. However, the height of rolling tire cannot keep constant in real life. Therefore, the force control method needs to be adopted in the future simulations and measurements whereby the tire/road contact force could be constant in the process of tire traversing an obstacle. This could provide better frequency response correlation by releasing the freedom of the spindle.

In this study, most of the work has been focused on the numerical simulation of a single tire. However, the objective of FTire model development is to use the model in quarter vehicle and full vehicle dynamic analysis. Derived FTire models should be implemented in quarter vehicle and full vehicle models and their dynamic behaviour validated against physical test results.

References

1. Gipser, M., *FTire: a physically based application-oriented tyre model for use with detailed MBS and finite-element suspension models.* Vehicle System Dynamics, 2005. **43**: p. 76-91.
2. Clark, S.K., *Rolling Tire under Load.* Sae Transactions, 1966. **74**: p. 126-&.
3. Tielking, J.T., *Plane Vibration Characteristics of a Pneumatic Tire Model.* Sae Transactions, 1966. **74**: p. 126-&.
4. Keltie, R.F., *Analytical Model of the Truck Tire Vibration Sound Mechanism.* Journal of the Acoustical Society of America, 1982. **71**(2): p. 359-367.
5. Soedel, W., *On the dynamic response of rolling tires according to thin shell approximations.* Journal of Sound and Vibration, 1975. **41**(2): p. 233-246.
6. Huang, S.C. and W. Soedel, *Effects of coriolis acceleration on the free and forced in-plane vibrations of rotating rings on elastic foundation.* Journal of Sound and Vibration, 1987. **115**(2): p. 253-274.
7. Gong, S., *A Study of In-Plane Dynamics of Tires.* Ph.D Thesis, Delft University of Technology, Faculty of Mechanical Engineering and Marine Technology, 1993.
8. Dohrmann, C.R., *Dynamics of a tire-wheel-suspension assembly.* Journal of Sound and Vibration, 1998. **210**(5): p. 627-642.
9. Kim, S.J. and A.R. Savkoor, *The contact problem of in-plane rolling of tires on a flat road.* Vehicle System Dynamics, 1997. **27**: p. 189-206.
10. Wei, Y.T., L. Nasdala, and H. Rothert, *Analysis of forced transient response for rotating tires using REF models.* Journal of Sound and Vibration, 2009. **320**(1-2): p. 145-162.
11. Springer, H., H. Ecker, and A. Slibar, *A New Analytical Model to Investigate Transient Rolling Conditions of a Steel-Belted Tire.* Vehicle System Dynamics, 1988. **17**: p. 448-459.
12. Qiu, X.D., J. Liu, and Y.X. Men, *A Modified Point-Contact Tire Model for the Simulation of Vehicle Ride Quality.* Journal of Terramechanics, 1993. **30**(3): p. 133-141.
13. Mastinu, G., et al., *A semi-analytical tyre model for steady- and transient-state simulations.* Vehicle System Dynamics, 1997. **27**: p. 2-21.
14. Goel, V. and K. Ramji, *Analytical predictions of steady state tyre characteristics.* International Journal of Vehicle Design, 2004. **34**(3): p. 260-285.
15. Srinivasa Rao, S., K. Ramji, and M.K. Naidu, *Analytical approach for the prediction of steady state tyre forces and moments under different normal pressure distributions.* Journal of Terramechanics, 2012. **49**(5): p. 281-289.

16. Kao, B.G., *A Three-Dimensional Dynamic Tire Model for Vehicle Dynamic Simulations.* Tire Science and Technology, 2000. **28**(2): p. 72-95.
17. Kao, B.G., *Tire Vibration Modes and Tire Stiffness.* Tire Science and Technology, 2002. **30**(3): p. 136-155.
18. Shim, T. and D. Margolis, *An analytical tyre model for vehicle simulation in normal driving conditions.* International Journal of Vehicle Design, 2004. **35**(3): p. 224-240.
19. Peng, C., et al., *Lateral Tyre Dynamic Characteristics.* Journal of Terramechanics, 1994. **31**(6): p. 395-414.
20. Wang, R.R. and J.M. Wang, *Tire-road friction coefficient and tire cornering stiffness estimation based on longitudinal tire force difference generation.* Control Engineering Practice, 2013. **21**(1): p. 65-75.
21. Kilner, J.R., *Pneumatic Tire Model for Aircraft Simulation.* Journal of Aircraft, 1982. **19**(10): p. 851-857.
22. Guo, K., *Tire Roller Contact Model for Simulation of Vehicle Vibration Input*. 1993, SAE International.
23. Guo, K. and Q. Liu, *A Model of Tire Enveloping Properties and Its Application on Modelling of Automobile Vibration Systems*. 1998, SAE International.
24. Wei, Y.T., L. Nasdala, and H. Rothert, *Analysis of Tire Rolling Contact Response by REF Model.* Tire Science and Technology, 2004. **32**(4): p. 214-235.
25. Pacejka, H.B. and E. Bakker, *The Magic Formula Tyre Model.* Tyre Models for Vehicle Dynamics Analysis, 1993: p. 1-18.
26. Pacejka, H.B. and I.J.M. Besselink, *Magic formula tyre model with transient properties.* Vehicle System Dynamics, 1997. **27**: p. 234-249.
27. Dihua, G., S. Jin, and L.H. Yam, *Establishment of model for tire steady state cornering properties using experimental modal parameters.* Vehicle System Dynamics, 2000. **34**(1): p. 43-56.
28. Shang, J., D.H. Guan, and L.H. Yam, *Study on tire dynamic cornering properties using experimental modal parameters.* Vehicle System Dynamics, 2002. **37**(2): p. 129-144.
29. Guo, K. and L. Ren, *A Unified Semi-Empirical Tire Model with HigherAccuracy and Less Parameters*. 1999, SAE International.
30. Guo, K. and D. Lu, *UniTire: unified tire model for vehicle dynamic simulation.* Vehicle System Dynamics, 2007. **45**(sup1): p. 79-99.
31. Guo, K.-H., *A Unified Tire Model for Braking Driving and Steering Simulation*, in *The 5th International Pacific Conference on Automotive Engineering*. 1989, Society of Automotive Engineers of China: Beijing.

32. Narasimha Rao, K.V., R.K. Kumar, and P.C. Bohara, *Prediction Of Tyre Force And Moment Characteristics During Vehicle Cornering Using Finite Element Techniques*. 2004, The Automotive Research Association of India.
33. Bandel, P. and C. Monguzzi, *Simulation Model of the Dynamic Behavior of a Tire Running Over an Obstacle*. Tire Science and Technology, 1988. **16**(2): p. 62-77.
34. Guan, D.H. and C.J. Fan, *Tire modeling for vertical properties including enveloping properties using experimental modal parameters.* Vehicle System Dynamics, 2003. **40**(6): p. 419-433.
35. Guan, D.H., C.J. Fan, and X.H. Xie, *A dynamic tyre model of vertical performance rolling over cleats.* Vehicle System Dynamics, 2005. **43**: p. 209-222.
36. Zienkiewicz, O.C. and R.L. Taylor, *The finite element method*. 5th ed. 2000, Oxford: Butterworth-Heinemann. 384p.
37. Burke, A.M. and O.A. Olatunbosun, *New techniques in tyre medal analysis using MSC/NASTRAN.* International Journal of Vehicle Design, 1997. **18**(2): p. 203-212.
38. Burke, A.M. and O.A. Olatunbosun, *Contact modelling of the tyre/road interface.* International Journal of Vehicle Design, 1997. **18**(2): p. 194-202.
39. Burke, A.M. and O.A. Olatunbosun, *Static tyre/road interaction modelling.* Meccanica, 1997. **32**(5): p. 473-479.
40. Bolarinwa, E. and A. Olatunbosun, *Finite element simulation of the tyre burst test.* Proceedings of the Institution of Mechanical Engineers Part D-Journal of Automobile Engineering, 2004. **218**(D11): p. 1251-1258.
41. Olatunbosun, O.A. and O. Bolarinwa, *FE Simulation of the Effect of Tire Design Parameters on Lateral Forces and Moments.* Tire Science and Technology, 2004. **32**(3): p. 146-163.
42. Yang, X., O. Olatunbosun, and E. Bolarinwa, *Materials Testing for Finite Element Tire Model.* SAE Int. J. Mater. Manuf., 2010. **3**(1): p. 211-220.
43. Yang, X. and O.A. Olatunbosun, *Optimization of reinforcement turn-up effect on tyre durability and operating characteristics for racing tyre design.* Materials & Design, 2012. **35**: p. 798-809.
44. Behroozi, M., O.A. Olatunbosun, and W. Ding, *Finite element analysis of aircraft tyre - Effect of model complexity on tyre performance characteristics.* Materials & Design, 2012. **35**: p. 810-819.
45. Mc Allen, J., A.M. Cuitiño, and V. Sernas, *Numerical investigation of the deformation characteristics and heat generation in pneumatic aircraft tires: Part I. Mechanical modeling.* Finite Elements in Analysis and Design, 1996. **23**(2–4): p. 241-263.
46. Pelc, J., *Static three-dimensional modelling of pneumatic tyres using the technique of element overlaying.* Proceedings of the Institution of Mechanical Engineers Part D-Journal of Automobile Engineering, 2002. **216**(D9): p. 709-716.

47. Ghoreishy, M.H.R., *Finite element analysis of the steel-belted radial tyre with tread pattern under contact load.* Iranian Polymer Journal, 2006. **15**(8): p. 667-674.
48. Hu, Y.K. and P.F.J. Abeels, *Agricultural Tire Deformation in the 2d Case by Finite-Element Methods.* Journal of Terramechanics, 1994. **31**(6): p. 353-370.
49. Xu, Y.H., L.P. Jia, and J.W. Zhang, *Modeling tire/road contact using piecewise Ritz procedure.* Journal of Terramechanics, 2005. **42**(2): p. 99-113.
50. Nakashima, H. and J.Y. Wong, *A three-dimensional tire model by the finite element method.* Journal of Terramechanics, 1993. **30**(1): p. 21-34.
51. Perumpral, J.V., J.B. Liljedahl, and W.H. Perloff, *A numerical method for predicting the stress distribution and soil deformation under a tractor wheel.* Journal of Terramechanics, 1971. **8**(1): p. 9-22.
52. Yong, R.N., E.A. Fattah, and P. Boonsinsuk, *Analysis and Prediction of Tyre-Soil Interaction and Performance Using Finite-Elements.* Journal of Terramechanics, 1978. **15**(1): p. 43-63.
53. Clark, S.K., *Mechanics of Pneumatic Tires - Preface.* National Bureau of Standards Monographs, 1971(M122): p. R5-&.
54. Mohsenimanesh, A. and S.M. Ward, *Estimation of a three-dimensional tyre footprint using dynamic soil-tyre contact pressures.* Journal of Terramechanics, 2010. **47**(6): p. 415-421.
55. Korunović, N., M. Trajanović, and M. Stojković, *Finite element model for steady-state rolling tire analysis.* Journal of the Serbian Society for Computational Mechanics/Vol, 2007. **1**(1): p. 63-79.
56. Korunovic, N., et al., *Finite Element Analysis of a Tire Steady Rolling on the Drum and Comparison with Experiment.* Strojniski Vestnik-Journal of Mechanical Engineering, 2011. **57**(12): p. 888-897.
57. XU Zhe, W.W., ZHAO Shu-gao, *FEA on static and cornering stiffness characteristics of radial tire.* China Rubber Industry, 2010.
58. Li, Z., Z.R. Li, and Y.M. Xia, *An Implicit to Explicit FEA Solving of Tire F&M with Detailed Tread Blocks.* Tire Science and Technology, 2012. **40**(2): p. 83-107.
59. Koishi, M., K. Kabe, and M. Shiratori, *Tire Cornering Simulation Using an Explicit Finite Element Analysis Code.* Tire Science and Technology, 1998. **26**(2): p. 109-119.
60. Rao, K., R. Kumar, and P. Bohara, *Transient Finite Element Analysis of Tire Dynamic Behavior.* Tire Science and Technology, 2003. **31**(2): p. 104-127.
61. Faria, L.O., et al., *Tire Modeling by Finite Elements.* Tire Science and Technology, 1992. **20**(1): p. 33-56.
62. Zhang, Y., T. Palmer, and A. Farahani, *A Finite Element Tire Model and Vibration Analysis: A New Approach.* Tire Science and Technology, 1998. **26**(3): p. 149-172.
63. Choi, J.H., et al., *Numerical investigation of snow traction characteristics of 3-D patterned tire.* Journal of Terramechanics, 2012. **49**(2): p. 81-93.

64. Lee, J.H., *Finite element modeling of interfacial forces and contact stresses of pneumatic tire on fresh snow for combined longitudinal and lateral slips.* Journal of Terramechanics, 2011. **48**(3): p. 171-197.
65. Xia, K., *A large deformation finite element model for soil compaction.* Geomechanics and Geoengineering, 2011. **7**(2): p. 123-137.
66. Fervers, C.W., *Improved FEM simulation model for tire–soil interaction.* Journal of Terramechanics, 2004. **41**(2–3): p. 87-100.
67. Mousseau, C.W. and S.K. Clark, *An Analytical and Experimental Study of a Tire Rolling Over a Stepped Obstacle at Low Velocity.* Tire Science and Technology, 1994. **22**(3): p. 162-181.
68. Mousseau, C.W. and G.M. Hulbert, *An efficient tire model for the analysis of spindle forces produced by a tire impacting large obstacles.* Computer Methods in Applied Mechanics and Engineering, 1996. **135**(1–2): p. 15-34.
69. Mousseau, C.W. and G.M. Hulbert, *THE DYNAMIC RESPONSE OF SPINDLE FORCES PRODUCED BY A TIRE IMPACTING LARGE OBSTACLES IN A PLANE.* Journal of Sound and Vibration, 1996. **195**(5): p. 775-796.
70. Mousseau, C.W., et al., *Vehicle dynamics simulations with coupled multibody and finite element models.* Finite Elements in Analysis and Design, 1999. **31**(4): p. 295-315.
71. Cho, J.R., et al., *Transient dynamic response analysis of 3-D patterned tire rolling over cleat.* European Journal of Mechanics a-Solids, 2005. **24**(3): p. 519-531.
72. Kamoulakos, A. and B.G. Kao, *Transient Dynamics of a Tire Rolling over Small Obstacles — A Finite Element Approach with PAM-SHOCK.* Tire Science and Technology, 1998. **26**(2): p. 84-108.
73. Olatunbosun, O.A. and A.M. Burke, *Finite Element Modelling of Rotating Tires in the Time Domain.* Tire Science and Technology, 2002. **30**(1): p. 19-33.
74. Yu, H.J. and H. Aboutorabi, *Dynamics of Tire, Wheel, and Suspension Assembly.* Tire Science and Technology, 2001. **29**(2): p. 66-78.
75. Kerchman, V., *Tire-Suspension-Chassis Dynamics in Rolling over Obstacles for Ride and Harshness Analysis.* Tire Science and Technology, 2008. **36**(3): p. 158-191.
76. Taylor, R.K., L.L. Bashford, and M.D. Schrock, *Methods for measuring vertical tire stiffness.* Transactions of the Asae, 2000. **43**(6): p. 1415-1419.
77. Alkan, V., S. Karamihas, and G. Anlas, *Experimental analysis of tyre-enveloping characteristics at low speed.* Vehicle System Dynamics, 2009. **47**(5): p. 575-587.
78. Upadhyaya, S.K., D. Wulfsohn, and G. Jubbal, *Traction Prediction Equations for Radial Ply Tyres.* Journal of Terramechanics, 1989. **26**(2): p. 149-175.
79. Lyasko, M.I., *The Determination of Deflection and Contact Characteristics of a Pneumatic Tire on a Rigid Surface.* Journal of Terramechanics, 1994. **31**(4): p. 239-246.

80. Gipser, M., *FTire, a New Fast Tire Model for Ride Comfort Simulations*, in *International ADAMS User's conference* 1999: Berlin.
81. Gipser M., H.R., Lugner P., *Dynamical Tyre Forces Response to Road Unevennesses.* Vehicle System Dynamics Supplement, 1997. **27**.
82. Mastinu, G. and M. Plöchl, *Road and off-road vehicle system dynamics handbook*. pages cm.
83. Gipser, M., *The FTire Tire Model Family.* Automotive Engineering, 1998.
84. Gipser, M., *FTire: 10 years of development and Application.* FTire Documentation. URL:http://www.ftire.com/documentation.htm.
85. Riepl, A., W. Reinalter, and M. Schmid, *Application of the tyre model FTire in the vehicle development process at MAGNA STEYR Fahrzeugtechnik.* Vehicle System Dynamics, 2005. **43**: p. 370-383.
86. Riepl, A., W. Reinalter, and G. Fruhmann, *Rough road simulation with tire model RMOD-K and FTire.* Dynamics of Vehicles on Roads and on Tracks, 2003: p. 734-743.
87. Haga, H., *Evaluation of tyre models for durability loads prediction using a suspension-on-a-drum environment.* Vehicle System Dynamics, 2005. **43**: p. 281-296.
88. Dorfi, H.R., *Tire Cleat Impact and Force Transmission: Modeling Based on FTIRE and Correlation to Experimental Data*. 2004, SAE International.
89. Dorfi, H.R., *A Study of the In-Plane Force Transmission of Tires.* Tire Science and Technology, 2004. **32**(4): p. 188-213.
90. Kenny, T.M. and R.A. Stechschulte, *Applications of Finite Element Analysis in Tire Design.* Tire Science and Technology, 1988. **16**(2): p. 96-117.
91. Konde, A.K., et al., *On the modeling of aircraft tire.* Aerospace Science and Technology, 2013. **27**(1): p. 67-75.
92. Mooney, M., *A Theory of Large Elastic Deformation.* Journal of Applied Physics, 1940. **11**(9): p. 582-592.
93. Rivlin, R.S., *Large Elastic Deformations of Isotropic Materials. I. Fundamental Concepts.* Philosophical Transactions of the Royal Society of London. Series A, Mathematical and Physical Sciences, 1948. **240**(822): p. 459-490.
94. Yeoh, O.H., *Some Forms of the Strain Energy Function for Rubber.* Rubber Chemistry and Technology, 1993. **66**(5): p. 754-771.
95. Yeoh, O.H. and P.D. Fleming, *A new attempt to reconcile the statistical and phenomenological theories of rubber elasticity.* Journal of Polymer Science Part B-Polymer Physics, 1997. **35**(12): p. 1919-1931.
96. Ogden, R.W., *Non-linear elastic deformations*. 1997: Courier Dover Publications.
97. Yeoh, O.H., *On the Ogden strain-energy function.* Rubber Chemistry and Technology, 1997. **70**(2): p. 175-182.

98. Ogden, R.W., G. Saccomandi, and I. Sgura, *Fitting hyperelastic models to experimental data.* Computational Mechanics, 2004. **34**(6): p. 484-502.
99. Beda, T., *Modeling hyperelastic behavior of rubber: A novel invariant-based and a review of constitutive models.* Journal of Polymer Science Part B-Polymer Physics, 2007. **45**(13): p. 1713-1732.
100. Kim, W.-D., et al., *Some considerations on mechanical testing methods of rubbery materials using nonlinear finite element analysis.* Polymer International, 2004. **53**(7): p. 850-856.
101. Castellucci, M.A., A.T. Hughes, and W.V. Mars, *Comparison of test specimens for characterizing the dynamic properties of rubber.* Experimental Mechanics, 2008. **48**(1): p. 1-8.
102. Kupchella, R., J. Kidney, and W. Hutchison, *Test Methods for Hyperelastic Characterization of Rubber4.* Tire Science and Technology, 2009. **37**(3): p. 165-186.
103. Duncan, B., et al., *Verification of hyperelastic test methods.* NPL Report No. CMMT (A), 1999. **226**.
104. Hitt, D.J., M. Gilbert, and M. Marfell, *Development of a machine for the stretching of polymers.* Polymer Testing, 2000. **19**(1): p. 27-41.
105. Sasso, M. and D. Amodio. *Development of a biaxial stretching machine for rubbers by optical methods*. in *Society for Experimental Mechanics Annual Conference*. 2006.
106. Martins, P.A.L.S., R.M.N. Jorge, and A.J.M. Ferreira, *A comparative study of several material models for prediction of hyperelastic properties: Application to silicone-rubber and soft tissues.* Strain, 2006. **42**(3): p. 135-147.
107. Guo, H., et al., *Development of a detailed aircraft tyre finite element model for safety assessment.* Materials & Design, 2014. **53**(0): p. 902-909.
108. Martins, J.A.C., et al., *A numerical model of passive and active behavior of skeletal muscles.* Computer Methods in Applied Mechanics and Engineering, 1998. **151**(3–4): p. 419-433.
109. Gracia, L.A., et al., *Finite element simulation of the hysteretic behaviour of an industrial rubber. Application to design of rubber components.* Finite Elements in Analysis and Design, 2010. **46**(4): p. 357-368.
110. Austrell, P.E., *Modeling of Elasticity and Damping for Filled Elastomers*, in *Structural Mechanics*. 1997, Lund University: Lund , Sweden.
111. Ghoreishy, M.H.R., et al., *Modeling the hyperviscoelastic behavior of a tire tread compound reinforced by silica and carbon black.* Journal of Applied Polymer Science, 2013. **128**(3): p. 1725-1731.
112. Dill, E.H., *Continuum mechanics : elasticity, plasticity, viscoelasticity*. 2007, Boca Raton, FL ; London: CRC Press. 352 p.

113. Bergström, J.S. and M.C. Boyce, *Constitutive modeling of the time-dependent and cyclic loading of elastomers and application to soft biological tissues.* Mechanics of Materials, 2001. **33**(9): p. 523-530.
114. Bergstrom, J.S. and M.C. Boyce, *Large strain time-dependent behavior of filled elastomers.* Mechanics of Materials, 2000. **32**(11): p. 627-644.
115. Bergstrom, J.S. and M.C. Boyce, *Constitutive modeling of the large strain time-dependent behavior of elastomers.* Journal of the Mechanics and Physics of Solids, 1998. **46**(5): p. 931-954.
116. Ghosh, P.S., A.; Bohara, P.C.; Mukhopadhyay, R. | Copyright, *Material property characterization for finite element analysis of tires.* Rubber World, 2006. **233**(4): p. 10.
117. *ASTM D412-06a Standard Test Methods for Vulcanized Rubber and Thermoplastic Elastomers—Tension.* 2006.
118. *ABAQUS™/CAE User's Manual . Dassault Systemes. ABAQUS™ Ver. 6.12.*
119. Yang, X., *Finite element analysis and experimental investigation of tyre characteristics for developing strain-based intelligent tyre system*, in *Mechanical Engineering*. 2009, University of Birmingham: Birmingham.
120. Fleming, R.A., *Tire Reinforcement and Tire Performance*. ASTM Special Technical Publication. 1979, Philadelphia: American Society for Testing and Materials.
121. Wang, X., *Finite Element Method*. 2003, Beijing, China: Tsinghua University Press.
122. Neves, R.R.V., G.B. Micheli, and M. Alves, *An experimental and numerical investigation on tyre impact.* International Journal of Impact Engineering, 2010. **37**(6): p. 685-693.
123. Reida, J.D., D.A. Boesch, and R.W. Bielenberg, *Detailed tire modeling for crash applications.* International Journal of Crashworthiness, 2007. **12**(5): p. 521-529.
124. Dunn, J.W. and O.A. Olatunbosun, *Linear and Nonlinear Modeling of Vehicle Rolling Tyre Low-Frequency Dynamic Behavior.* Vehicle System Dynamics, 1989. **18**: p. 179-189.
125. Ebbott, T.G., et al., *Tire Temperature and Rolling Resistance Prediction with Finite Element Analysis.* Tire Science and Technology, 1999. **27**(1): p. 2-21.
126. Shida, Z., et al., *A Rolling Resistance Simulation of Tires Using Static Finite Element Analysis.* Tire Science and Technology, 1999. **27**(2): p. 84-105.
127. Ghosh, S., R.A. Sengupta, and G. Heinrich, *Investigations on Rolling Resistance of Nanocomposite Based Passenger Car Radial Tyre Tread Compounds Using Simulation Technique.* Tire Science and Technology, 2011. **39**(3): p. 210-222.
128. Cho, J.R., et al., *Numerical estimation of rolling resistance and temperature distribution of 3-D periodic patterned tire.* International Journal of Solids and Structures, 2013. **50**(1): p. 86-96.
129. Luchini, J.R. and J.A. Popio, *Modeling Transient Rolling Resistance of Tires.* Tire Science and Technology, 2007. **35**(2): p. 118-140.
130. Wong, J.Y., *Theory of ground vehicles*. 4th ed. 2008, Hoboken, N.J.: Wiley. xxxi, 560 p.

131. Kerchman, V., *Tire-Suspension-Chassis Dynamics in Rolling over Obstacles for Ride and Harshness Analysis2.* Tire Science and Technology, 2008. **36**(3): p. 158-191.
132. Litak, G., et al., *Chaotic vibration of a quarter-car model excited by the road surface profile.* Communications in Nonlinear Science and Numerical Simulation, 2008. **13**(7): p. 1373-1383.
133. Jack, H., *Dynamic System Modeling and Control*. 2004.
134. Robert Bosch GmbH., *Automotive handbook*. 8th ed. 2011, Plochingen: Robert Bosch ;. 1265 p.
135. Clark, S.K., *Rolling Resistance of Pneumatic Tires.* Tire Science and Technology, 1978. **6**(3): p. 163-175.